Author Manuscript:
Published in final edited form as: *Surf. Interface Anal*. Volume 51, Issue 4, Pages 427-457, April 2019
https://doi.org/10.1002/sia.6598

Calculations of electron inelastic mean free paths. XII. Data for 42 inorganic compounds over the 50 eV to 200 keV range with the full Penn algorithm.

Hiroshi Shinotsuka,[1] Shigeo Tanuma,[1†] Cedric J. Powell,[2] and Dave R. Penn[2]

[1]National Institute for Materials Science, 1-2-1 Sengen, Tsukuba, Ibaraki 305-0047, Japan
[2]National Institute of Standards and Technology, Gaithersburg, MD 20899, USA

ABSTRACT

We have calculated inelastic mean free paths (IMFPs) for 42 inorganic compounds (AgBr, AgCl, AgI, Al_2O_3, AlAs, AlN, AlSb, cubic BN, hexagonal BN, CdS, CdSe, CdTe, GaAs, GaN, GaP, GaSb, GaSe, InAs, InP, InSb, KBr, KCl, MgF_2, MgO, NaCl, $NbC_{0.712}$, $NbC_{0.844}$, $NbC_{0.93}$, PbS, PbSe, PbTe, SiC, SiO_2, SnTe, $TiC_{0.7}$, $TiC_{0.95}$, $VC_{0.76}$, $VC_{0.86}$, $Y_3Al_5O_{12}$, ZnS, ZnSe, and ZnTe) for electron energies from 50 eV to 200 keV. These calculations were made with energy-loss functions (ELFs) obtained from measured optical constants for 15 compounds while calculated ELFs were utilized for the other 27 compounds. Checks based on ELF sum rules showed that the calculated ELFs were superior to the measured ELFs that we had used previously. Our calculated IMFPs could be fitted to a modified form of the relativistic Bethe equation for inelastic scattering of electrons in matter for energies from 50 eV to 200 keV. The average root-mean-square (RMS) deviation in these fits was 0.60 %. The IMFPs were also compared with a relativistic version of our predictive Tanuma-Powell-Penn (TPP-2M) equation. The average RMS deviation in these comparisons was 10.7 % for energies between 50 eV and 200 keV. This average RMS deviation is almost the same as that found in a similar comparison for a group of 41 elemental solids (11.9 %) although relatively large deviations were found for cubic BN (65.6 %) and hexagonal BN (34.3%). If these two compounds are excluded in the comparisons, the average RMS deviation becomes 8.7 %. We found generally satisfactory agreement between our calculated IMFPs and values from other calculations and from experiments.

† *Correspondence to*: S. Tanuma, National Institute for Materials Science, 1-2-1 Sengen, Tsukuba, Ibaraki 305-0047, Japan.
E-mail: tanuma.shigeo@nims.go.jp

Author Manuscript:
Published in final edited form as: *Surf. Interface Anal*. Volume 51, Issue 4, Pages 427-457, April 2019
https://doi.org/10.1002/sia.6598

1. Introduction

Values of electron inelastic mean free paths (IMFPs) in solids are of fundamental physical importance for describing the inelastic scattering of electrons in different materials. The IMFPs also define the surface sensitivity of Auger electron spectroscopy (AES) and X-ray photoelectron spectroscopy (XPS) and are used in quantitative applications of these techniques.[1,2]

We have previously calculated IMFPs for many solid materials over a wide energy range.[3,4,5,6,7,8] Initially, we reported IMFPs for 50 eV to 2,000 eV electrons for 27 elemental solids,[3,4] 15 inorganic compounds,[5] and 14 organic compounds.[6] These IMFPs were calculated from experimental optical data with the non-relativistic full Penn algorithm (FPA)[9] for electron energies under 200 eV and the single-pole approximation or simple Penn algorithm (SPA)[9] for higher energies. We analyzed these calculated IMFPs with the Bethe equation for inelastic scattering of electrons in matter[10] to develop an IMFP predictive formula (designated TPP-2M).[6] The TPP-2M equation could be used to estimate IMFPs in other materials, again for energies between 50 eV and 2,000 eV, the energy range of interest for many AES and XPS experiments.

In recent years, there has been growing interest in XPS and related experiments performed with X-rays of much higher energies for both scientific and industrial purposes. We then published IMFPs for 41 elemental solids for electron energies up to 30 keV.[7] Since there is also a need for IMFPs in transmission electron microscopy (TEM), we also calculated IMFPs in 41 elemental solids for energies up to 200 keV with a relativistic version of the FPA.[8] In addition, we developed a relativistic version of the TPP-2M equation that provides reasonable IMFP estimates for energies between 50 eV and 200 keV. The root-mean-square (RMS) deviation between the estimated IMFPs from the TPP-2M equation and the directly calculated values was 11.9 % for the group of 41 elemental solids.[8] This RMS deviation was similar to that found (10.2 %) in a similar comparison for our original group of 27 elemental solids for the 50 eV to 2 keV energy range.[6]

In this paper, we extend our previous calculations[5] of IMFPs for 15 inorganic compounds and electron energies between 50 eV and 2,000 eV. We report here new calculations of IMFPs with the relativistic FPA for 42 inorganic compounds (AgBr, AgCl, AgI, Al_2O_3, AlAs, AlN, AlSb, cubic BN (*c*-BN), hexagonal BN (*h*-BN), CdS, CdSe, CdTe, GaAs, GaN, GaP, GaSb, GaSe, InAs, InP, InSb, KBr, KCl, MgF_2, MgO, NaCl, $NbC_{0.712}$, $NbC_{0.844}$, $NbC_{0.93}$, PbS, PbSe, PbTe, SiC, SiO_2, SnTe, $TiC_{0.7}$, $TiC_{0.95}$, $VC_{0.76}$, $VC_{0.86}$, $Y_3Al_5O_{12}$, ZnS, ZnSe, and ZnTe) for energies between 50 eV and 200 keV. These inorganic compounds were chosen because they had experimental ELF data below the bandgap energy and the errors in the two sum rules for evaluating ELFs were less than 10 %. Two inorganic compounds that we considered previously [5], LiF and Si_3N_4, were omitted in this study because their ELFs gave large errors in the sum rules discussed in Section 3.2. The relativistic TPP-2M formula[8] must therefore be a more reliable means for determining IMFPs for these two compounds.

The IMFP calculations with the FPA require knowledge of the energy-loss

Author Manuscript:
Published in final edited form as: *Surf. Interface Anal.* Volume 51, Issue 4, Pages 427-457, April 2019
https://doi.org/10.1002/sia.6598

functions (ELFs) of each material, typically for photon energies (or, equivalently, electron energy losses) between 1 eV and 200 keV. Our previous IMFP calculations were based on ELFs obtained from experimental optical data or from electron energy-loss spectroscopy (EELS). However, optical constants and optical ELFs as well as EELS ELFs are lacking for most semiconductor materials for energy losses larger than about 10 eV. We therefore calculated ELFs for the 27 compound semiconductors in our group of 42 inorganic compounds. We utilized the WIEN2k[11] and FEFF[12] codes to compute the imaginary part of the complex dielectric constant, typically for photon energies from several eV to 1 MeV, from which we calculated the real part and then the ELF. We note here that Werner *et al.*[13] successfully used the WIEN2k code to calculate optical constants and ELFs for 16 elemental metals and one semimetal that agreed satisfactorily with corresponding data obtained from an analysis of reflection EELS data.

We also report comparisons of our calculated IMFPs for the 42 inorganic compounds with IMFPs calculated by Reich *et al.*[14], Akkerman *et al.*[15], Pandya *et al.*[16], Kwei and Li[17], Kwei *et al.*[18], Boutboul *et al.*[19], Ashley and Anderson[20], Dapor and Miotello[21,22], and Dapor[23], and with IMFPs measured by lakoubovskii *et al.*[24], Egerton[25, 26], Meltzman *et al.*[27], Gurban *et al.*[28], Pi *et al.*[29], Krawczyk *et al.*[30], Chung *et al.*[31], Wang *et al.*[32], MacCartney *et al.*[33], Lee *et al.*[34], and Bideux *et al.*[35], Zommer *et al.*[36], and Jung *et al.*[37]. We also make comparisons between the measured IMFPs and IMFPs from the relativistic TPP-2M equation.

2. IMFP Calculations with the Relativistic Full Penn Algorithm

We utilized the relativistic FPA to calculate IMFPs for energies in the 50 eV to 200 keV range in order to be consistent with our previous IMFP calculations for elemental solids.[8] The IMFPs were calculated at equal energy intervals on a logarithmic scale corresponding to increments of 10 % from 10 eV to 1 MeV. We will present IMFPs for energies between 10 eV and 50 eV and between 200 keV and 1 MeV in Figures but these results are shown only to illustrate trends.

The relativistic differential cross section (DCS) for inelastic scattering can be expressed as the sum of a longitudinal DCS and a transverse DCS.[38] Since the transverse DCS can be neglected for electron energies less than about 0.5 MeV,[39] the relativistic DCS can be written using Hartree atomic units ($m_e = e = \hbar = 1$, where m_e is the electron rest mass, e is the elementary charge, and $\hbar$ is the reduced Planck constant), as

$$\frac{d^2\sigma}{d\omega dQ} = \frac{d^2\sigma_L}{d\omega dQ} + \frac{d^2\sigma_T}{d\omega dQ} \approx \frac{d^2\sigma_L}{d\omega dQ} = \frac{1}{v^2}\frac{1+Q/c^2}{Q\left(1+Q/2c^2\right)}\frac{1}{\pi N}\mathrm{Im}\left(\frac{-1}{\varepsilon(Q,\omega)}\right) \qquad (1)$$

where ω is the energy loss, c is the speed of light, Q is the recoil energy defined by[40]

$$Q(Q+2c^2) = (cq)^2 , \qquad (2)$$

q is the momentum transfer, N is the number of molecules per unit volume, v is the electron velocity, and $\mathrm{Im}\left[-1/\varepsilon(Q,\omega)\right]$ is the ELF expressed as a function of energy loss

Author Manuscript:
Published in final edited form as: *Surf. Interface Anal.* Volume 51, Issue 4, Pages 427-457, April 2019
https://doi.org/10.1002/sia.6598

ω and recoil energy Q. Using Eqn (2) and $dQ = q/\left[1+\left(Q/c^2\right)\right]\cdot dq$, the ELF in Eqn (1) can be conveniently written as a function of ω and momentum transfer q.

We write the DCS as

$$\frac{d^2\sigma}{d\omega dq} \approx \frac{2}{\pi N v^2}\mathrm{Im}\left(\frac{-1}{\varepsilon(q,\omega)}\right)\frac{1}{q}, \tag{3}$$

where $\mathrm{Im}\left[-1/\varepsilon(q,\omega)\right]$ is the ELF. We will use the Penn algorithm[9] to evaluate Eqn (3). The dependence of the ELF on ω can be obtained from the measured ELF for each material (typically from optical experiments) while the dependence of the ELF on q can be obtained from the Lindhard model dielectric function.[41] In this paper, we will show that we can also use calculated ELFs for materials for which there are no measured ELFs over key energy ranges.

The ELF in Eqn (3) can be expressed using the full Penn algorithm as

$$\mathrm{Im}\left[\frac{-1}{\varepsilon(q,\omega)}\right] = \int_0^\infty d\omega_p g(\omega_p)\,\mathrm{Im}\left[\frac{-1}{\varepsilon^L(q,\omega;\omega_p)}\right] \tag{4}$$

where ε^L denotes the Lindhard model dielectric function of a free-electron gas with plasmon energy $\omega_p\left(=\sqrt{4\pi n}\right)$, n is the electron density, $g(\omega_p)$ is a coefficient introduced to satisfy the condition $\mathrm{Im}[-1/\varepsilon(q=0,\omega)] = \mathrm{Im}[-1/\varepsilon(\omega)]$, and $\mathrm{Im}[-1/\varepsilon(\omega)]$ is the measured or calculated ELF. The coefficient $g(\omega_p)$ is then given by

$$g(\omega) = \frac{2}{\pi\omega}\mathrm{Im}\left[\frac{-1}{\varepsilon(\omega)}\right] \tag{5}$$

The ELF from the FPA in Eqn (4) can be described as the sum of two contributions, one associated with the plasmon pole and the other with single-electron excitations:

$$\mathrm{Im}\left[\frac{-1}{\varepsilon(q,\omega)}\right] = \mathrm{Im}\left[\frac{-1}{\varepsilon(q,\omega)}\right]_{pl} + \mathrm{Im}\left[\frac{-1}{\varepsilon(q,\omega)}\right]_{se} \tag{6}$$

Details of the evaluations of the plasmon-pole and single-electron contributions were given in a previous paper [8].

We calculated IMFPs from Eqns (3) to (6) using the approach of Boutboul *et al.*[19] to include the effect of the bandgap energy in semiconductors and insulators. The IMFP, λ, at electron energy T ($>E_g + E_v$), which is measured from the bottom of the valence band for semiconductors and insulators, can be expressed as [8]:

$$\lambda(T)^{-1} = \frac{\left(1+T'/c^2\right)^2}{1+T'/\left(2c^2\right)}\frac{1}{\pi T'}\iint_D \frac{1}{q}\,\mathrm{Im}\left[\frac{-1}{\varepsilon(\omega,q)}\right] dq\,d\omega \tag{7}$$

Author Manuscript:
Published in final edited form as: *Surf. Interface Anal*. Volume 51, Issue 4, Pages 427-457, April 2019
https://doi.org/10.1002/sia.6598

where $T' = T - E_g$ and E_g is the bandgap energy. The integration domain D is determined from the maximum and minimum energy losses and the largest and smallest kinematically-allowed momentum transfers for a given energy T and ω:

$$D = \{(\omega, q): E_g \leq \omega \leq (T' - E_v), q_- \leq q \leq q_+ \} \ , \tag{8}$$

where E_v is the width of the valence band for semiconductors and insulators, and $q_\pm = \sqrt{T'(2 + T'/c^2)} \pm \sqrt{(T' - \omega)[2 + (T' - \omega)/c^2]}$.

Table 1 shows the material-property data used in our IMFP calculations and in our analyses of the ELFs and IMFPs. We show values of the molecular weight M, bulk density ρ (g cm^{-3}), number of valence electrons per molecule (N_v), free-electron plasmon energy (E_p), bandgap energy (E_g), and valence-band width (E_v) for each compound. The bandgap energy is also an important material parameter in the use of our TPP-2M predictive equation for IMFPs [6]. We chose the median of the E_g values in the literature [42,43,44,45,46,47,48] for most of our compounds; however, only single values of E_g were available for NaCl [49] and $Y_3Al_5O_{12}$ [47]. The E_v values were obtained from the WIEN2k calculations for 27 compound semiconductors and values for the other eight insulators were estimated from the literature: Al_2O_3 [50, 51], KBr [52], KCl [52], MgF_2 [53], MgO [54], NaCl, [52], SiO_2 [55], $Y_3Al_5O_{12}$ [56]. For the niobium, titanium, and vanadium carbides, the E_v values correspond to the Fermi energies that were estimated from the literature [86, 87].

3. Optical energy-loss functions

We have shown that IMFPs can be calculated with the FPA and SPA from ELFs obtained from experimental optical data (i.e., optical ELFs) for many materials of interest.[3-8] The ELF is thus the critical material-dependent parameter in our IMFP calculations. Ideally, optical ELFs should be determined from measured optical constants. In many cases, we utilized optical constants from Handbooks[45-47] although we have occasionally used optical constants derived from analyses of electron energy-loss experiments.[7] Our choices from sets of optical data were guided by evaluations of the ELFs using the two important sum rules described in the 'Evaluations of energy-loss functions' subsection.

Unfortunately, experimental optical constants are generally not available for many inorganic compounds, especially for the 20 eV to 50 eV energy range that is particularly important for the IMFP calculations. As an alternative, we have made first-principles calculations of optical constants using the WIEN2k[11] and FEFF[12] codes, as described in the next subsection. These calculations were made for 27 inorganic compounds (*c*-AgBr, *c*- AgCl, *h*- AgI, *c*- AlAs, *h*-AlN, c- AlSb, *c*- BN, *h*-BN, CdS, *h*-CdSe, *c*- CdTe, *c*-GaAs, *h*-GaN, c- GaP, c- GaSb, *h*- GaSe, *c*- InAs, *c*- InP, *c*- InSb, *c*- PbS, *c*- PbSe, *c*- PbTe, *c*- SiC, *c*- SnTe, *c*- ZnS, *c*- ZnS, and *c*- ZnTe). These compounds were selected because

Author Manuscript:
Published in final edited form as: *Surf. Interface Anal*. Volume 51, Issue 4, Pages 427-457, April 2019
https://doi.org/10.1002/sia.6598

optical data for photon energies less than 0.1 eV were needed for evaluation of one of the sum rules and were mostly available in the literature.[44, 45, 46, 47] Details of the first-principle calculations of ELFs will be published elsewhere.

Table 2 shows the sources of optical data used in our IMFP calculations. For 15 of the compounds (Al_2O_3, KBr, KCl, MgF_2, MgO, NaCl, $NbC_{0.712}$, $NbC_{0.844}$, $NbC_{0.93}$, SiO_2, $TiC_{0.7}$, $TiC_{0.95}$, $VC_{0.76}$, $VC_{0.86}$, and $Y_3Al_5O_{12}$), optical data from literature sources were available for photon energies up to at least 50 eV.

3.1 Optical energy-loss functions from first-principles calculations

Crystal information for the inorganic compounds used in the WIEN2k[11] and FEFF[12] calculations is shown in Table 3.[57] The WIEN2k code performs calculations of the electronic structure of solids using density functional theory (DFT). We used WIEN2k Version 08.02. The generalized gradient approximation (GGA) as parameterized by Perdew, Bruke, and Ernzerhof was adopted for the exchange-correlation potential [58]. We calculated the imaginary part of the dielectric function, ε_2, from the optically-allowed transition amplitudes for photon energies between 0.1 eV and 136 eV. For hexagonal crystals, we calculated the optical constants under the condition that the electric field was perpendicular to the c-axis of the crystal.

The FEFF 8.2 code is an automated program for calculating X-ray absorption spectra based on an *ab initio* all-electron, real-space relativistic Green's function formalism[12]. This code gives photoabsorption cross sections for all elements in a compound. Only crystal-structure information is needed to obtain the absorption spectra. We can then easily calculate ε_2. These calculations were made for photon energies between 10 eV and 1 MeV.

Our calculations of ε_2 with the FEFF and WIEN2k codes were made independently, and we found the values of ε_2 from each code to be reasonably consistent for energies between 30 and 80 eV, as will be shown shortly. We made a dataset of ε_2 values calculated by the FEFF and WIEN2K codes for each compound for photon energies from 0.1 eV to 1 MeV, and Table 2 shows the energy range utilized for the ε_2 values from each code. The real part of the dielectric function, ε_1, was calculated by use of the Kramers-Kronig relation[59]:

$$\varepsilon_1(\omega) = 1 + \frac{2}{\pi} P \int_0^\infty \frac{\omega' \varepsilon_2(\omega')}{(\omega')^2 - \omega^2} d\omega' \ , \tag{9}$$

where P is the Cauchy principal value. The actual integration range of Eqn (9) was between 0.1 eV and 1 MeV. We then calculated the optical ELF, $\mathrm{Im}[-1/\varepsilon(\omega)]$, from the data sets of ε_1 and ε_2.[5]

We now give brief comments on the calculated ELFs for two compound semiconductors, GaAs and InSb, to assess the accuracy of our first-principles calculations

Author Manuscript:
Published in final edited form as: *Surf. Interface Anal*. Volume 51, Issue 4, Pages 427-457, April 2019
https://doi.org/10.1002/sia.6598

of the ELFs. Figure 1 shows the plots of ε_2 for GaAs and InSb calculated from the WIEN2k and FEFF codes for energies from 0.1 eV to 100 eV together with ε_2 values calculated from the atomic scattering factors of Henke *et al.* [60]. We see that there is good agreement in Fig. 1(a) among the ε_2 data for GaAs for energies between 30 eV and 60 eV. For energies over 60 eV, the ε_2 values from WIEN2k are smaller than those from FEFF and from Henke *et al*. On the other hand, the ε_2 values from FEFF are in good agreement with those from Henke *et al*. for energies between 30 eV and 100 eV. This agreement occurs because the FEFF code was developed mainly to calculate inner-shell X-ray absorption spectra, and it is thus expected to be particularly useful for energy losses greater than about 100 eV. In contrast, the WIEN2k was developed mainly for calculating the electronic states of the outer shells, and is particularly useful for energy losses less than about 50 eV.[13]

For InSb, as shown in Fig. 1(b), the ε_2 data from WIEN2k are in good agreement with those from FEFF for energies between 30 eV and 50 eV. We also see that the ε_2 data of Henke *et al.* are slightly smaller than the WIEN2k and FEFF values for the same energy range. For energies over 60 eV, the ε_2 results from FEFF are larger than those from WIEN2k, as found for GaAs.

Figure 1 also shows ELFs of GaAs and InSb calculated from the WIEN2k code together with ELFs obtained from the transmission-EELS experiments of von Festenberg,[61] as analyzed by Chen *et al*.,[62] and the reflection-EELS experiments of Jin *et al*.[63] The GaAs ELF from WIEN2k for energy losses up to 30 eV is in excellent agreement with the ELF determined by Jin *et al.* except at around 20 eV, as shown in Fig. 1(c). It is also in good agreement with the ELF obtained by Chen *et al*.,[62] especially for the large peak at around 16 eV that corresponds to bulk-plasmon excitation, although there are some differences at around 10 eV and over 20 eV. However, the peak found by Chen *et al.* at around 10 eV is not seen in the ELF of Jin *et al*. The plasmon peak is at 15.6 eV in the WIEN2k ELF, in good agreement with the peak positions in the ELFs of Jin *et al.* (15.4 eV) and Chen *et al.* (15.7 eV), and with the tabulation of Egerton[26] (15.8 eV).

On the other hand, the GaAs ELF from WIEN2k is very different from the ELF shown in Fig. 1(c) that was calculated from experimental optical constants tabulated by Palik[45] and which we used in our previous IMFP calculations for GaAs[5]. For photon energies between 6 eV and 23 eV, we utilized optical constants that were obtained from near-normal-incidence reflectance measurements in a vacuum spectrometer[45, 64]. The GaAs sample used by Philipp and Ehrenreich[64] was prepared by chemical etching to remove distorted layers produced by mechanical polishing but was exposed to air before mounting in their sample chamber. The sample was also exposed to "the poor vacuum" of their monochromator during their measurements; at the time of this work, reflectance measurements in the ultraviolet spectral region were typically made in high-vacuum

Author Manuscript:
Published in final edited form as: *Surf. Interface Anal*. Volume 51, Issue 4, Pages 427-457, April 2019
https://doi.org/10.1002/sia.6598

chambers. As noted by Palik[45], the GaAs sample of Ehrenreich and Philipp probably had a ≈ 2 nm thick native oxide on its surface. It is therefore not surprising now that the GaAs ELF in Fig. 1(c) from the Palik optical data differs considerably from the other ELFs. We note particularly that the plasmon peak from the Palik data is at 14.0 eV and is much weaker than for the other ELFs in Fig. 1(c).

The ELF for InSb from the WIEN2k code is shown in Fig. 1(d) and is in good agreement with the ELF determined by von Festenberg[61] from transmission-EELS experiments. The bulk-plasmon peak is at 13.2 eV in the WIEN2k ELF which is also in good agreement with the peak position in the von Festenberg ELF (12.9 eV). As for InSb, the ELF from the optical data of Palik[45] (also used in our previous IMFP calculations for InSb[5]) shows a plasmon peak at 12.0 eV that is much weaker than the plasmon peak found in the ELFs from WIEN2k and von Festenberg[61]. The optical constants tabulated by Palik for InSb were also obtained from the reflectivity measurements of Philipp and Ehrenreich[64] for photon energies between 6 eV and 24 eV. Their InSb sample was prepared and handled in the same way as their GaAs sample, and it is again likely that the InSb sample had a surface oxide.

We conclude that the ELFs of GaAs and InSb obtained from WIEN2k are superior to the ELFs obtained from published optical data[45]. We also point out that small differences in peak positions and peak heights in ELFs from different sources are expected to have insignificant effects on calculated IMFPs since these IMFPs are derived from an integration of the ELF using Eqn (7). Further evaluations of the ELFs from WIEN2k and FEFF are given in the following subsection.

3.2 Evaluations of energy-loss functions

We checked the internal consistency of our ELF data for each compound with the oscillator-strength or f-sum rule and a limiting form of the Kramers-Kronig integral (or KK-sum rule).[5,65] The f-sum can be evaluated as the total effective number of electrons per molecule, $Z_{\rm eff}$, contributing to the inelastic scattering:

$$Z_{\rm eff} = (2/\pi\hbar^2\Omega_p^2)\int_{E_g}^{\Delta E_{\rm max}} \Delta E\,{\rm Im}[-1/\varepsilon(\Delta E)]d(\Delta E) \qquad (10)$$

where $\Delta E = \hbar\omega$, $\Omega_p = (4\pi n_a e^2/m)^{1/2}$, $n_a = N_a\rho/M$ is the density of atoms, $N_{\rm a}$ is Avogadro's number, ρ is the mass density, and M is the molecular weight. The maximum energy loss in Eqn (10), $\Delta E_{\rm max}$, was chosen to be 1 MeV. Ideally, the value of Z_{eff} should be equal to (or otherwise close to) the total number of electrons per molecule, Z. The KK-sum can be expressed as:

$$P_{eff} = (2/\pi)\int_0^{\Delta E_{\rm max}} \Delta E^{-1}\,{\rm Im}[-1/\varepsilon(\Delta E)]d(\Delta E) + n^{-2}(0) \qquad (11)$$

Author Manuscript:
Published in final edited form as: *Surf. Interface Anal*. Volume 51, Issue 4, Pages 427-457, April 2019
https://doi.org/10.1002/sia.6598

where $n(0)$ is the limiting value of the refractive index at low photon energies.

In the limit $\Delta E_{\max} \to \infty$, $Z_{eff} \to Z$ and $P_{eff} \to 1$. We determined Z_{eff} and P_{eff} from Eqns (10) and (11) for each compound as a function of $\Delta E_{\max}$ up to a maximum value of 1 MeV. Table 4 lists the errors in the f-sum and KK-sum rules for each inorganic compound, that is, the differences between the computed values of Z_{eff} and P_{eff} and the expected values (the total number of electrons per molecule and unity, respectively). The average RMS errors in the f-sum and KK-sum rules were 4.1 % and 3.5 %, respectively, for our sets of ELF data. These average RMS errors are comparable to those found in our ELF data sets for a group of 41 elemental solids[7], 4.2 % for the f-sum error and 7.7 % for the KK-sum error. Over 80 % of our compounds had sum-rule errors less than 5 % for both sum rules. In our previous analyses of optical ELFs, obtained from experimental optical data for 15 inorganic compounds, the average sum-rule errors were 8 % and 24 % for the f-sum and KK-sum rules, respectively[5].

For the example case of GaAs in Fig. 1(c), we previously found large sum-rule errors (-13 % for the f-sum rule and -37 % for the KK-sum rule) for the GaAs ELF obtained from the Palik[45] optical data for photon energies between 1.5 eV and 100 eV and from Henke *et al*.[60] for higher energies.[5] In contrast, the sum-rule errors for the GaAs ELF from the WIEN2k and FEFF calculations were -1.9 % for the f-sum rule and 1.4 % for the KK-sum rule. This large reduction in the sum-rule errors is due mainly to the more reliable ELF from WIEN2k for photon energies less than 30 eV in Fig. 1(c). As noted in the previous subsection, the ELF from WIEN2k generally agrees well with the ELFs from the EELS experiments of von Festenberg[61] (analyzed by Chen *et al*.[62]) and of Jin *et al*. [63] The large improvement in the results of the KK-sum rule is due to the fact that this evaluation emphasizes the ELF for relatively small energy losses [Eqn (11)] whereas the f-sum rule [Eqn (10)] emphasizes the ELF for relatively large energy losses. As we can see from Fig. 1(c), there is a substantial difference in the GaAs ELF from the Palik data and the more recent ELFs from WIEN2k and EELS data. We reach similar conclusions for the example case of InSb in Fig. 1(d).

Figure 2 shows comparisons of the f-sum and KK-sum errors for the 15 inorganic compounds in our previous work[5] and the corresponding values for the same compounds in the present work. We see that the new values cluster much closer to the origin with sum-rule errors generally less than 10 %. The present ELF data are clearly superior to the previous ELF data, especially in the KK-sum rule results.

4. Results

4.1 Calculated IMFPs from the relativistic full Penn algorithm

Table 5 shows our calculated IMFPs for the 42 inorganic compounds as a function of the electron kinetic energy E (= $T - E_g - E_v$) with respect to the bottom of the conduction band between 50 eV and 200 keV. Plots of IMFPs as a function of electron

Author Manuscript:
Published in final edited form as: *Surf. Interface Anal*. Volume 51, Issue 4, Pages 427-457, April 2019
https://doi.org/10.1002/sia.6598

energy are shown as solid circles in Figs. 3 to 10. IMFPs are included in these plots for energies less than 50 eV and over 200 keV to illustrate trends. The IMFPs for energies less than 50 eV, however, are not considered as reliable as those at higher energies[4,7] while the IMFPs for energies larger than 200 keV must be slightly larger than the correct values because we neglected the contribution of the transverse DCS shown in Eqn (1).[8]

The plots of calculated IMFPs in Figs. 3 to 10 show similar dependences on electron energy for energies over 200 eV for all of the compounds. For energies less than 200 eV, however, there are appreciable variations in the shapes of the plots (i.e., the positions and the shapes of the minima) that are due to different shapes of the ELFs for each material. For energies over 50 keV, the slopes of the IMFP *vs*. electron energy plots become smaller than those for energies between about 1 keV and 30 keV; these slope changes must be due to relativistic effects.

4.2 Effects of the bandgap energy on the calculated IMFPs

The value of the bandgap energy E_g is an important parameter in the calculations of IMFPs for nonconductors, as shown by Eqns (7) and (8). We therefore investigated the influence of including the E_g value on the calculated IMFPs for SiO_2, KBr, and InP. We chose these compounds as representative materials because one compound (SiO_2) has a relatively large E_g value (9.1 eV), another (KBr) has an intermediate E_g value (7.26 eV), and the other (InP) has a small E_g value (1.38 eV).

Figures 11(a) – (c) show IMFPs calculated from optical ELFs by the FPA-Boutboul approach for InP, KBr, and SiO_2 as a function of electron energy from 10 eV to 10 keV both with the E_g values for each compound included in the calculation (dashed lines) and with E_g set equal to zero (solid lines). Figure 11(d) shows ratios of the IMFPs for the three compounds with finite E_g values to those with E_g set to zero as a function of energy. These ratios are less than 1.01 (i.e., IMFP differences of less than 1 %) for $E \geq$ 100 eV. For 50 eV $\leq E \leq$ 100 eV, however, the differences could be up to about 10 % for KBr and SiO_2 although the differences for InP were less than 1 %.

Figure 11 indicates that inclusion of the bandgap energy in the IMFP calculation generally leads to IMFP increases for $E <$ 100 eV. This increase is due to the decrease in the ω (or energy) integral domain D as given in Eqn (8). The lower limit of the ω integral, ΔE_{min}, is set equal to the bandgap energy for nonconductors. This limit corresponds to the minimum excitation energy of electron in the material. The maximum excitation energy corresponds to the upper limit of the ω integral, ΔE_{max}. This upper limit ensures that an incident electron will always have sufficient energy to remain in the conduction band. The upper limit is then given by $\Delta E_{max} = T - E_v - E_g$. On the other hand, ΔE_{min} and ΔE_{max} for conductors are given by 0 and T - E_f, respectively, where E_f is the Fermi energy.

In our previous papers [3 – 8,69], we did not consider the effect of the bandgap energy in the IMFP calculations for nonconductors. For example, IMFPs for water were reported for energies between 50 eV and 30 keV with the same procedure (i.e., the same

Author Manuscript:
Published in final edited form as: *Surf. Interface Anal*. Volume 51, Issue 4, Pages 427-457, April 2019
https://doi.org/10.1002/sia.6598

integral domain) we used for conductors [69]. We will therefore show a comparison of water IMFPs that were calculated with and without consideration of E_g as one more example.

Figure 12(a) shows IMFPs of water calculated from the FPA-Boutbul approach with E_g = 7.9 eV (dashed line) and from the FPA with E_g = 0 (solid line) as a function of electron energy above the bottom of the conduction band. Figure 12(b) shows the ratio of these IMFPs as a function of electron energy. For $E \geq 100$ eV, we see that the IMFPs from the FPA-Boutboul approach are up to 1.5 % larger than the IMFPs from the FPA with E_g assumed to be zero. For lower energies, the IMFP differences become larger due to the decrease in the ω integral domain, reaching 6.5 % at 54.6 eV.

We conclude that the effect of the bandgap energy on IMFPs calculations with the FPA is generally small (< 1.5 %) for energies over 100 eV even for the materials that have large bandgap energies such as SiO_2.

4.3 Comparison of IMFPs calculated from the present and previous energy loss functions.

Figure 13(a) shows plots of the ratios of IMFPs in Table 5 for 13 inorganic compounds with the newer ELFs that we used here (λ_{new}) to the corresponding IMFPs that we published previously [5] (λ_{old}). Over 100 eV, the largest changes occurred for GaAs (a decrease) and for InP (an increase). While the ratios are nearly constant for energies above about 300 eV, different energy dependences are seen for lower energies. The various magnitudes of the ratios in Fig. 13(a) and the different energy dependences are associated with the new ELFs that we adopted for the present IMFP calculations.

Figures 13(b) and (c) show the averages of the IMFP ratios, $< \lambda_{new} / \lambda_{old} >$, between 100 eV and 2000 eV for each compound as a function of the f-sum and KK-sum-rule errors for the previous ELFs, respectively. We see a clear linear dependence between the averages of the IMFP ratios and the KK-sum-rule errors in Fig. 13(c) except for four compounds (NaCl, Al_2O_3, KCl and PbTe). This linear dependence for most compounds is reasonable because IMFPs of a material are roughly proportional to the inverse of its ELF, as shown by Eqn (7). For example, a smaller ELF that gives a negative sum-rule error will give larger IMFPs than those calculated from the correct ELF. On the other hand, three compounds (Al_2O_3, KCl, and NaCl) show $< \lambda_{new} / \lambda_{old} >$ values of about unity despite having large KK sum-rule errors for the previous ELF data sets (-25 %, -25%, and -32 % for Al_2O_3, KCl, and NaCl, respectively, as shown in Fig.11(c)) but relatively small f-sum errors (-6 %, -1 %, and -5% for Al_2O_3, KCl, and NaCl, respectively, as shown in Fig.13(b)). In the evaluations of the KK-sum from Eqn (11), the contributions from low-energy excitations (e.g., less than 1 eV) are very important. However, the minimum excitation energies in our previous ELFs were 6 eV for Al_2O_3, 6.9 eV for KCl, and 7.6 eV for NaCl. It was thus not possible to evaluate the KK-sum rule correctly for these compounds in our earlier work[5]. The low-energy excitations, however, do not contribute

Author Manuscript:
Published in final edited form as: *Surf. Interface Anal*. Volume 51, Issue 4, Pages 427-457, April 2019
https://doi.org/10.1002/sia.6598

significantly to the calculated IMFPs, and thus the $< \lambda_{new} / \lambda_{old} >$ values are roughly unity even though the KK-sum-rule errors for the previous ELF data sets are relatively large for Al_2O_3, KCl, and NaCl.

On the other hand, PbTe showed large sum-rule errors, -12 % for the f-sum and 12 % for the KK-sum, as shown in Figs. 13(b) and (c). Since $< \lambda_{new} / \lambda_{old} >= 0.85$ for PbTe, this result must be due to the relatively large contribution of energy losses under 100 eV in the new ELF to the KK-sum-rule error.

As shown in Table 4 and Fig. 2, our new IMFPs for inorganic compounds are believed to be more reliable than those we published previously[5] because of the smaller sum-rule errors of the new ELFs compared to those for the previous ELFs.

4.4 Energy dependence of IMFPs

In previous work [4, 5, 7, 8,66, 67], we analyzed the dependence of the calculated IMFPs on energy for each material with a modified form of the Bethe equation for inelastic-electron scattering in matter.[68] The relativistic form of the modified Bethe equation can be described approximately as:[8]

$$\lambda(E) = \frac{\alpha(E)E}{E_p^2 \left\{ \beta[\ln(\gamma\alpha(E)E)] - (C/E) + \left(D/E^2\right) \right\}} , \qquad \text{(nm)} \qquad (12)$$

where

$$\alpha(E) = \frac{1 + E/\left(2m_e c^2\right)}{\left[1 + E/\left(m_e c^2\right)\right]^2} \approx \frac{1 + E/1021999.8}{(1 + E/510998.9)^2} , \qquad (13)$$

$$E_p = 28.816 \left(\frac{N_v \cdot \rho}{M} \right)^{0.5} , \qquad \text{(eV)}$$

where E is the electron kinetic energy (in eV) above the bottom of the conduction band (= $T - E_v - E_g$), ρ is the bulk density (in g cm^{-3}), N_v is the number of valence electrons per atom or molecule, and β, γ, C, and D are parameters. Satisfactory fits were made with Eqns (12) and (13) to the calculated IMFPs for the 42 inorganic compounds for energies between 50 eV and 200 keV, as shown by the solid lines in Figs. 3 to 10, and the values of β, γ, C, and D from each fit are shown in Table 6.

The quality of each fit was assessed from the *RMS* percentage difference, *RMS*:

$$RMS = 100 \times \left[\sum_{i=1}^{n} \left(\frac{\lambda_{fit}\left(E_i\right) - \lambda\left(E_i\right)}{\lambda\left(E_i\right)} \right)^2 / n \right]^{0.5} , \qquad (\%) \qquad (14)$$

where n = 83 is the number of electron energies in Table 5. Values of *RMS* for each solid are shown in Table 6. These values range from 0.18 % (for *h*-BN) to 1.04 % (for MgF_2), while the average value of *RMS* for the 42 compounds was 0.60 ± 0.22 %. This average

Author Manuscript:
Published in final edited form as: *Surf. Interface Anal*. Volume 51, Issue 4, Pages 427-457, April 2019
https://doi.org/10.1002/sia.6598

value of *RMS* is similar to that found for our group of 41 elemental solids (0.68 %).[8] Equations (12) and (13) are thus convenient analytical representations of the calculated IMFPs (e.g., for interpolation).

4.5 Comparison of calculated IMFPs with IMFPs from the relativistic TPP-2M equation

We recently developed a relativistic version of our earlier predictive IMFP formula[6], designated the relativistic TPP-2M equation[8], to estimate IMFPs in materials for electron energies between 50 eV and 200 keV. Our original non-relativistic TPP-2M equation was developed from an analysis of calculated IMFPs for a group of 27 elemental solids[4] and a group of 14 organic compounds[6] for electron energies between 50 eV and 2 keV. The relativistic TPP-2M formula is based on Eqns (12) and (13), and the following expressions for the material-dependent parameters in this equation:[8]

$$\beta = -1.0 + 9.44 / \left(E_p^2 + E_g^2\right)^{0.5} + 0.69\rho^{0.1} \qquad (\mathrm{eV^{-1}nm^{-1}}) \tag{15a}$$

$$\gamma = 0.191\rho^{-0.5} \qquad (\mathrm{eV^{-1}}) \tag{15b}$$

$$C = 19.7 - 9.1U \qquad (\mathrm{nm^{-1}}) \tag{15c}$$

$$D = 534 - 208U \qquad (\mathrm{eV\,nm^{-1}}) \tag{15d}$$

$$U = \frac{N_v \rho}{M} = \left(E_p / 28.816\right)^2 \tag{15e}$$

where the bandgap energy E_g is in eV. Equations (15) are the same as those for our non-relativistic TPP-2M equation.[6]

IMFPs calculated from the relativistic TPP-2M equation for our 42 compounds are shown in Figs. 3 to 10 as dashed lines, and Table 7 shows values of RMS deviations between these IMFPs and the IMFPs calculated from optical data as shown in Table 5. The average RMS deviation for the 42 inorganic compounds over the 50 eV to 200 keV range was 10.7 %. This average deviation is almost the same as that found in a similar comparison for our group of 41 elemental solids for the same energy range (11.9 %).[8] Nevertheless, we see relatively large RMS deviations for *c*-BN and *h*- BN in Table 7 (65.6 % and 34.3 %, respectively). Possible reasons for these large deviations will be discussed in the next section. If the RMS deviations for the two types of BN are ignored, the average RMS deviation for the remaining compounds becomes 8.7 %.

Figure 14 shows plots of ratios of IMFPs calculated from the relativistic TPP-2M equation [Eqns (12), (13), and (15)] to IMFPs calculated from optical data for the 42 inorganic compounds as a function of electron energy in order to assess visually the reliability of the TPP-2M equation for energies up to 200 keV. Ideally, these ratios should not change with energy and should be close to unity. The ratios in Fig. 14 are nearly constant for energies between about 200 eV and 200 keV (the relative deviations are less than 2.8%) but there are often substantial changes at lower energies (typically less than 100 eV). We see large values of the ratios for *c*-BN (ratios > 1.6 for energies over 100 eV) and *h*-BN (ratios >1.3 for energies over 100 eV). We also see that the ratios for NaCl

Author Manuscript:
Published in final edited form as: *Surf. Interface Anal*. Volume 51, Issue 4, Pages 427-457, April 2019
https://doi.org/10.1002/sia.6598

are < 0.8 for energies less than 300 eV. If we ignore the two BN compounds, the TPP-2M values deviate by ±15% to ±20% from the corresponding optical IMFPs for energies between 100 eV and 200 keV. We conclude that the relativistic TPP-2M formula consisting of Eqns (12), (13) and (15) is useful for estimating IMFPs in solid materials for energies between 50 eV and 200 keV although the accuracy of these estimates is likely to be poorer for energies less than about 200 eV.

5. Discussion

We will make comparisons of our calculated IMFPs for inorganic compounds with other IMFP calculations and with IMFP measurements from EELS, different types of transmission electron microscopy (TEM) experiments, elastic-peak electron spectroscopy (EPES), and photoemission experiments. Although IMFP calculations from the relativistic FPA are expected to provide only a qualitative guide for energies over 200 keV, we show the calculated IMFPs for energies up to 500 keV in Fig.16 to make comparisons with IMFP measurements at 300 keV. We will also discuss the reliability of the relativistic TPP-2M equation for predicting IMFPs.

5.1 Comparison of inelastic mean free paths with other calculated inelastic mean free paths

Figure 15 shows comparisons of our IMFPs with IMFPs calculated for Al_2O_3 [14,15, 16, 21], GaAs [17], KBr [15], KCl [15], MgO [15, 18, 21], NaCl [19] and SiO_2 [14, 15, 16, 18, 20, 21, 22, 23] for energies between 10 eV and 10 keV. We have plotted the IMFP data in the literature, listed above, in Fig. 15 without any energy-scaling corrections. That is, our IMFPs are shown as a function of energy above the bottom of the conduction band (as in Figs. 3 to 10) and the IMFPs from the literature are shown as they were reported. We thus assumed that these IMFPs were also determined as a function of energy above the bottom of the conduction band even if this was not stated in the original papers.

Ashley and Anderson [20] calculated IMFPs for SiO_2 in 1981 for energies from 15 eV to 10 keV using a model ELF. This ELF consisted of a fit to measured ε_2 and EELS data to describe valence-electron excitations and generalized oscillator strengths to represent inner-shell excitations. They also made a correction for the exchange effect between the incident electron and electrons in the medium. Their IMFPs for SiO_2 are shown in Fig. 15(e) where we see excellent agreement with our IMFPs for energies between 80 eV and 10 keV, where the RMS difference between them is 6.8 %. At lower energies, however, we see larger difference between their IMFPs and ours. At 15 eV, the Ashley and Anderson IMFP was larger than our IMFP by over 300 %. This difference at low energies must be mainly due to the contribution of single-electron excitations to the ELF, as shown in Eqn (6), which were neglected in the algorithm of Ashley *et al*. Their algorithm is based on the simplified single-pole approximation (SSPA)[69] which is expected to give substantially larger IMFPs at energies less than 50 eV than those calculated with the FPA as in our work.

Author Manuscript:
Published in final edited form as: *Surf. Interface Anal*. Volume 51, Issue 4, Pages 427-457, April 2019
https://doi.org/10.1002/sia.6598

Reich *et al*.[14] calculated IMFPs for Al_2O_3, SiO_2, and GeO_2 in 1988 for energies from 200 eV to 3700 eV using an independent atomic-center approximation. The total inelastic-scattering cross sections of O, Al, Si and Ge atoms were calculated within the framework of the Born approximation with consideration of both ionization processes and excitation to discrete levels. The IMFPs for compounds were determined from the sum of total cross sections for their constituent atoms.

Figure 15(a) shows that the IMFPs of Reich *et al*. for Al_2O_3 are considerably smaller than our IMFPs with an RMS difference between them of 43 %. Figure 15(e) shows a similar comparison for SiO_2 where again the Reich *et al*. IMFPs are substantially smaller than our IMFPs. For SiO_2, the RMS difference between them is 32 %.

In 1993, Kwei *et al.*[18] calculated IMFPs for MgO and for the crystalline and glassy forms of SiO_2 for energies from 10 eV or 20 eV to 2000 eV using extended Drude dielectric functions to describe plasmon excitations and interband transitions. The parameters in the Drude functions were determined from fits to experimental values of ε_2. They used a simple quadratic dispersion equation to extend the optical dielectric function into the $q > 0$ region.

Figures 15(d) and (e) show comparisons of our IMFPs with the IMFPs of Kwei *et al*. for MgO and SiO_2, respectively. The IMFPs of Kwei *et al.* for MgO are substantially larger than our IMFPs for energies less than 40 eV and slightly larger than our IMFPs for energies between 500 eV and 2000 eV. Their IMFPs are in good agreement with our IMFPs for energies between 50 eV and 400 eV where the differences are less than 10 %. The relatively small differences between the MgO IMFPs of Kwei *et al.* and our IMFPs for energies between 50 eV and 2000 eV are believed due to their use of a different ELF and/or a different dispersion equation for q. Because Kwei *et al.* used the SSPA, their IMFPs at energies less than 50 eV are expected to be substantially larger than our values from the FPA.

The energy dependence of the IMFPs of Kwei *et al.* for crystalline SiO_2 in Fig. 15 (e) is similar to that for MgO. Their IMFPs are slightly smaller than our IMFPs for energies between 50 eV and 2000 eV where the RMS difference is 14.5 %. The IMFP differences are mainly due to the use of different ELFs because our IMFPs were calculated from the ELF for glassy SiO_2. On the other hand, the IMFPs of Kwei *et al*. for glassy SiO_2 in Fig. 13(e) are in excellent agreement with our IMFPs for energies between 50 eV and 2000 eV where the RMS difference is 4.6 %. At lower energies, however, there are increasing differences between the Kwei *et al.* IMFPs and our IMFPs for both crystalline and glassy SiO_2, with a difference of over 400 % at 20 eV for both materials. These divergences are due to the neglect of single-electron excitations by Kwei *et al*.

Akkerman *et al.*[15] calculated IMFPs for Al_2O_3, KBr, KCl, MgO, and SiO_2 in 1996 for energies between 50 eV and 10 keV. They used a dielectric model with a quadratic dispersion equation and took the bandgap energy into account. They fitted Drude functions to the optical ELFs for each material to describe valence-electron excitations. They performed separate IMFP calculations for core-electron excitations with

Author Manuscript:
Published in final edited form as: *Surf. Interface Anal*. Volume 51, Issue 4, Pages 427-457, April 2019
https://doi.org/10.1002/sia.6598

Gryzinski's binary-encounter theory [70]. Total inverse IMFP values were obtained by the summation of inverse IMFPs for valence- and core-electron excitations.

Figures 15(a), (c), (d), and (e) show comparisons of our IMFPs with the IMFPs of Akkerman *et al*. for Al_2O_3, KBr, KCl, MgO, and SiO_2 for electron energies from 50 eV to 10 keV. The IMFPs of Akkerman *et al.* for Al_2O_3 in Fig. 15(a) are in good agreement with our IMFPs for energies between 100 eV and 10 keV with an RMS difference of 8.8 %. At lower energies, however, there are increasing differences between the Akkerman *et al*. IMFPs and our IMFPs with a difference of 43 % at 53 eV. Our smaller IMFPs in this energy range must be due to the contribution of single-electron excitations to the ELF, as shown in Eqn (6), which were neglected in the algorithm of Akkerman *et al*.[15]. Similar trends are found in the comparisons of the Akkerman *et al.* IMFPs for KBr and KCl in Fig. 15(c) and for SiO_2 in Fig. 15(e). The IMFPs of Akkerman *et al.* for KBr and KCl are also in excellent agreement with our IMFPs between 100 eV and 10 keV, as shown in Fig. 15(c) where the RMS differences are 2.7 % for KBr and 4.0 % for KCl. At lower energies, we see increasing differences between the Akkerman *et al*. IMFPs and our IMFPs for both compounds, as for Al_2O_3. Our IMFPs at 50 eV are smaller than the Akkerman *et al.* IMFPs by 43 % for KBr and 57 % for KCl. For SiO_2, the IMFPs of Akkerman *et al*. in Fig. 15(e) are in good agreement with our IMFPs for energies between 80 eV and 900 eV where the differences are less than 10 %. At lower energies, we also see increasing differences between the Akkerman IMFPs and our IMFPs that are similar to those found for the other compounds; at 50 eV, the Akkerman *et al.* IMFPs are larger than our IMFPs by 42 %. For the IMFP comparisons for MgO in Fig. 15(d), however, we find good agreement between our IMFPs and the Akkerman *et al*. IMFPs for energies between 50 eV and 10 keV with an RMS difference of 7.7 %. We have no explanation for the much better agreement between the IMFP results for MgO at energies between 50 eV and 100 eV than for the other four compounds.

Boutboul *et al.*[19] calculated IMFPs of LiF, NaCl, KCl, and CsI in 1996 for energies between 50 eV and 10 keV. They used a dielectric model with a quadratic dispersion equation and also took the bandgap energy into account. Their algorithm was the same as that used by Akkerman *et al.* [15]

Figure 15(c) shows comparisons of our IMFPs for NaCl with those of Boutboul *et al.* for electron energies between 40 eV and 10 keV. The IMFPs of Boutboul *et al.* are in excellent agreement with our IMFPs for energies between 500 eV and 6000 eV where the differences between them are less than 5 %. For energies less than 500 eV, we see slightly different energy dependences and the energy for the minimum IMFP is at a higher energy than for our IMFPs. At 40 eV, the Boutboul *et al.* IMFP is 14 % larger than our IMFP. Our smaller IMFP at 50 eV is similar to the results in the comparisons with the Akkerman IMFPs for Al_2O_3, MgO, and SiO_2 and must also be due to the contribution of single-electron excitations to the ELF that were neglected by Boutboul *et al*.

In 1997, Dapor and Miotello[22] used the Ashley algorithm[71, 74] (i.e., the SSPA) to calculate IMFPs for SiO_2 for energies between 20 eV and 4000 eV. Their ELF for SiO_2

Author Manuscript:
Published in final edited form as: *Surf. Interface Anal*. Volume 51, Issue 4, Pages 427-457, April 2019
https://doi.org/10.1002/sia.6598

was obtained from the data of Buechner ($\Delta E < 40$ eV) [72] and Henke ($\Delta E > 100$ eV) [60]. A linear interpolation was used for energies between 40 and 100 eV. Figure 15(f) shows good agreement between the IMFPs of Dapor and Miotello and our IMFPs for energies between 100 eV and 4000 eV where the RMS difference is 10.7 %. At lower energies, however, there are increasing differences between the their IMFPs and our IMFPs, with a difference of over 360 % at 20 eV due to the limitations of the SSPA.

In 1999, Dapor and Miotello[21] calculated IMFPs for Al_2O_3, MgO, and SiO_2 for energies from 50 eV to 10 keV using the SSPA algorithm of Ashley *et al.* [71, 74] and the non-relativistic Møller cross section [73] for the exchange correction proposed by Ashley [74]. They determined optical ELFs from optical constants (the refraction index n and the extinction coefficient k) that were derived from the atomic scattering factors published by Henke *et al*. in 1982 [75]. Since the lowest energy in the latter compilation was 30.5 eV, they performed a polynomial extrapolation of the Henke *et al*. data to lower energies.

Figures 15(a), (d) and (f) show comparisons of our IMFPs with those of Dapor and Miotello for Al_2O_3, MgO, and SiO_2, respectively. Their IMFPs for Al_2O_3 are smaller than our IMFPs by between 12 % and 23 % for energies between 100 eV and 10 keV. At 50 eV, however, their IMFP is 12 % larger than our IMFP. The MgO IMFPs of Dapor and Miotello are also smaller than our IMFPs by between 3 % and 21 % for energies between 50 eV and 10 keV. The Dapor and Miotello IMFPs for SiO_2 in Fig. 15(f) are smaller than our IMFPs by between 27 % and 34 %. A major reason for the differences between the Dapor-Miotello IMFPs and our results is the different optical ELFs for Al_2O_3, MgO, and SiO_2 in the IMFP calculations. Since Dapor and Miotello determined their ELFs for energies less than 30 eV by extrapolation of optical data from higher energies, their ELFs have large uncertainties in the low-energy region.

In 2004, Kwei and Li[17] calculated IMFPs and surface-excitation parameters for electrons crossing a GaAs surface using dielectric response theory. Figure 15(b) shows a comparison of their IMFPs for valence-band excitations with our results for energies between 200 eV and 2000 eV. Their IMFPs are clearly larger than our values, and the RMS difference is 25.4 %. We see increasing differences at higher energies with a difference of over 30 % at 2000 eV. This result must be must be due to the lack of inner-shell excitations in the dielectric function used by Kwei and Li.

In 2006, Dapor[23] reported new calculations of IMFPs for SiO_2 for energies between 50 eV and 10 keV using the Ashley algorithm[71, 74]. The ELF used in this calculation was slightly different from that of Dapor and Miotello in 1997[22].The ELF was constructed from the optical data of Buechner[72] for energies less than 33.6 eV, the data of Henke *et al*.[60] for energies above 42 eV, and a linear interpolation was made between 33.6 eV and 42 eV. Figure 15(f) show a comparison of our IMFPs for SiO_2 with those of Dapor for electron energies from 50 eV to 10 keV. The Dapor IMFPs are in good agreement with our IMFPs for energies between 100 eV and 10 keV where the RMS difference is 8.5 %. At lower energies, however, there are also increasing differences

Author Manuscript:
Published in final edited form as: *Surf. Interface Anal*. Volume 51, Issue 4, Pages 427-457, April 2019
https://doi.org/10.1002/sia.6598

between the Dapor IMFPs and our values, with a difference of over 220 % at 50 eV. This large difference must again be due to the neglect of single-electron excitations in the Ashley algorithm.

Pandya *et al.*[16] determined IMFPs for Si, SiO_2, SiO, and Al_2O_3 in 2012 using a semi-empirical quantum-mechanical method[76] to determine total inelastic-scattering cross sections for free atoms or molecules from complex optical potentials for energies between 20 eV and 2000 eV. Their complex potentials included the effect of the bulk medium through the atomic charge density for solids as given by Salvat *et al.*[77].

Figures 15(a) and (f) show comparisons of our IMFPs with those of Pandya *et al.* for Al_2O_3 and SiO_2, respectively. The IMFPs of Pandya *et al.* for Al_2O_3 in Fig. 15(a) are clearly smaller than our IMFPs for energies between 100 eV and 2000 eV, where the RMS difference is 20 %. At lower energies, however, their IMFPs become much larger than our IMFPs. The IMFPs of Pandya *et al.* for SiO_2 in Fig. 15(f) are in good agreement with our IMFPs for energies between 100 eV and 1800 eV, where the RMS difference is 8.1 %. At lower energies, however, their IMFPs also become larger than our IMFPs, where a difference of 28 % is found at 50 eV.

Finally, we mention that Bourke and Chantler[78] reported IMFP calculations for ZnSe in 2014. They performed DFT calculations of the ELF for excitation energies between 20 eV and 120 eV using the WIEN2k code, as in our work. Their IMFPs agree closely with our values for energies between 50 eV and 120 eV.

5.2 Comparison of inelastic mean free paths with measured inelastic mean free paths

Many IMFP measurements have been made by transmission EELS at electron energies of 100 keV or 200 keV [24,26]. Most of these measurements were made on metal oxide specimens by analyses of the electron energy-loss spectra, typically over an energy-loss range of about 150 eV, as described by Egerton [26]. The uncertainties of IMFPs from the EELS experiments have been estimated to be about 10 % but intercomparisons of IMFPs from different laboratories suggest that the uncertainties could be up to about 25 %[26]. One group determined IMFPs for MgO by off-axis electron holography[33] and another group used a combination of this technique and convergent-beam electron diffraction for AlAs and GaAs.[31] The reported uncertainties of these IMFP measurements were between 5 % and 8 %. Another group derived an IMFP for MgO from a comparison of energy-filtered and unfiltered images in high-resolution TEM.[32]

IMFP measurements have also been made by EPES on a limited number of inorganic compounds (Al_2O_3, GaAs, InP, MgO, and SiO_2). These IMFPs were obtained from measurements of ratios of intensities of elastically backscattered electrons from the specimen of interest and a reference material for which the IMFP is known [1,79]. The intensity ratios, determined for a range of incident electron energies (typically between 100 eV and 5000 eV), are then compared with corresponding ratios from Monte Carlo simulations in which the sample IMFP is a parameter. Ni, Cu, Ag, or Au are often chosen as reference materials since these materials showed good consistencies in comparisons of

Author Manuscript:
Published in final edited form as: *Surf. Interface Anal*. Volume 51, Issue 4, Pages 427-457, April 2019
https://doi.org/10.1002/sia.6598

IMFPs calculated from optical data and IMFPs determined from EPES experiments[79]. Finally, a correction needs to be made for surface excitations[80]. An important requirement in EPES experiments is that specimen surfaces generally need to be cleaned of impurities that have arisen from sample handling and exposure to the ambient vacuum environment. Surface cleaning can be readily accomplished by ion sputtering but ion bombardment of compounds also generally causes changes in the surface composition as well as surface roughening.

Iakoubovskii *et al*.[24] determined IMFPs for 42 oxides from EELS experiments at 200 keV. Unfortunately, we calculated IMFPs for only three of these oxides (MgO, Al_2O_3, and SiO_2). We make comparisons below of the measured IMFPs for these oxides with our calculated IMFPs. The other IMFPs measured by Iakoubovskii *et al*. will be compared with IMFPs from the relativistic TPP-2M predictive formula [Eqns (12), (13), and (15)] in Section 5.3.

Figure 16 shows comparisons of our calculated IMFPs with measured IMFPs for Al_2O_3, AlAs, *h*-BN, GaAs, InP, MgO, and SiO_2 for electron energies between 10 eV and 500 keV. As for the comparisons in Fig. 15, our IMFPs are shown as a function of energy above the bottom of the conduction band and the measured IMFPs from the literature are shown as they were reported. We thus assumed that these IMFPs were also determined as a function of energy above the bottom of the conduction band even if this was not stated in the original papers.

Figure 16(a) shows the comparisons for Al_2O_3 with the IMFPs measured by Egerton[26], Iakoubovskii *et al*.[24] and Meltzman *et al.*[27] from EELS experiments at energies of 100, 200, and 300 keV, respectively. We see that our IMFPs are in good agreement with the measured IMFPs of Iakoubovskii *et al*. and Meltzman *et al*. (the differences between them are -12 % and 5 %, respectively). However, our calculated IMFP at 100 keV is smaller than Egerton's measured IMFP by 24 %.

Gurban *et al*. [28] used EPES to determine IMFPs of a 30 nm Al_2O_3 film on Al at electron energies of 200 eV, 500 eV, 1000 eV, 1500 eV, and 2000 eV and applied a correction for surface excitations. A Cu specimen cleaned by Ar^+ sputtering was used as the reference material. We see good agreement in Fig.16(a) between our IMFPs and the IMFPs of Gurban *et al*. for energies between 200 and 2000 eV. The differences between the calculated and measured IMFPs are less than 10 % except at 500 eV where the measured IMFP is smaller than our IMFP by about 18 %. Overall, our IMFPs for Al_2O_3 are generally in good agreement with the measured IMFPs for energies between 200 eV and 300 keV, with a RMS difference of 13.3 %.

Figure 16(b) shows the comparison of our IMFPs with measured IMFPs for AlAs [31] and *h*-BN [26]. The IMFP for *h*-BN was measured by EELS at 100 keV and is larger than our calculated IMFP by 18 %. Chung *et al.*[31] determined IMFPs for AlAs and GaAs at 200 keV based on a comparison of film thicknesses measured by electron holography and convergent-beam electron diffraction. Their IMFP for AlAs is smaller than our IMFP by 46 %.

Author Manuscript:
Published in final edited form as: *Surf. Interface Anal*. Volume 51, Issue 4, Pages 427-457, April 2019
https://doi.org/10.1002/sia.6598

Figure 16(c) shows comparisons of our IMFPs for GaAs with IMFPs measured by photoelectron spectroscopy (PES), EPES, and EELS for energies between 24 eV and 200 keV. Pi *et al*. [29] used PES and a method developed by Wertheim *et al*.[81] to determine IMFPs of Ga 3d and As 3d photoelectrons from a reconstructed GaAs(111) surface for electron energies between 24 eV and 140 eV. Their analysis of the measured spectra for a range of photon energies and photoelectron emission angles showed separate Ga 3d and As 3d peaks due to photoemission from the surface layer of atoms as well as corresponding peaks arising from the bulk of the solid. With the use of model descriptions of surface and bulk lineshapes, they determined the fractional intensity of bulk emission, f_B, for each spectrum and equated this fraction to $\exp(-d/\lambda)$ where d is the layer spacing. Pi *et al*. could thus determine IMFPs as a function of photoelectron energy. While there is some scatter in the IMFPs from the PES experiments, we see generally good agreement between the calculated and measured IMFPs. We note, however, that no account was taken of elastic-scattering effects in the Wertheim *et al*. model.

Krawczyk *et al.*[30] determined IMFPs of GaAs with EPES using a Ni reference for energies between 1 keV and 5 keV. Their GaAs sample was bombarded by Ar^+ ions both to clean the surface and to amorphize the surface region. As a result, the surface region was Ga-enriched due to preferential sputtering of As. Although the enrichment was estimated to be up to 80 %, this had little effect on the derived IMFPs since Ga and As have very similar atomic numbers (31 and 33, respectively) and thus similar elastic-scattering properties. The IMFPs of Krawczyk *et al*. are larger than our IMFPs by between 7 % and 16 %.

Egerton[26] determined IMFPs for GaAs from EELS measurements with two collection angles (10 mrad and 100 mrad) at 100 keV. Our IMFP is 12 % smaller than Egerton's value for the 10 mrad acceptance angle and 13 % larger than Egerton's result for the 100 mrad angle.

Chung *et al*. [31] also reported an IMFP for GaAs at 200 keV that, as for AlAs, was determined using a combination of off-axis electron holography and convergent-beam electron diffraction. This IMFP is smaller than our IMFP by 48 %. Their IMFP at 200 keV is also smaller than the IMFP measured by Egerton at 100 keV (100 mrad) by 10 %. Since the energy-dependence of IMFPs is well-described by the modified Bethe equation [Eqn (12)] and the GaAs IMFPs measured by Krawczyk *et al*., Pi *et al*., and Egerton agree satisfactorily with our calculated IMFPs over a wide energy range, as seen in Fig.16(c), it is clear that the IMFP determined by Chung *et al*. is significantly underestimated. Their IMFP for AlAs in Fig.16(b) was also 45 % lower than our calculated IMFP, and we conclude that their measurement method had an unsuspected systematic error. With exclusion of the Chung *et al*. result, the RMS difference between the calculated and measured IMFPs for GaAs and energies between 24 eV and 100 keV was 19.3 %.

Figure 16(d) shows comparisons of our IMFPs for InP with IMFPs measured by Bideux *et al*.[35] and Zommer *et al*.[36] with EPES. Bideux *et al.* bombarded their

Author Manuscript:
Published in final edited form as: *Surf. Interface Anal*. Volume 51, Issue 4, Pages 427-457, April 2019
https://doi.org/10.1002/sia.6598

sample with 300 eV Ar^+ ions to clean the surface and to amorphize the surface region, made direct measurements of their primary and elastically backscattered currents, and determined IMFPs for energies between 100 eV and 1 keV. Zommer *et al*. reported IMFPs for energies between 100 eV and 3 keV. Zommer *et al*. employed Ar^+ beams of much higher energies (100 keV to 400 keV) to amorphize their sample and then cleaned their sample with 400 eV or 500 eV Ar^+ beams. They used a Ni reference sample and reported IMFPs for energies between 100 eV and 3 keV. After ion bombardment, Zommer *et al*. used XPS to find that the average composition of their sample was $In_{68}P_{32}$.

There is excellent agreement in Fig.16(d) between our IMFPs and the IMFPs of Bideux *et al*. for energies between 600 eV and 1000 eV where the differences are less than 15 %. However, our IMFPs are larger than those of Bideux *et al*. by between 30 % and 60 % for energies between 100 eV and 400 eV. Since their InP specimen was cleaned by ion sputtering, its surface composition is expected to be In rich. Although we cannot estimate the extent and depth of In enrichment on the IMFP measurements of Bideux *et al*., it is reasonable to believe that the enrichment effects would be smaller for the more bulk-sensitive measurements at higher energies.

While there is good agreement in Fig.16(d) between the IMFPs of Zommer *et al*. and our IMFPs for energies between 200 eV and 1000 eV (with differences of less than 10 %), there are larger differences at 100 eV (39 %) and for energies between 1500 eV and 3000 eV (where the differences are up to 37 %). It is difficult to assess these differences since the average sample composition after high-energy ion bombardment was found to be $In_{68}P_{32}$. Nevertheless, the average RMS difference between the calculated and measured IMFPs for InP (or $In_{68}P_{32}$) was 26 %.

Figure 16(e) shows comparisons of our IMFPs for MgO with IMFPs measured by EPES, [28] EELS, [24, 33] and TEM[32]. Gurban *et al*.[28] used a Cu reference and determined IMFPs of a 30 nm MgO thin film at 200 eV, 500 eV, 1000 eV, 1500 eV, and 2000 eV after applying a correction for surface excitations. Their IMFPs are in excellent agreement with our IMFPs with differences of less than 10 % except at 500 eV where the difference was 19 %. McCartney *et al*.[33], Iakoubovskii *et al*.[24], and Wang and Shapiro[32] reported IMFPs at energies of 100 keV, 200 keV, and 300 keV, respectively. We see satisfactory agreement between our IMFPs and their IMFPs with differences of 20 %, -2 %, and -13 %, respectively. The RMS difference between our IMFPs for MgO and the measured IMFPs was 11.5 % for energies between 200 eV and 300 keV.

Figure 16(f) shows comparisons of our calculated IMFPs for SiO_2 with IMFPs measured by EPES and EELS. Jung *et al*.[37] determined IMFPs of SiO_2 by EPES for energies between 300 eV and 2000 eV using a Si reference and applied corrections for surface excitations. Their sample films were bombarded by Ar^+ ions with energies between 300 eV and 1 keV. They reported two series of IMFP results, one from measurements at a primary-electron incidence angle of 0° and the other with an incidence angle of 55° (both with respect to the surface normal). Both sets of IMFPs agreed well

Author Manuscript:
Published in final edited form as: *Surf. Interface Anal*. Volume 51, Issue 4, Pages 427-457, April 2019
https://doi.org/10.1002/sia.6598

with each other. Our calculated IMFPs are in excellent agreement with the measured IMFPs (with differences of less than 3 % except at 300 eV where the difference was 19 %).

Egerton[26], Iakoubovskii *et al*.[24], Lee *et al*.[34], and Meltzman *et al*.[27] measured IMFPs of SiO_2 from EELS experiments in the TEM at incident energies of 100 keV, 200 keV, or 300 keV. We see good agreement in Fig.16(f) between our calculated IMFPs and their measured IMFPs with differences between -12 % and 18 %. The RMS difference between our calculated IMFPs and the measured IMFPs for SiO_2 was 9.1 % for energies between 300 eV and 300 keV.

We would like to comment here that the comparisons in Fig.16 were made for IMFP measurements made over a very large energy range, 24 eV to 300 keV. While the magnitudes of our calculated IMFPs have various sources of uncertainty[7], the energy dependences of these IMFPs is expected to be well-described by the modified Bethe equation [Eqn (12)].[82] It is thus possible to make useful comparisons of IMFP measurements over a wide energy range. This approach has also been found useful in evaluations of calculated and measured cross sections for inner-shell ionization, again over wide energy ranges.[83,84] Figure 17 shows a summary plot of the comparisons of our calculated IMFPs for the seven inorganic compounds in Fig.16 with measured IMFPs for energies between 24 eV and 300 keV. We see an excellent correlation between the calculated and measured IMFPs except for the IMFPs measured for AlAs and GaAs at 200 keV by Chung *et al*.[31] As discussed earlier, we believe that there was an unrecognized systematic error in the these IMFPs.

The average RMS difference between the calculated and 71 measured IMFPs in Figs. 16 and 17 is 23.5 %. If the AlAs and GaAs IMFPs measured by Chung *et al*. are excluded from this comparison, the average RMS difference is reduced to 18.7 %. This average RMS difference is comparable to the average RMS difference between calculated and measured IMFPs of 13.6 % for 11 elemental solids at 100 keV and for 32 elemental solids at 200 keV.[8] The average RMS difference between calculated and measured IMFPs in Fig.17 (again with the exclusion of the Chung *et al*. IMFPs) is also similar to those found in comparisons of calculated IMFPs for elemental solids[7] with IMFPs from EPES experiments. These comparisons showed RMS differences of 12 % for a group of 11 elemental solids and energies between 100 eV and 5 keV from one set of EPES experiments and of 15 % for a group of 17 elemental solids and energies between 300 eV and 3.4 keV in another set of EPES experiments.[7]

5.3 Comparison of IMFPs from the TPP-2M formula with measured IMFPs

Figure 18 shows a comparison of IMFPs calculated from the relativistic TPP-2M equation [Eqns (12), (13), and (15)]] with IMFPs measured for energies between 50 eV and 300 keV. We have included the measured IMFPs (solid squares) shown in Fig.16 as well as the additional IMFP measurements of Iakoubovskii *et al*.[24] (solid circles) for 37 oxides (B_2O_3, CaO, Sc_2O_3, TiO, V_2O_5, CrO_3, Fe_2O_3, CoO, NiO, ZnO, GeO_2, SeO_2, SrO, Y_2O_3, ZrO_2, MoO_3, PdO, Ag_2O, SnO_2, TeO_2, BaO, La_2O_3, Ce_2O_3, Pr_2O_3, Nd_2O_3,

Author Manuscript:
Published in final edited form as: *Surf. Interface Anal*. Volume 51, Issue 4, Pages 427-457, April 2019
https://doi.org/10.1002/sia.6598

Sm_2O_3, Eu_2O_3, Gd_2O_3, Tb_2O_3, Dy_2O_3, Ho_2O_3, Er_2O_3, Yb_2O_3, WO_3, HgO, PbO, Bi_2O_3) from EELs experiments at 200 keV. There is a total of 103 IMFP measurements on 44 inorganic compounds shown in Fig.18. In general, we see a satisfactory correlation between IMFPs from the TPP-2M equation and the measured IMFPs. However, we see relatively large positive deviations for IMFPs less than 1 nm that correspond to electron energies under 200 eV. The TPP-2M equation is less reliable for energies less than 200 eV compared to higher energies[7], as indicated in Fig. 14. The average RMS difference between IMFPs from the TPP-2M equation and the 103 measured IMFPs for 44 inorganic compounds in Fig.18 was 24.8 % for energies between 50 eV and 300 keV. If the AlAs and GaAs IMFPs measured by Chung *et al*.[31] are again excluded from this comparison, the average RMS difference becomes 21.7 %. This average RMS difference is slightly larger than the average RMS difference of 17.4 % found in a similar comparisons of IMFPs from the TPP-2M equation and IMFPs measured by EELs at energies of 100 keV and 200 keV for our group of 41 elemental solids.[8] The average RMS difference of 21.7 % found here is larger than found in a similar comparison with one set of IMFPs from EPES experiments (11 % for a group of 11 elemental solids for energies between 100 eV and 5 keV[7]) but is almost the same as in a comparison for another set of IMFPs from EPES experiments (19 % for a group of 17 elemental solids for energies between 300 eV and 3.4 keV[7]).

5.4 Reliability of the TPP-2M equation

We now comment on the reliability of the relativistic TPP-2M equation [Eqns (12), (13) and (15)] for estimating IMFPs in solids. While Fig.18 shows that there is generally good correlation between IMFPs from the TPP-2M equation and measured IMFPs for IMFPs over 1 nm (i.e., for energies greater than about 200 eV), we found disturbingly large RMS deviations of 65.6 % and 34.3 % between IMFPs from the TPP-2M equation and our calculated IMFPs for *c*-BN and *h*-BN, respectively. There were also smaller but still significant RMS deviations of 17.1 % and 19.3 % for Al_2O_3 and MgF_2, respectively. We have previously found similar large RMS deviations of 46.6 %, 70.7 %, and 34.7 % between IMFPs from the relativistic TPP-2M equation and our calculated IMFPs for graphite, diamond, and Cs, respectively.[8] Possible reasons for the latter RMS deviations have been discussed in previous papers.[7,67]

In principle, the large RMS deviations between IMFPs from the TPP-2M equation and our calculated IMFPs for *c*-BN and *h*-BN and, to a lesser extent, for Al_2O_3 and MgF_2 could be due to limitations of the TPP-2M equation, errors in the calculations of the optical data and ELFs for *c*-BN and *h*-BN, uncertainties in the optical data and ELFs for Al_2O_3 and MgF_2, and/or a deficiency in the algorithm used for the IMFP calculations. However, the optical data and ELFs for these four compounds appear to be generally satisfactory as indicated by the sum-rule errors listed in Table 4. While there was a 9.2 % error in the f-sum rule for MgF_2 and a -7.8 % error in the KK-sum rule for Al_2O_3, there were comparable or larger sum-rule errors for other compounds that did not

Author Manuscript:
Published in final edited form as: *Surf. Interface Anal*. Volume 51, Issue 4, Pages 427-457, April 2019
https://doi.org/10.1002/sia.6598

lead to relatively large RMS deviations between IMFPs from the TPP-2M equation and our calculated IMFPs. We also point out that our calculated IMFPs from the Penn algorithm generally agree well with measured IMFPs, as shown in Figs. 16 and 17 for many inorganic compounds and for many elemental solids.[7, 8]

The large RMS deviations between IMFPs from the TPP-2M equation and our calculated IMFPs for *c*-BN and *h*-BN and the smaller RMS deviations for Al_2O_3 and MgF_2 occur for relatively small values of the TPP-2M parameter β from Eqn (15a). Figure 19 shows a plot of β values from Eqn (15a), $\beta_{TPP\text{-}2M}$, versus β values obtained from fits of Eqn (12) to our calculated IMFPs for each compound, β_{fit}, as shown in Table 6. We see that there is generally a linear correlation between $\beta_{TPP\text{-}2M}$ and β_{fit} although the $\beta_{TPP\text{-}2M}$ values for *c*-BN, *h*-BN, Al_2O_3 and MgF_2 are smaller than the corresponding β_{fit} values. Figure 19 also includes plots of $\beta_{TPP\text{-}2M}$ versus β_{fit} for our group of 41 elemental solids[8] from which we can see that $\beta_{TPP\text{-}2M}$ is systematically smaller than β_{fit} for diamond and graphite. Although the deviations of $\beta_{TPP\text{-}2M}$ from β_{fit} for *c*-BN(BN), *h*-BN, Al_2O_3, MgF_2, diamond and graphite are roughly similar to those for the other elements and compounds in Fig.19, the deviations relative to the corresponding β_{fit} values are larger. These large relative deviations lead to the substantial RMS deviations between IMFPs from the TPP-2M formula and the calculated IMFPs. This shortcoming of the TPP-2M formula can occur for β_{fit} values less than about 0.18 or, equivalently, $\beta_{TPP\text{-}2M}$ values less than about 0.13. It is apparent from Fig.19 that this overestimation of IMFPs from the TPP-2M formula does not always occur for $\beta_{fit} < 0.18$ (e.g., for glassy C, Fe, Co, Ni, and Cu), and we are unable to suggest a further improvement to Eqn (12) or Eqn (15).

6. Summary

We report new calculations of IMFPs with the relativistic full Penn algorithm for 42 inorganic compounds (AgBr, AgCl, AgI, Al_2O_3, AlAs, AlN, AlSb, *c*-BN, *h*-BN, CdS, CdSe, CdTe, GaAs, GaN, GaP, GaSb, GaSe, InAs, InP, InSb, KBr, KCl, MgF_2, MgO, NaCl, $NbC_{0.712}$, $NbC_{0.844}$, $NbC_{0.93}$, PbS, PbSe, PbTe, SiC, SiO_2, SnTe, $TiC_{0.7}$, $TiC_{0.95}$, $VC_{0.76}$, $VC_{0.86}$, $Y_3Al_5O_{12}$, ZnS, ZnSe, and ZnTe) for energies between 50 eV and 200 keV. For 15 of these compounds, the IMFPs were calculated from ELFs obtained from experimental measurements of optical constants, the procedure we used in our previous IMFP calculations.[3-8] Sufficient experimental data of this type were not available for the other 27 compounds (all compound semiconductors) for photon energies above about 10 eV, and we computed the imaginary part of the complex dielectric constant, ε_2, from the WIEN2k and FEFF codes after which we calculated ε_1 and then the ELF.

We compared the ELFs calculated from the WIEN2k code for GaAs and InSb with corresponding ELFs derived from EELS experiments[61-63] and found satisfactory agreement. However, there was significant disagreement with ELFs obtained from optical data[45] that we had utilized in our previous IMFP calculations for these two compounds.[5] The optical data had been obtained from samples exposed to air before reflectance

Author Manuscript:
Published in final edited form as: *Surf. Interface Anal*. Volume 51, Issue 4, Pages 427-457, April 2019
https://doi.org/10.1002/sia.6598

measurements, and it is likely that they had surface contamination. We therefore concluded that the calculated ELFs for GaAs and InSb were superior to those obtained from optical experiments.

We evaluated the ELFs for each compound with the f-sum and KK-sum rules.[5,65] The average RMS errors in these sum rules were found to be 4.1 % and 3.5 % for the f-sum and KK-sum rules, respectively. These average RMS errors were comparable to those found in the ELF data sets for our group of 41 elemental solids (4.2 % for the f-sum error and 7.7 % for the KK-sum error). The average RMS sum-rule errors for our 42 inorganic compounds are also appreciably less than those found in our previous use of ELFs from experimental optical data for 15 inorganic compounds (8 % for the f-sum error and 24 % for the KK-sum error).[5] The present ELF data sets are clearly superior to our previous data sets.

The calculated IMFPs for the 42 inorganic compounds could be fitted with a modification of the relativistic Bethe equation for inelastic scattering of electrons in matter. The average RMS deviation in these fits was 0.60 %, a value similar to that found in similar fits for our group of 41 elemental solids (0.68 %).[8]

We compared our calculated IMFPs for the 42 compounds with values obtained from the relativistic TPP-2M predictive formula [Eqns. (12), (13), and (15)] that can be used to estimate IMFPs for electron energies between 50 eV and 200 keV.[8] These comparisons showed an average RMS deviation of 10.7 %. This average deviation is almost the same as that found in a similar comparison for our group of 41 elemental solids (11.9 %).[8] However, relatively large RMS deviations were found for *c*-BN (65.6 %) and *h*-BN (34.3 %). If the RMS deviations for these two compounds are ignored, the average RMS deviation for the remaining 40 compounds becomes 8.7 %. We found that the large RMS deviations between the calculated IMFPs and values from the TPP-2M formula for BN as well as for graphite and diamond occurred for relatively small values of the TPP-2M parameter β from Eqn (15a), i.e., for $\beta_{\text{TPP-2M}}$ values less than about 0.13. While the TPP-2M formula is useful for estimating IMFPs in a variety of solids (and also liquid water[69]) for energies between 50 eV and 200 keV, the accuracy of these estimates is likely to be poorer for energies less than about 200 eV.

We compared our calculated IMFPs for Al_2O_3, GaAs, KBr, KCl, MgO, NaCl, and SiO_2 with results from other calculations for energies typically between 50 eV and 10 keV. There was generally satisfactory agreement except for differences at energies between 50 eV and 100 eV that could be attributed to the neglect of single-electron excitations in most previous calculations. Other differences could be attributed to the use of different ELFs or to other features of the chosen algorithms.

We also compared our calculated IMFPs for Al_2O_3, AlAs, *h*-BN, GaAs, InP, MgO, and SiO_2 with 71 measured IMFPs for these compounds. These IMFP measurements had most often been made by EPES for energies between 100 eV and 5 keV and by TEM at energies of 100 keV, 200 keV or 300 keV, while some PES measurements were made for GaAs at energies between 24 eV and 140 eV. We found

Author Manuscript:
Published in final edited form as: *Surf. Interface Anal*. Volume 51, Issue 4, Pages 427-457, April 2019
https://doi.org/10.1002/sia.6598

generally satisfactory agreement between the calculated and measured IMFPs with an average RMS deviation of 23.5 % although the IMFPs of Chung *et al*.[31] for AlAs and GaAs were smaller than our values by 48 % and 45 %, respectively. If these two measurements are disregarded, the average RMS difference between our calculated IMFPs and the 69 other measured IMFPs was 18.7 %. This average RMS difference is comparable to the average RMS difference between calculated and measured IMFPs of 13.6 % for 11 elemental solids at 100 keV and for 32 elemental solids at 200 keV.[8] The average RMS difference is also similar to those found in comparisons of calculated IMFPs for elemental solids[7] with IMFPs from EPES experiments. These comparisons showed RMS differences of 12 % for a group of 11 elemental solids and energies between 100 eV and 5 keV from one set of EPES experiments and of 15 % for a group of 17 elemental solids and energies between 300 eV and 3.4 keV in another set of EPES experiments.[7]

Finally, we compared IMFPs calculated from the predictive TPP-2M formula with the measured IMFPs for Al_2O_3, AlAs, *h*-BN, GaAs, InP, MgO, and SiO_2 and with the additional IMFP measurements of Iakoubovskii *et al*.[24] for 37 oxides (B_2O_3, CaO, Sc_2O_3, TiO, V_2O_5, CrO_3, Fe_2O_3, CoO, NiO, ZnO, GeO_2, SeO_2, SrO, Y_2O_3, ZrO_2, MoO_3, PdO, Ag_2O, SnO_2, TeO_2, BaO, La_2O_3, Ce_2O_3, Pr_2O_3, Nd_2O_3, Sm_2O_3, Eu_2O_3, Gd_2O_3, Tb_2O_3, Dy_2O_3, Ho_2O_3, Er_2O_3, Yb_2O_3, WO_3, HgO, PbO, Bi_2O_3) at 200 keV. If the Chung *et al.*[31] results for AlAs and GaAs are again excluded, the average RMS deviation between the 101 measured IMFPs and the corresponding predicted IMFPs was 21.7 %. While this average RMS deviation is similar to that found in a similar comparison at 100 keV and 200 keV for our group of 41 elemental solids (17.4 %),[8] the predicted IMFPs were systematically larger than the measured IMFPs for energies less than about 200 eV. The TPP-2M equation is thus less reliable at energies less than 200 eV compared to higher energies.

Acknowledgments
We thank Professor T. Koide for supplying optical constants for niobium carbides, titanium carbides and vanadium carbides. We also thank Dr. John Villarrubia for useful comments on IMFP calculations for nonconductors at low electron energies.

Author Manuscript:
Published in final edited form as: *Surf. Interface Anal.* Volume 51, Issue 4, Pages 427-457, April 2019
https://doi.org/10.1002/sia.6598

Table 1. Values of material parameters used in the IMFP calculations and in the analysis of IMFP results for our 42 inorganic compounds.

Compound	M	ρ (g cm^{-3})	N_v	E_p (eV)	E_g(eV)	E_v (eV)
AgBr	187.772	6.48	18	22.71	2.68	4.27
AgCl	143.321	5.59	18	24.14	3.25	4.26
h-AgI	234.773	5.72	18	19.08	2.92	3.23
Al_2O_3	101.961	3.97	24	27.86	8.63	8.0
AlAs	101.903	3.73	8	15.59	2.16	5.27
h-AlN	40.988	3.26	8	22.99	6	6.03
AlSb	148.742	4.28	8	13.83	1.62	5.32
c-BN	24.818	3.49	8	30.56	7.2	8.51
h-BN	24.818	2.3	8	24.81	5	8.77
h-CdS	144.476	4.8	18	22.28	2.46	4.42
h-CdSe	191.371	5.66	18	21.03	1.7	4.53
CdTe	240.011	5.85	18	19.09	1.51	4.62
GaAs	144.645	5.32	8	15.63	1.47	7.07
h-GaN	83.7297	6.09	8	21.98	3.4	7.09
GaP	100.697	4.13	8	16.51	2.26	6.67
GaSb	191.483	5.61	8	13.95	0.73	7.02
h-GaSe	148.683	5.07	9	15.96	1.98	7.73
InAs	189.74	5.67	8	14.09	0.36	6.12
InP	145.792	4.79	8	14.77	1.38	5.98
InSb	236.578	5.78	8	12.74	0.18	6.18
KBr	119.002	2.75	8	12.39	7.26	2.6
KCl	74.548	1.98	8	13.28	7.4	2.7
MgF_2	62.302	3.177	16	26.03	10.95	5.5
MgO	40.304	3.576	8	24.28	7.69	6.3
NaCl	58.443	2.165	8	15.69	9	4.1
$NbC_{0.712}$	101.458	7.746	7.848	22.31	0	7.4*
$NbC_{0.844}$	103.044	7.769	8.376	22.90	0	7.4*
$NbC_{0.93}$	104.077	7.781	8.72	23.27	0	7.4*
PbS	239.265	7.62	10	16.26	0.42	5.21
PbSe	286.16	8.29	10	15.51	0.29	5.00
PbTe	334.8	8.27	10	14.32	0.32	4.54
SiC	40.096	3.22	8	23.10	2.31	6.95
SiO_2	60.008	2.19	16	22.02	9.1	10.0

Author Manuscript:
Published in final edited form as: *Surf. Interface Anal*. Volume 51, Issue 4, Pages 427-457, April 2019
https://doi.org/10.1002/sia.6598

SnTe	246.31	6.47	10	14.77	0.19	8.25
$TiC_{0.7}$	56.288	4.627	6.8	21.54	0	5.7*
$TiC_{0.95}$	59.290	4.843	7.8	23.00	0	5.7*
$VC_{0.76}$	60.070	5.582	8.04	24.91	0	7.5*
$VC_{0.86}$	61.271	5.605	8.44	25.32	0	7.5*
$Y_3Al_5O_{12}$	593.618	4.554	96	24.73	6.5	6.5
ZnS	97.445	4.09	18	25.05	3.81	5.37
ZnSe	144.34	5.26	18	23.34	2.68	5.42
ZnTe	192.98	5.64	18	20.9	2.25	5.42

* Fermi energy (eV).

Author Manuscript:
Published in final edited form as: *Surf. Interface Anal*. Volume 51, Issue 4, Pages 427-457, April 2019
https://doi.org/10.1002/sia.6598

Table 2. Sources of optical data used in the IMFP calculations for the 42 inorganic compounds.

Compound	Photon energy range (eV)	Source of data
AgBr	0.005283 to 0.02254	Ref.[47]
	2.6 to 30	Calculation with WIEN2k
	30.40 to 1000000	Calculation with FEFF
AgCl	0.01 to 0.023	Ref.[47]
	3.0 to 30	Calculation with WIEN2k
	30.40 to 1000000	Calculation with FEFF
AgI	0.004138 to 0.02857	Ref.[47]
	1.4 to 30	Calculation with WIEN2k
	30.40 to 1000000	Calculation with FEFF
Al_2O_3	0.0496 to 100.0	Ref. [46]
	101.94 to 30000	Ref. [60]
	30156.09 to 988553.1	Ref. [85]
AlAs	0.01 to 0.1	Ref. [44]
	2.1 to 50	Calculation with WIEN2k
	50.5 to 1000000	Calculation with FEFF
AlN	0.01 to 1.0	Ref. [44]
	4.3 to 70	Calculation with WIEN2k
	70.5 to 10413.56	Calculation with FEFF
	10570.17 to 1000000	Ref. [85]
AlSb	0.01 to 0.3	Ref. [44]
	1.70 to 50	Calculation with WIEN2k
	50.5 to 1000000	Calculation with FEFF
c-BN	0.01 to 0.14	Ref. [44]
	8.90 to 80.0	Calculation with WIEN2k
	80.5 to 9821.20	Calculation with FEFF
	10413.56 to 1000000	Ref. [85]
h-BN	0.01 to 1	Ref. [44]
	4.7 to 80.0	Calculation with WIEN2k
	80.5 to 9821.20	Calculation with FEFF
	10413.56 to 1000000	Ref. [85]
CdS	0.01 to 0.06	Ref. [44]
	1.2 to 30	Calculation with WIEN2k
	30.4 to 1000000	Calculation with FEFF
CdSe	0.01 to 0.1	Ref. [44]
	0.7 to 30	Calculation with WIEN2k
	30.4 to 1000000	Calculation with FEFF
CdTe	0.004 to 0.1	Ref. [44]
	0.8 to 30	Calculation with WIEN2k
	30.4 to 1000000	Calculation with FEFF
GaAs	0.01 to 0.4	Ref. [44]
	0.6 to 50	Calculation with WIEN2k

Author Manuscript:
Published in final edited form as: *Surf. Interface Anal*. Volume 51, Issue 4, Pages 427-457, April 2019
https://doi.org/10.1002/sia.6598

	50.5 to 1000000	Calculation with FEFF
GaN	0.01 to 0.5	Ref. [44]
	1.9 to 50	Calculation with WIEN2k
	50.5 to 1000000	Calculation with FEFF
GaP	0.01 to 0.1	Ref. [44]
	1.8 to 50	Calculation with WIEN2k
	50.5 to 1000000	Calculation with FEFF
GaSb	0.01 to 0.3	Ref. [44]
	0.4 to 50	Calculation with WIEN2k
	50.5 to 1000000	Calculation with FEFF
GaSe	0.0031 to 0.3105	Ref. [46]
	0.9 to 46	Calculation with WIEN2k
	46.4 to 1000000	Calculation with FEFF
InAs	0.01 to 0.1	Ref. [44]
	0.2 to 30	Calculation with WIEN2k
	30.40 to 1000000	Calculation with FEFF
InP	0.01 to 0.3	Ref. [44]
	0.7 to 30	Calculation with WIEN2k
	30.40 to 1000000	Calculation with FEFF
InSb	0.001 to 0.04	Ref. [44]
	0.1 to 30	Calculation with WIEN2k
	30.40 to 1000000	Calculation with FEFF
KBr	0.00003682 to 40.0	Ref. [46]
	41.85834 to 1070165	Ref. [85]
KCl	0.007439 to 43	Ref. [45]
	44.4673 to 30000.0	Ref. [60]
	30309.08 to 944060.9	Ref. [85]
MgF_2	0.0006 to 83	Ref. [46]
	84.164 to 977240	Ref. [85]
MgO	0.002 to 75.0	Ref. [46]
	76.01 to 30000.0	Ref. [60]
	30156.09 to 988553.13	Ref. [85]
NaCl	0.00004053 to 26	Ref. [45]
	27.032 to 1011600	Ref. [85]
$NbC_{0.712}$	0.02 to 79	Ref. [86]
	80.177 to 30000	Ref. [60]
	30070.87 to 1120601	Ref. [85]
$NbC_{0.844}$	0.02 to 79	Ref. [86]
	80.177 to 30000	Ref. [60]
	30070.87 to 1120601	Ref. [85]
$NbC_{0.93}$	0.02 to 79	Ref. [87]
	80.177 to 30000	Ref. [60]
	30070.87 to 1120601	Ref. [85]
PbS	0.001 to 0.035	Ref. [44]
	0.4 to 50	Calculation with WIEN2k

Author Manuscript:
Published in final edited form as: *Surf. Interface Anal*. Volume 51, Issue 4, Pages 427-457, April 2019
https://doi.org/10.1002/sia.6598

	50.5 to 1000000	Calculation with FEFF
PbSe	0.001 to 0.007	Ref. [44]
	0.3 to 50	Calculation with WIEN2k
	50.5 to 1000000	Calculation with FEFF
PbTe	0.001 to 5.4	Ref. [44]
	5.5 to 50	Calculation with WIEN2k
	50.5 to 1000000	Calculation with FEFF
SiC	0.01 to 0.4	Ref. [44]
	4.6 to 50	Calculation with WIEN2k
	80.5 to 9821.20	Calculation with FEFF
	10143.01 to 1000000	Ref. [85]
SiO_2	0.002 to 2000	Ref. [45]
	2025.3 to 30000	Ref. [60]
	30156.09 to 1000000	Ref. [85]
SnTe	0.1 to 36.8	Calculation with WIEN2k
	37.2 to 1000000	Calculation with FEFF
$TiC_{0.7}$	0.02 to 79.6	Ref. [86]
	80.177 to 30000	Ref. [60]
	30070.87 to 1120600	Ref. [85]
$TiC_{0.95}$	0.02 to 79.6	Ref. [87]
	80.177 to 30000	Ref. [60]
	30070.87 to 1120600	Ref. [85]
$VC_{0.76}$	0.02 to 79	Ref. [87]
	80.177 to 30000	Ref. [60]
	30071 to 1120600	Ref. [85]
$VC_{0.86}$	0.02 to 79	Ref. [87]
	80.177 to 30000	Ref. [60]
	30071 to 1120600	Ref. [85]
$Y_3Al_5O_{12}$	0.0031 to 49.45	Ref. [47]
	50.935 to 30000	Ref. [60]
	30156 to 1022000	Ref. [85]
ZnS	0.01 to 0.07	Ref. [44]
	2.1 to 50	Calculation with WIEN2k
	50.5 to 1000000	Calculation with FEFF
ZnSe	0.01 to 0.0744	Ref. [44]
	1.4 to 50	Calculation with WIEN2k
	50.5 to 1000000	Calculation with FEFF
ZnTe	0.01 to 0.04	Ref. [44]
	1.3 to 38	Calculation with WIEN2k
	38.4 to 1000000	Calculation with FEFF

Author Manuscript:
Published in final edited form as: *Surf. Interface Anal*. Volume 51, Issue 4, Pages 427-457, April 2019
https://doi.org/10.1002/sia.6598

Table 3. Crystal information used in the FEFF and WIEN2k calculations for the indicated compound semiconductors. The cell parameters were obtained from the AtomWork database[57].

Material	Space Group	Cell parameter (nm)
AgBr	F m -3 m	a = 0. 5775
AgCl	F m -3 m	a = 0.5543
AgI	P 63 m c	a = 0.45856 c = 0.749 γ = 120°
AlAs	F -4 3 m	a = 0.56605
AlN	P 63 m c	a = 0.311 c = 0.498 γ = 120°
AlSb	F -4 3 m	a = 0.6135
c-BN	F -4 3 m	a =0.36159
h-BN	P 63 /mmc	a = 0.2.5045 c =0.6606 γ = 120°
CdS	P 63 m c	a = 0.4142 c =0.6724 γ = 120°
CdSe	P 63 m c	a = 0.4299 c = 0.701 γ = 120°
CdTe	F -4 3 m	a = 0.6482
GaAs	F -4 3 m	a = 0.56532
GaN	P 63 m c	a =0.31891 c = 0.51855 γ = 120°
GaP	F -4 3 m	a = 0.54508
GaSb	F -4 3 m	a = 0.60959
GaSe	P 63 /mmc	a = 0.375 c = 1.5995 γ = 120°
InAs	F -4 3 m	a = 0.60577
InP	F -4 3 m	a = 0.58687
InSb	F -4 3 m	a = 0.64794
PbS	F m -3 m	a = 0.59315
PbSe	F m -3 m	a = 0.61213
PbTe	F m -3 m	a = 0.64541
SiC	F -4 3 m	a = 0.43581
SnTe	F m -3 m	a = 0.6323
ZnS	F -4 3 m	a = 0.54102
ZnSe	F -4 3 m	a = 0.56692
ZnTe	F -4 3 m	a = 0.61026

Author Manuscript:
Published in final edited form as: *Surf. Interface Anal*. Volume 51, Issue 4, Pages 427-457, April 2019
https://doi.org/10.1002/sia.6598

Table 4. List of 42 inorganic compounds with values of the number of electrons per molecule, Z, Z_{eff} from Eqn (10), errors in the f-sum rule, values of P_{eff} from Eqn (11), and errors in the KK-sum rule. Values of Z_{eff} and P_{eff} were determined with ΔE_{max} = 1 MeV.

Compound	Z	Z_{eff}	Error in f-sum rule (%)	P_{eff}	Error in KK-sum rule (%)
AgBr	82	80.10	-2.3	1.023	2.3
AgCl	64	62.48	-2.4	0.977	-2.3
AgI	100	98.40	-1.6	1.035	3.5
Al_2O_3	50	49.39	-1.2	0.922	-7.8
AlAs	46	46.22	0.5	1.012	1.2
AlN	20	20.25	1.3	0.937	-6.3
AlSb	64	62.75	-1.9	1.018	1.8
c-BN	12	11.96	-0.3	0.953	-4.7
h-BN	12	12.18	1.5	0.997	-0.3
CdS	64	62.84	-1.8	1.005	0.5
CdSe	82	80.35	-2.0	1.058	5.8
CdTe	100	100.07	0.1	1.036	3.6
GaAs	64	62.76	-1.9	1.014	1.4
GaN	38	37.70	-0.8	1.033	3.3
GaP	46	45.04	-2.1	1.076	7.6
GaSb	82	79.95	-2.5	1.014	1.4
GaSe	65	63.98	-1.6	1.003	0.3
InAs	82	80.18	-2.2	1.031	3.1
InP	64	62.45	-2.4	1.001	0.1
InSb	100	97.09	-2.9	1.018	1.8
KBr	54	54.07	0.1	0.943	-5.7
KCl	36	35.33	-1.9	0.984	-1.6
MgF_2	30	32.76	9.2	1.038	3.8
MgO	20	20.22	1.1	1.003	0.3
NaCl	28	27.01	-3.6	0.917	-8.3
$NbC_{0.712}$	45.272	41.05	-9.3	0.996	-0.4
$NbC_{0.844}$	46.064	41.55	-9.8	0.996	-0.4
$NbC_{0.93}$	46.58	41.87	-10.1	0.996	-0.4
PbS	98	95.38	-2.7	0.993	-0.7
PbSe	116	112.70	-2.8	0.989	-1.1
PbTe	134	130.47	-2.6	1.012	1.2

Author Manuscript:
Published in final edited form as: *Surf. Interface Anal*. Volume 51, Issue 4, Pages 427-457, April 2019
https://doi.org/10.1002/sia.6598

SiC	20	19.91	-0.4	1.070	7.0
SiO_2	30	28.14	-6.2	1.045	4.5
SnTe	102	100.20	-1.8	0.999	-0.1
$TiC_{0.7}$	26.2	26.23	0.1	1.005	0.5
$TiC_{0.95}$	27.7	27.66	-0.1	1.006	0.6
$VC_{0.76}$	27.56	24.83	-9.9	1.011	1.1
$VC_{0.86}$	28.16	25.68	-8.8	1.011	1.1
$Y_3Al_5O_{12}$	278	280.24	0.8	0.962	-3.8
ZnS	46	44.83	-2.6	1.022	2.2
ZnSe	64	63.13	-1.4	0.992	-0.8
ZnTe	82	82.28	0.4	1.032	3.2

Author Manuscript:
Published in final edited form as: *Surf. Interface Anal*. Volume 51, Issue 4, Pages 427-457, April 2019
https://doi.org/10.1002/sia.6598

Table 5. Calculated IMFPs for the 42 inorganic compounds as a function of electron energy E with respect to the bottom of the conduction band.

	Inelastic mean free path (nm)										
E(eV)	AgBr	AgCl	AgI	Al_2O_3	AlAs	AlN	AlSb	*c*-BN	*h*-BN	CdS	CdSe
54.6	0.533	0.562	0.524	0.757	0.401	0.533	0.416	0.718	0.597	0.503	0.489
60.3	0.524	0.550	0.524	0.711	0.410	0.513	0.430	0.652	0.550	0.504	0.492
66.7	0.520	0.543	0.529	0.677	0.424	0.502	0.446	0.597	0.522	0.509	0.498
73.7	0.520	0.539	0.537	0.654	0.440	0.499	0.464	0.555	0.510	0.516	0.507
81.5	0.523	0.540	0.547	0.640	0.459	0.501	0.485	0.521	0.504	0.526	0.518
90.0	0.528	0.543	0.560	0.634	0.481	0.510	0.507	0.498	0.504	0.538	0.531
99.5	0.536	0.548	0.575	0.634	0.506	0.523	0.532	0.491	0.512	0.552	0.547
109.9	0.546	0.557	0.593	0.640	0.533	0.540	0.559	0.491	0.525	0.568	0.565
121.5	0.560	0.569	0.614	0.651	0.563	0.560	0.588	0.497	0.542	0.587	0.585
134.3	0.578	0.584	0.638	0.667	0.597	0.585	0.619	0.508	0.563	0.608	0.608
148.4	0.599	0.604	0.665	0.688	0.633	0.613	0.652	0.524	0.588	0.632	0.634
164.0	0.625	0.628	0.694	0.713	0.672	0.644	0.687	0.543	0.616	0.659	0.663
181.3	0.655	0.657	0.723	0.743	0.715	0.679	0.724	0.567	0.649	0.691	0.696
200.3	0.690	0.690	0.752	0.776	0.760	0.717	0.764	0.595	0.685	0.728	0.734
221.4	0.728	0.728	0.788	0.814	0.810	0.758	0.808	0.626	0.725	0.769	0.776
244.7	0.772	0.770	0.830	0.856	0.862	0.803	0.856	0.661	0.770	0.816	0.823
270.4	0.819	0.818	0.878	0.903	0.919	0.851	0.910	0.699	0.819	0.867	0.874
298.9	0.872	0.871	0.933	0.954	0.980	0.903	0.969	0.742	0.873	0.925	0.931
330.3	0.930	0.929	0.993	1.01	1.05	0.960	1.03	0.789	0.932	0.988	0.993
365.0	0.992	0.992	1.06	1.07	1.12	1.02	1.11	0.841	0.996	1.06	1.06
403.4	1.06	1.06	1.13	1.14	1.20	1.09	1.18	0.898	1.07	1.13	1.13
445.9	1.13	1.14	1.22	1.21	1.28	1.16	1.27	0.961	1.14	1.21	1.21
492.7	1.22	1.22	1.30	1.29	1.37	1.24	1.36	1.03	1.23	1.30	1.30
544.6	1.30	1.31	1.40	1.38	1.47	1.33	1.47	1.10	1.32	1.40	1.40
601.8	1.40	1.41	1.51	1.47	1.58	1.43	1.58	1.18	1.42	1.51	1.50
665.1	1.50	1.52	1.62	1.58	1.70	1.53	1.70	1.27	1.53	1.62	1.62
735.1	1.62	1.64	1.75	1.69	1.83	1.65	1.83	1.37	1.65	1.75	1.74
812.4	1.74	1.76	1.89	1.81	1.97	1.77	1.98	1.47	1.78	1.88	1.87
897.8	1.88	1.90	2.03	1.95	2.12	1.91	2.13	1.59	1.92	2.03	2.02
992.3	2.02	2.05	2.20	2.10	2.29	2.06	2.31	1.71	2.07	2.19	2.18
1096.6	2.18	2.21	2.37	2.26	2.47	2.22	2.49	1.85	2.24	2.37	2.35
1212.0	2.35	2.39	2.57	2.44	2.67	2.40	2.70	2.00	2.42	2.56	2.54
1339.4	2.54	2.58	2.77	2.63	2.89	2.59	2.92	2.16	2.62	2.77	2.74
1480.3	2.75	2.79	3.00	2.84	3.12	2.81	3.16	2.33	2.83	3.00	2.97
1636.0	2.97	3.02	3.25	3.07	3.38	3.03	3.42	2.52	3.07	3.24	3.21
1808.0	3.21	3.27	3.52	3.32	3.66	3.28	3.71	2.73	3.32	3.51	3.47
1998.2	3.48	3.53	3.81	3.59	3.97	3.56	4.02	2.95	3.60	3.80	3.76
2208.3	3.76	3.83	4.13	3.88	4.30	3.85	4.36	3.20	3.91	4.12	4.07
2440.6	4.07	4.14	4.47	4.20	4.66	4.18	4.73	3.47	4.24	4.47	4.41
2697.3	4.41	4.49	4.85	4.55	5.06	4.53	5.14	3.76	4.60	4.84	4.78
2981.0	4.78	4.87	5.26	4.94	5.49	4.91	5.57	4.08	4.99	5.25	5.19
3294.5	5.19	5.28	5.70	5.35	5.96	5.33	6.05	4.42	5.42	5.70	5.63
3641.0	5.63	5.73	6.19	5.80	6.47	5.78	6.57	4.80	5.88	6.18	6.11
4023.9	6.10	6.21	6.71	6.29	7.03	6.28	7.13	5.21	6.39	6.71	6.63
4447.1	6.62	6.74	7.29	6.83	7.64	6.82	7.75	5.65	6.94	7.29	7.19
4914.8	7.19	7.32	7.91	7.41	8.30	7.41	8.42	6.14	7.54	7.91	7.81
5431.7	7.80	7.95	8.59	8.04	9.02	8.04	9.15	6.67	8.19	8.60	8.48
6002.9	8.48	8.63	9.33	8.73	9.80	8.74	9.95	7.24	8.91	9.34	9.21
6634.2	9.20	9.38	10.14	9.48	10.7	9.50	10.8	7.87	9.68	10.1	10.0

Author Manuscript:
Published in final edited form as: *Surf. Interface Anal*. Volume 51, Issue 4, Pages 427-457, April 2019
https://doi.org/10.1002/sia.6598

7332.0	10.0	10.2	11.01	10.3	11.6	10.3	11.8	8.55	10.5	11.0	10.9
8103.1	10.9	11.1	11.96	11.2	12.6	11.2	12.8	9.29	11.4	12.0	11.8
8955.3	11.8	12.0	13.00	12.2	13.7	12.2	13.9	10.1	12.4	13.0	12.8
9897.1	12.8	13.1	14.13	13.2	14.9	13.2	15.1	11.0	13.5	14.2	14.0
10938.0	13.9	14.2	15.35	14.3	16.2	14.4	16.4	11.9	14.7	15.4	15.2
12088.4	15.1	15.4	16.68	15.6	17.6	15.6	17.8	13.0	16.0	16.7	16.5
13359.7	16.4	16.8	18.12	16.9	19.1	17.0	19.4	14.1	17.4	18.2	17.9
14764.8	17.8	18.2	19.69	18.4	20.8	18.5	21.1	15.3	18.9	19.7	19.4
16317.6	19.4	19.8	21.38	19.9	22.6	20.1	22.9	16.6	20.5	21.4	21.1
18033.7	21.0	21.5	23.22	21.7	24.5	21.8	24.9	18.0	22.3	23.3	22.9
19930.4	22.8	23.3	25.21	23.5	26.6	23.7	27.0	19.6	24.2	25.3	24.9
22026.5	24.8	25.3	27.36	25.5	28.9	25.7	29.4	21.3	26.3	27.5	27.0
24343.0	26.9	27.4	29.69	27.7	31.4	27.9	31.9	23.1	28.5	29.8	29.3
26903.2	29.2	29.8	32.20	30.0	34.1	30.2	34.6	25.0	31.0	32.3	31.8
29732.6	31.6	32.3	34.90	32.5	36.9	32.8	37.5	27.1	33.6	35.0	34.5
32859.6	34.2	35.0	37.81	35.2	40.0	35.5	40.6	29.4	36.4	38.0	37.4
36315.5	37.1	37.8	40.94	38.1	43.4	38.4	44.0	31.8	39.4	41.1	40.5
40134.8	40.1	41.0	44.30	41.2	46.9	41.6	47.6	34.4	42.7	44.5	43.8
44355.9	43.4	44.3	47.90	44.6	50.8	45.0	51.5	37.2	46.1	48.1	47.3
49020.8	46.8	47.8	51.75	48.1	54.9	48.6	55.7	40.2	49.9	52.0	51.1
54176.4	50.6	51.6	55.86	51.9	59.2	52.5	60.1	43.4	53.8	56.1	55.2
59874.1	54.5	55.7	60.24	56.0	63.9	56.6	64.8	46.8	58.1	60.5	59.5
66171.2	58.7	60.0	64.88	60.3	68.8	60.9	69.9	50.4	62.5	65.2	64.1
73130.4	63.2	64.5	69.80	64.9	74.1	65.6	75.2	54.2	67.3	70.1	69.0
80821.6	67.8	69.3	74.99	69.7	79.6	70.4	80.8	58.3	72.3	75.3	74.1
89321.7	72.8	74.3	80.46	74.7	85.4	75.6	86.7	62.5	77.6	80.8	79.5
98715.8	78.0	79.6	86.19	80.0	91.5	81.0	92.9	66.9	83.2	86.6	85.2
109097.8	83.4	85.2	92.19	85.6	97.9	86.6	99.4	71.6	89.0	92.6	91.1
120571.7	89.0	90.9	98.42	91.4	105	92.5	106	76.4	95.0	98.9	97.3
133252.4	94.9	96.9	105	97.3	111	98.6	113	81.5	101	105	104
147266.6	101	103	112	104	119	105	120	86.6	108	112	110
162754.8	107	109	118	110	126	111	128	92.0	114	119	117
179871.9	113	116	125	116	133	118	135	97.4	121	126	124
198789.2	120	122	133	123	141	125	143	103	128	133	131

Author Manuscript:
Published in final edited form as: *Surf. Interface Anal*. Volume 51, Issue 4, Pages 427-457, April 2019
https://doi.org/10.1002/sia.6598

Table 5. (continued)

Inelastic mean free path (nm)

E(eV)	CdTe	GaAs	GaN	GaP	GaSb	GaSe	InAs	InP	InSb	KBr	KCl
54.6	0.489	0.415	0.531	0.408	0.428	0.428	0.446	0.445	0.452	0.838	0.785
60.3	0.497	0.422	0.516	0.414	0.439	0.435	0.454	0.451	0.463	0.812	0.755
66.7	0.507	0.433	0.507	0.424	0.453	0.445	0.464	0.461	0.477	0.793	0.732
73.7	0.519	0.447	0.505	0.437	0.469	0.458	0.478	0.473	0.492	0.783	0.721
81.5	0.533	0.464	0.508	0.453	0.487	0.474	0.493	0.488	0.510	0.782	0.722
90.0	0.549	0.483	0.515	0.471	0.507	0.493	0.510	0.504	0.528	0.788	0.733
99.5	0.567	0.505	0.525	0.492	0.529	0.515	0.529	0.522	0.549	0.805	0.753
109.9	0.587	0.529	0.538	0.516	0.552	0.539	0.550	0.542	0.570	0.831	0.780
121.5	0.608	0.555	0.555	0.542	0.578	0.566	0.572	0.564	0.593	0.866	0.814
134.3	0.630	0.584	0.574	0.571	0.606	0.596	0.597	0.587	0.618	0.907	0.854
148.4	0.651	0.616	0.595	0.603	0.635	0.629	0.623	0.613	0.643	0.955	0.899
164.0	0.672	0.651	0.620	0.638	0.665	0.665	0.652	0.641	0.670	1.01	0.951
181.3	0.696	0.688	0.647	0.676	0.697	0.704	0.684	0.673	0.699	1.07	1.01
200.3	0.725	0.729	0.677	0.717	0.732	0.746	0.720	0.709	0.732	1.13	1.07
221.4	0.760	0.773	0.711	0.762	0.771	0.791	0.760	0.750	0.769	1.21	1.14
244.7	0.801	0.820	0.748	0.811	0.815	0.841	0.805	0.795	0.811	1.29	1.22
270.4	0.848	0.871	0.789	0.864	0.863	0.894	0.855	0.846	0.859	1.37	1.30
298.9	0.901	0.927	0.834	0.922	0.917	0.953	0.909	0.902	0.913	1.47	1.39
330.3	0.960	0.987	0.883	0.985	0.976	1.02	0.969	0.964	0.973	1.57	1.49
365.0	1.02	1.05	0.937	1.05	1.04	1.08	1.03	1.03	1.04	1.68	1.60
403.4	1.10	1.12	0.996	1.13	1.11	1.16	1.11	1.11	1.11	1.80	1.72
445.9	1.17	1.20	1.06	1.21	1.19	1.24	1.18	1.19	1.19	1.93	1.85
492.7	1.26	1.28	1.13	1.29	1.28	1.32	1.27	1.27	1.28	2.07	1.99
544.6	1.35	1.37	1.21	1.39	1.37	1.42	1.36	1.37	1.38	2.23	2.14
601.8	1.46	1.47	1.29	1.49	1.47	1.52	1.46	1.47	1.48	2.39	2.31
665.1	1.57	1.58	1.39	1.60	1.58	1.63	1.57	1.58	1.59	2.58	2.49
735.1	1.69	1.70	1.49	1.72	1.70	1.76	1.69	1.71	1.72	2.77	2.68
812.4	1.82	1.83	1.60	1.85	1.84	1.89	1.82	1.84	1.85	2.99	2.90
897.8	1.96	1.97	1.72	2.00	1.98	2.03	1.97	1.99	2.00	3.22	3.13
992.3	2.12	2.12	1.85	2.15	2.14	2.19	2.12	2.14	2.16	3.47	3.38
1096.6	2.29	2.28	1.99	2.32	2.31	2.36	2.29	2.32	2.33	3.75	3.65
1212.0	2.48	2.47	2.14	2.51	2.49	2.55	2.48	2.50	2.52	4.05	3.95
1339.4	2.68	2.66	2.31	2.71	2.69	2.75	2.68	2.71	2.73	4.38	4.27
1480.3	2.90	2.88	2.50	2.93	2.91	2.98	2.89	2.93	2.96	4.73	4.62
1636.0	3.14	3.11	2.70	3.17	3.15	3.22	3.13	3.17	3.20	5.12	5.00
1808.0	3.40	3.37	2.92	3.44	3.41	3.48	3.39	3.44	3.47	5.54	5.42
1998.2	3.68	3.65	3.15	3.72	3.70	3.77	3.67	3.72	3.76	6.00	5.87
2208.3	3.99	3.95	3.41	4.04	4.01	4.08	3.98	4.04	4.07	6.50	6.37
2440.6	4.32	4.28	3.70	4.38	4.34	4.43	4.31	4.38	4.41	7.04	6.90
2697.3	4.68	4.64	4.00	4.75	4.71	4.80	4.67	4.75	4.78	7.63	7.49
2981.0	5.08	5.03	4.34	5.15	5.11	5.20	5.07	5.15	5.19	8.28	8.13
3294.5	5.51	5.46	4.70	5.59	5.54	5.65	5.49	5.59	5.63	8.98	8.83
3641.0	5.98	5.92	5.10	6.07	6.01	6.13	5.96	6.06	6.11	9.75	9.59
4023.9	6.49	6.43	5.53	6.59	6.53	6.65	6.47	6.58	6.63	10.6	10.4
4447.1	7.04	6.98	6.00	7.16	7.09	7.22	7.03	7.15	7.20	11.5	11.3
4914.8	7.64	7.58	6.51	7.78	7.70	7.84	7.63	7.76	7.81	12.5	12.3
5431.7	8.30	8.23	7.07	8.45	8.36	8.52	8.29	8.44	8.49	13.6	13.4
6002.9	9.02	8.94	7.68	9.18	9.08	9.26	9.00	9.17	9.22	14.7	14.5
6634.2	9.80	9.72	8.33	9.98	9.87	10.1	9.78	9.96	10.0	16.0	15.8
7332.0	10.6	10.6	9.05	10.8	10.7	10.9	10.6	10.8	10.9	17.4	17.2
8103.1	11.6	11.5	9.83	11.8	11.7	11.9	11.5	11.8	11.8	18.9	18.7
8955.3	12.6	12.5	10.7	12.8	12.7	12.9	12.5	12.8	12.9	20.6	20.3

Author Manuscript:
Published in final edited form as: *Surf. Interface Anal*. Volume 51, Issue 4, Pages 427-457, April 2019
https://doi.org/10.1002/sia.6598

9897.1	13.7	13.5	11.6	13.9	13.8	14.0	13.6	13.9	14.0	22.3	22.1
10938.0	14.8	14.7	12.6	15.1	15.0	15.2	14.8	15.1	15.2	24.3	24.0
12088.4	16.1	16.0	13.7	16.5	16.3	16.6	16.1	16.4	16.5	26.4	26.1
13359.7	17.5	17.4	14.9	17.9	17.7	18.0	17.5	17.9	17.9	28.7	28.3
14764.8	19.0	18.9	16.1	19.4	19.2	19.6	19.0	19.4	19.5	31.2	30.8
16317.6	20.7	20.5	17.5	21.1	20.8	21.2	20.6	21.1	21.2	33.8	33.5
18033.7	22.4	22.3	19.0	22.9	22.6	23.1	22.4	22.9	23.0	36.8	36.4
19930.4	24.4	24.2	20.6	24.9	24.6	25.0	24.3	24.9	25.0	39.9	39.5
22026.5	26.5	26.3	22.4	27.1	26.7	27.2	26.4	27.0	27.1	43.3	42.9
24343.0	28.7	28.5	24.3	29.4	29.0	29.5	28.7	29.3	29.4	47.0	46.5
26903.2	31.1	30.9	26.3	31.9	31.4	32.0	31.1	31.8	31.9	51.0	50.5
29732.6	33.7	33.5	28.5	34.5	34.0	34.7	33.7	34.5	34.6	55.3	54.8
32859.6	36.6	36.3	30.9	37.4	36.9	37.6	36.5	37.3	37.5	59.9	59.4
36315.5	39.6	39.3	33.5	40.5	40.0	40.7	39.6	40.4	40.6	64.9	64.3
40134.8	42.8	42.5	36.2	43.9	43.2	44.0	42.8	43.8	43.9	70.2	69.6
44355.9	46.3	46.0	39.1	47.5	46.8	47.6	46.3	47.3	47.5	75.9	75.3
49020.8	50.1	49.7	42.3	51.3	50.5	51.5	50.0	51.1	51.3	82.0	81.3
54176.4	54.0	53.6	45.6	55.4	54.5	55.6	54.0	55.2	55.4	88.6	87.8
59874.1	58.3	57.8	49.2	59.7	58.8	59.9	58.2	59.5	59.7	95.5	94.7
66171.2	62.7	62.3	53.0	64.3	63.3	64.5	62.7	64.1	64.3	103	102
73130.4	67.5	67.0	57.0	69.2	68.2	69.4	67.5	69.0	69.2	111	110
80821.6	72.5	72.0	61.2	74.4	73.2	74.6	72.5	74.2	74.4	119	118
89321.7	77.8	77.3	65.6	79.8	78.6	80.0	77.8	79.6	79.8	128	127
98715.8	83.4	82.8	70.3	85.5	84.2	85.8	83.3	85.3	85.5	137	136
109097.8	89.2	88.5	75.2	91.5	90.0	91.7	89.1	91.2	91.5	146	145
120571.7	95.2	94.5	80.2	97.7	96.1	97.9	95.2	97.4	97.7	156	155
133252.4	101	101	85.5	104	102	104	101	104	104	166	165
147266.6	108	107	90.9	111	109	111	108	110	111	177	176
162754.8	115	114	96.5	118	116	118	115	117	118	188	187
179871.9	121	120	102	125	123	125	121	124	124	199	198
198789.2	128	127	108	132	129	132	128	131	132	210	209

Author Manuscript:
Published in final edited form as: *Surf. Interface Anal*. Volume 51, Issue 4, Pages 427-457, April 2019
https://doi.org/10.1002/sia.6598

Table 5. (continued)

Inelastic mean free path (nm)

E(eV)	MgF_2	MgO	NaCl	$NbC_{0.712}$	$NbC_{0.844}$	$NbC_{0.93}$	PbS	PbSe	PbTe	SiC	SiO_2
54.6	1.06	0.705	0.819	0.466	0.466	0.466	0.449	0.442	0.439	0.451	0.831
60.3	0.985	0.671	0.808	0.455	0.454	0.454	0.452	0.446	0.446	0.433	0.801
66.7	0.933	0.654	0.815	0.451	0.449	0.449	0.458	0.453	0.456	0.426	0.782
73.7	0.898	0.646	0.830	0.451	0.449	0.448	0.467	0.463	0.469	0.425	0.773
81.5	0.874	0.644	0.854	0.454	0.452	0.451	0.478	0.474	0.483	0.430	0.772
90.0	0.860	0.647	0.883	0.458	0.456	0.455	0.491	0.488	0.498	0.440	0.778
99.5	0.853	0.655	0.917	0.465	0.463	0.462	0.503	0.501	0.514	0.453	0.791
109.9	0.853	0.667	0.956	0.473	0.470	0.469	0.517	0.517	0.531	0.470	0.808
121.5	0.859	0.684	0.999	0.483	0.480	0.479	0.534	0.535	0.551	0.490	0.831
134.3	0.871	0.704	1.05	0.497	0.494	0.493	0.553	0.555	0.572	0.513	0.859
148.4	0.888	0.727	1.10	0.515	0.512	0.511	0.575	0.578	0.594	0.539	0.892
164.0	0.909	0.753	1.15	0.537	0.534	0.533	0.599	0.604	0.618	0.569	0.930
181.3	0.935	0.783	1.22	0.563	0.560	0.559	0.628	0.634	0.642	0.602	0.973
200.3	0.966	0.817	1.28	0.593	0.590	0.589	0.660	0.667	0.670	0.638	1.02
221.4	1.00	0.854	1.36	0.626	0.623	0.622	0.697	0.704	0.702	0.678	1.08
244.7	1.04	0.896	1.44	0.663	0.660	0.659	0.738	0.746	0.739	0.722	1.14
270.4	1.09	0.943	1.53	0.705	0.701	0.700	0.783	0.791	0.782	0.769	1.21
298.9	1.14	0.994	1.62	0.750	0.747	0.745	0.834	0.842	0.830	0.821	1.28
330.3	1.20	1.05	1.73	0.801	0.797	0.795	0.890	0.897	0.883	0.877	1.36
365.0	1.27	1.11	1.85	0.856	0.851	0.850	0.951	0.957	0.942	0.937	1.45
403.4	1.35	1.18	1.98	0.916	0.911	0.909	1.02	1.02	1.01	1.00	1.55
445.9	1.43	1.26	2.12	0.982	0.977	0.975	1.09	1.09	1.08	1.07	1.66
492.7	1.52	1.34	2.27	1.05	1.05	1.05	1.17	1.17	1.16	1.15	1.78
544.6	1.62	1.43	2.43	1.13	1.13	1.12	1.26	1.26	1.24	1.23	1.90
601.8	1.73	1.53	2.61	1.22	1.21	1.21	1.35	1.35	1.34	1.33	2.04
665.1	1.85	1.64	2.81	1.31	1.30	1.30	1.45	1.45	1.44	1.42	2.19
735.1	1.98	1.76	3.03	1.41	1.40	1.40	1.56	1.56	1.55	1.53	2.36
812.4	2.13	1.89	3.26	1.52	1.51	1.51	1.69	1.68	1.67	1.65	2.54
897.8	2.29	2.04	3.51	1.64	1.63	1.62	1.82	1.81	1.80	1.78	2.73
992.3	2.46	2.19	3.78	1.76	1.76	1.75	1.96	1.95	1.94	1.92	2.95
1096.6	2.65	2.36	4.08	1.90	1.89	1.89	2.11	2.11	2.10	2.07	3.18
1212.0	2.86	2.55	4.40	2.05	2.04	2.04	2.28	2.27	2.26	2.24	3.44
1339.4	3.08	2.75	4.76	2.22	2.21	2.20	2.47	2.45	2.45	2.42	3.71
1480.3	3.33	2.97	5.14	2.40	2.38	2.38	2.66	2.65	2.65	2.62	4.02
1636.0	3.59	3.21	5.56	2.59	2.57	2.57	2.88	2.87	2.86	2.83	4.35
1808.0	3.88	3.47	6.02	2.80	2.78	2.78	3.12	3.10	3.10	3.07	4.70
1998.2	4.20	3.76	6.52	3.03	3.01	3.01	3.37	3.35	3.35	3.32	5.09
2208.3	4.55	4.07	7.06	3.28	3.26	3.25	3.65	3.63	3.63	3.60	5.52
2440.6	4.92	4.41	7.66	3.55	3.53	3.52	3.96	3.93	3.93	3.90	5.98
2697.3	5.33	4.77	8.30	3.85	3.82	3.82	4.29	4.26	4.26	4.23	6.49
2981.0	5.77	5.18	9.01	4.17	4.15	4.14	4.65	4.62	4.62	4.59	7.04
3294.5	6.26	5.61	9.77	4.52	4.49	4.48	5.04	5.01	5.01	4.98	7.63
3641.0	6.78	6.09	10.6	4.90	4.87	4.86	5.47	5.43	5.43	5.41	8.28
4023.9	7.36	6.60	11.5	5.32	5.29	5.28	5.93	5.89	5.89	5.88	8.99
4447.1	7.98	7.17	12.5	5.77	5.74	5.73	6.44	6.39	6.40	6.38	9.77
4914.8	8.66	7.78	13.6	6.26	6.23	6.22	6.99	6.94	6.94	6.94	10.6
5431.7	9.40	8.44	14.8	6.80	6.76	6.75	7.59	7.53	7.54	7.54	11.5
6002.9	10.2	9.17	16.0	7.39	7.35	7.33	8.25	8.18	8.19	8.19	12.5
6634.2	11.1	9.96	17.4	8.02	7.98	7.96	8.96	8.89	8.89	8.90	13.6
7332.0	12.0	10.8	18.9	8.71	8.67	8.65	9.73	9.65	9.66	9.68	14.8
8103.1	13.1	11.7	20.6	9.47	9.42	9.39	10.6	10.5	10.5	10.5	16.1
8955.3	14.2	12.8	22.4	10.3	10.2	10.2	11.5	11.4	11.4	11.4	17.5

Author Manuscript:
Published in final edited form as: *Surf. Interface Anal*. Volume 51, Issue 4, Pages 427-457, April 2019
https://doi.org/10.1002/sia.6598

9897.1	15.4	13.9	24.3	11.2	11.1	11.1	12.5	12.4	12.4	12.4	19.0
10938.0	16.7	15.1	26.4	12.1	12.1	12.0	13.6	13.4	13.5	13.5	20.6
12088.4	18.2	16.4	28.7	13.2	13.1	13.1	14.7	14.6	14.6	14.7	22.4
13359.7	19.7	17.8	31.2	14.3	14.3	14.2	16.0	15.9	15.9	16.0	24.4
14764.8	21.4	19.3	33.9	15.6	15.5	15.4	17.4	17.2	17.3	17.3	26.5
16317.6	23.2	21.0	36.8	16.9	16.8	16.8	18.9	18.7	18.7	18.8	28.7
18033.7	25.2	22.8	40.0	18.4	18.3	18.2	20.5	20.3	20.4	20.5	31.2
19930.4	27.4	24.7	43.4	19.9	19.8	19.8	22.3	22.1	22.1	22.2	33.9
22026.5	29.7	26.8	47.2	21.6	21.5	21.5	24.2	23.9	24.0	24.1	36.8
24343.0	32.2	29.1	51.2	23.5	23.3	23.3	26.2	26.0	26.0	26.2	39.9
26903.2	34.9	31.5	55.5	25.4	25.3	25.2	28.4	28.2	28.2	28.4	43.3
29732.6	37.8	34.2	60.2	27.6	27.4	27.4	30.8	30.5	30.6	30.8	46.9
32859.6	41.0	37.0	65.2	29.9	29.7	29.6	33.4	33.1	33.1	33.4	50.9
36315.5	44.3	40.0	70.6	32.3	32.2	32.1	36.1	35.8	35.9	36.2	55.1
40134.8	48.0	43.3	76.4	35.0	34.8	34.7	39.1	38.7	38.8	39.1	59.6
44355.9	51.8	46.8	82.6	37.8	37.6	37.5	42.3	41.9	41.9	42.3	64.4
49020.8	56.0	50.6	89.3	40.9	40.6	40.6	45.7	45.2	45.3	45.7	69.6
54176.4	60.4	54.6	96.4	44.1	43.9	43.8	49.3	48.8	48.9	49.4	75.2
59874.1	65.1	58.9	104	47.6	47.3	47.2	53.2	52.7	52.7	53.3	81.0
66171.2	70.1	63.4	112	51.2	50.9	50.8	57.3	56.7	56.8	57.4	87.3
73130.4	75.4	68.2	120	55.1	54.8	54.7	61.6	61.0	61.1	61.7	93.9
80821.6	81.0	73.2	129	59.2	58.9	58.7	66.2	65.5	65.6	66.3	101
89321.7	86.9	78.6	139	63.5	63.2	63.0	71.0	70.3	70.4	71.2	108
98715.8	93.0	84.2	149	68.0	67.7	67.5	76.1	75.3	75.4	76.3	116
109097.8	99.5	90.0	159	72.8	72.4	72.2	81.4	80.5	80.7	81.6	124
120571.7	106	96.1	170	77.7	77.3	77.1	86.9	86.0	86.1	87.1	132
133252.4	113	102	181	82.8	82.3	82.1	92.6	91.6	91.8	92.8	141
147266.6	120	109	193	88.0	87.6	87.4	98.5	97.5	97.6	98.8	150
162754.8	128	116	205	93.4	92.9	92.7	104	103	104	105	159
179871.9	135	122	217	99.0	98.4	98.2	111	110	110	111	169
198789.2	143	129	229	105	104	104	117	116	116	117	178

Author Manuscript:
Published in final edited form as: *Surf. Interface Anal*. Volume 51, Issue 4, Pages 427-457, April 2019
https://doi.org/10.1002/sia.6598

Table 5. (continued)

Inelastic mean free path (nm)

E(eV)	SnTe	$TiC_{0.7}$	$TiC_{0.95}$	$VC_{0.76}$	$VC_{0.86}$	$Y_3Al_5O_{12}$	ZnS	ZnSe	ZnTe
54.6	0.427	0.486	0.492	0.463	0.471	0.807	0.460	0.449	0.460
60.3	0.437	0.476	0.475	0.453	0.458	0.767	0.461	0.452	0.468
66.7	0.449	0.471	0.465	0.449	0.452	0.736	0.467	0.459	0.480
73.7	0.463	0.470	0.462	0.450	0.452	0.713	0.476	0.470	0.494
81.5	0.480	0.474	0.462	0.456	0.455	0.692	0.490	0.484	0.511
90.0	0.498	0.479	0.466	0.464	0.462	0.674	0.507	0.501	0.531
99.5	0.518	0.487	0.471	0.475	0.472	0.662	0.526	0.521	0.552
109.9	0.539	0.494	0.478	0.487	0.483	0.659	0.548	0.544	0.575
121.5	0.561	0.502	0.484	0.501	0.496	0.663	0.573	0.570	0.599
134.3	0.585	0.511	0.491	0.516	0.510	0.674	0.601	0.599	0.624
148.4	0.609	0.524	0.504	0.534	0.527	0.692	0.632	0.631	0.648
164	0.633	0.543	0.521	0.556	0.548	0.715	0.666	0.665	0.672
181.3	0.658	0.566	0.543	0.582	0.573	0.743	0.704	0.703	0.698
200.3	0.685	0.594	0.569	0.612	0.602	0.776	0.744	0.744	0.729
221.4	0.718	0.625	0.599	0.645	0.634	0.813	0.789	0.788	0.765
244.7	0.755	0.660	0.632	0.682	0.670	0.856	0.838	0.836	0.806
270.4	0.798	0.699	0.670	0.723	0.710	0.902	0.892	0.889	0.853
298.9	0.847	0.743	0.711	0.769	0.754	0.955	0.950	0.945	0.905
330.3	0.902	0.791	0.757	0.818	0.802	1.01	1.01	1.01	0.962
365.0	0.962	0.844	0.807	0.872	0.855	1.07	1.08	1.07	1.03
403.4	1.03	0.902	0.862	0.932	0.913	1.14	1.16	1.14	1.10
445.9	1.10	0.965	0.922	0.997	0.977	1.22	1.24	1.22	1.17
492.7	1.18	1.03	0.988	1.07	1.05	1.30	1.33	1.31	1.25
544.6	1.27	1.11	1.06	1.15	1.12	1.39	1.43	1.40	1.35
601.8	1.36	1.19	1.14	1.23	1.21	1.49	1.53	1.50	1.44
665.1	1.47	1.28	1.22	1.32	1.30	1.60	1.64	1.61	1.55
735.1	1.58	1.38	1.32	1.42	1.39	1.72	1.77	1.73	1.67
812.4	1.71	1.49	1.42	1.53	1.50	1.84	1.90	1.86	1.80
897.8	1.84	1.60	1.53	1.65	1.62	1.98	2.05	2.00	1.94
992.3	1.99	1.73	1.65	1.79	1.75	2.13	2.21	2.16	2.09
1096.6	2.15	1.87	1.78	1.93	1.89	2.30	2.38	2.33	2.26
1212.0	2.32	2.02	1.93	2.08	2.04	2.48	2.57	2.51	2.44
1339.4	2.51	2.18	2.08	2.25	2.20	2.67	2.78	2.71	2.64
1480.3	2.71	2.36	2.25	2.43	2.38	2.89	3.00	2.93	2.85
1636.0	2.94	2.56	2.44	2.63	2.58	3.12	3.25	3.17	3.09
1808.0	3.18	2.77	2.64	2.85	2.79	3.37	3.52	3.43	3.34
1998.2	3.45	3.00	2.86	3.09	3.02	3.65	3.81	3.71	3.62
2208.3	3.73	3.25	3.10	3.34	3.27	3.94	4.13	4.02	3.92
2440.6	4.05	3.52	3.35	3.62	3.54	4.27	4.47	4.36	4.25
2697.3	4.39	3.81	3.64	3.93	3.84	4.62	4.85	4.72	4.61
2981.0	4.76	4.14	3.94	4.26	4.16	5.01	5.26	5.12	5.00
3294.5	5.16	4.49	4.28	4.62	4.52	5.43	5.71	5.55	5.42
3641.0	5.60	4.87	4.64	5.01	4.90	5.89	6.20	6.03	5.88
4023.9	6.08	5.28	5.04	5.44	5.32	6.39	6.73	6.54	6.38
4447.1	6.59	5.74	5.47	5.90	5.77	6.93	7.31	7.10	6.93
4914.8	7.16	6.23	5.94	6.41	6.27	7.52	7.94	7.71	7.52
5431.7	7.78	6.77	6.45	6.96	6.81	8.16	8.63	8.38	8.17
6002.9	8.45	7.35	7.00	7.56	7.39	8.86	9.37	9.10	8.87
6634.2	9.18	7.99	7.61	8.22	8.03	9.62	10.2	9.89	9.64
7332.0	9.97	8.68	8.27	8.93	8.73	10.5	11.1	10.7	10.5
8103.1	10.8	9.43	8.98	9.70	9.48	11.4	12.0	11.7	11.4
8955.3	11.8	10.3	9.76	10.5	10.3	12.3	13.1	12.7	12.4
9897.1	12.8	11.1	10.6	11.5	11.2	13.4	14.2	13.8	13.4

Author Manuscript:
Published in final edited form as: *Surf. Interface Anal*. Volume 51, Issue 4, Pages 427-457, April 2019
https://doi.org/10.1002/sia.6598

10938.0	13.9	12.1	11.5	12.5	12.2	14.5	15.4	15.0	14.6
12088.4	15.1	13.2	12.5	13.5	13.2	15.8	16.8	16.3	15.9
13359.7	16.4	14.3	13.6	14.7	14.4	17.2	18.2	17.7	17.2
14764.8	17.8	15.5	14.8	16.0	15.6	18.6	19.8	19.2	18.7
16317.6	19.4	16.9	16.1	17.3	17.0	20.2	21.5	20.9	20.3
18033.7	21.0	18.3	17.4	18.8	18.4	22.0	23.4	22.7	22.1
19930.4	22.8	19.9	18.9	20.5	20.0	23.8	25.4	24.6	24.0
22026.5	24.8	21.6	20.6	22.2	21.7	25.9	27.6	26.7	26.0
24343.0	26.9	23.4	22.3	24.1	23.5	28.0	29.9	29.0	28.2
26903.2	29.2	25.4	24.2	26.1	25.5	30.4	32.4	31.4	30.6
29732.6	31.6	27.5	26.2	28.3	27.7	33.0	35.2	34.1	33.2
32859.6	34.3	29.8	28.4	30.7	30.0	35.7	38.1	36.9	35.9
36315.5	37.1	32.3	30.8	33.2	32.5	38.6	41.3	40.0	38.9
40134.8	40.2	35.0	33.3	36.0	35.1	41.8	44.7	43.2	42.1
44355.9	43.4	37.8	36.0	38.9	38.0	45.2	48.3	46.8	45.5
49020.8	46.9	40.9	38.9	42.0	41.0	48.8	52.2	50.5	49.2
54176.4	50.6	44.1	42.0	45.4	44.3	52.7	56.3	54.5	53.1
59874.1	54.6	47.6	45.3	48.9	47.8	56.8	60.7	58.8	57.3
66171.2	58.8	51.2	48.8	52.7	51.5	61.1	65.4	63.3	61.7
73130.4	63.3	55.1	52.5	56.7	55.4	65.7	70.4	68.1	66.4
80821.6	68.0	59.2	56.4	60.9	59.5	70.6	75.6	73.2	71.3
89321.7	73.0	63.5	60.5	65.3	63.8	75.7	81.2	78.5	76.5
98715.8	78.2	68.1	64.8	70.0	68.4	81.1	87.0	84.1	81.9
109097.8	83.6	72.8	69.3	74.9	73.1	86.8	93.0	90.0	87.6
120571.7	89.3	77.7	74.0	79.9	78.1	92.6	99.3	96.1	93.6
133252.4	95.1	82.8	78.8	85.2	83.2	98.7	106	102	99.7
147266.6	101	88.1	83.8	90.6	88.5	105	113	109	106
162754.8	107	93.5	89.0	96.2	93.9	111	119	116	113
179871.9	114	99.1	94.3	102	99.5	118	127	122	119
198789.2	120	105	99.6	108	105	125	134	129	126

Author Manuscript:
Published in final edited form as: *Surf. Interface Anal*. Volume 51, Issue 4, Pages 427-457, April 2019
https://doi.org/10.1002/sia.6598

Table 6. Values of the parameters β, γ, C, D found in the fits of Eqns (12) and (13) to the calculated IMFPs for each inorganic compound for electron energies between 50 eV and 200 keV and values of *RMS* calculated from Eqn (14).

Compound	β (eV^{-1} nm^{-1})	γ (eV^{-1})	C (nm^{-1})	D (eV nm^{-1})	*RMS* (%)
AgBr	0.2134	0.09402	15.45	393.8	0.32
AgCl	0.1810	0.11103	15.99	394.5	0.52
AgI	0.2668	0.11547	25.21	778.8	0.57
Al_2O_3	0.1419	0.07707	12.04	330.0	0.63
AlAs	0.3835	0.10386	14.93	541.2	0.92
AlN	0.2018	0.09304	11.56	241.0	0.81
AlSb	0.4651	0.13373	35.42	1265.5	0.55
c-BN	0.1332	0.12011	14.35	273.7	0.77
h-BN	0.1616	0.13144	11.01	95.0	0.18
CdS	0.1937	0.12136	15.97	433.5	0.34
CdSe	0.2254	0.10395	16.04	467.0	0.22
CdTe	0.2735	0.12323	30.13	1023.3	0.78
GaAs	0.4321	0.08464	19.48	737.8	0.93
GaN	0.2621	0.07160	18.05	570.5	0.89
GaP	0.3671	0.10127	16.00	492.8	0.74
GaSb	0.5171	0.10726	41.08	1524.3	0.65
GaSe	0.3989	0.08646	16.27	566.5	0.88
InAs	0.5126	0.10566	38.61	1299.9	0.40
InP	0.4462	0.12591	35.84	1085.8	0.30
InSb	0.5975	0.12641	59.44	2067.9	0.63
KBr	0.4047	0.10413	15.32	0.0	0.61
KCl	0.3426	0.13926	16.26	0.0	0.55
MgF_2	0.1407	0.07291	15.65	509.8	1.04
MgO	0.1772	0.07941	15.75	489.3	0.94
NaCl	0.2341	0.09818	13.07	369.9	0.71
$NbC_{0.712}$	0.2516	0.09973	18.73	452.1	0.53
$NbC_{0.844}$	0.2401	0.09944	17.75	422.2	0.52
$NbC_{0.93}$	0.2332	0.09926	17.20	407.7	0.52
PbS	0.4222	0.10263	32.51	985.2	0.36
PbSe	0.4760	0.09097	32.34	1036.9	0.30
PbTe	0.5469	0.10544	51.52	1804.8	0.64
SiC	0.2097	0.10298	8.52	69.5	0.65
SiO_2	0.1505	0.10741	12.84	314.9	0.34
SnTe	0.4910	0.11692	50.10	1819.4	0.83

Author Manuscript:
Published in final edited form as: *Surf. Interface Anal*. Volume 51, Issue 4, Pages 427-457, April 2019
https://doi.org/10.1002/sia.6598

$TiC_{0.7}$	0.2622	0.12641	30.08	860.9	0.52
$TiC_{0.95}$	0.2425	0.12272	27.61	763.8	0.54
$VC_{0.76}$	0.1944	0.10915	16.89	461.5	0.32
$VC_{0.86}$	0.1928	0.10810	17.33	472.6	0.34
$Y_3Al_5O_{12}$	0.1741	0.08825	18.50	522.4	0.41
ZnS	0.1576	0.09638	7.76	217.2	0.64
ZnSe	0.1909	0.08349	8.47	278.9	0.90
ZnTe	0.2368	0.10591	22.67	835.5	0.82

Author Manuscript:
Published in final edited form as: *Surf. Interface Anal.* Volume 51, Issue 4, Pages 427-457, April 2019
https://doi.org/10.1002/sia.6598

Table 7. Root-mean-square (RMS) deviations between IMFPs from the relativistic TPP-2M equation [Eqns (12), (13) and (15)] and IMFPs calculated from optical data for energies between 50 eV and 200 keV.

Compound	RMS deviation (%)	Compound	RMS deviation (%)
AgBr	9.2	KCl	6.8
AgCl	8.1	MgF_2	19.3
AgI	9.1	MgO	9.4
Al_2O_3	17.1	NaCl	17.5
AlAs	3.2	$NbC_{0.712}$	2.5
AlN	13.9	$NbC_{0.844}$	2.6
AlSb	4.5	$NbC_{0.93}$	2.8
c-BN	65.6	PbS	6.6
h-BN	34.3	PbSe	9.6
CdS	9.9	PbTe	15.4
CdSe	11.6	SiC	16.3
CdTe	7.7	SiO_2	3.0
GaAs	5.0	SnTe	11.6
GaN	3.4	$TiC_{0.7}$	13.2
GaP	4.3	$TiC_{0.95}$	16.2
GaSb	9.0	$VC_{0.76}$	3.7
GaSe	2.4	$VC_{0.86}$	5.4
InAs	8.9	$Y_3Al_5O_{12}$	7.2
InP	6.6	ZnS	5.7
InSb	13.4	ZnSe	10.8
KBr	8.1	ZnTe	8.2

Author Manuscript:
Published in final edited form as: *Surf. Interface Anal.* Volume 51, Issue 4, Pages 427-457, April 2019
https://doi.org/10.1002/sia.6598

Figures

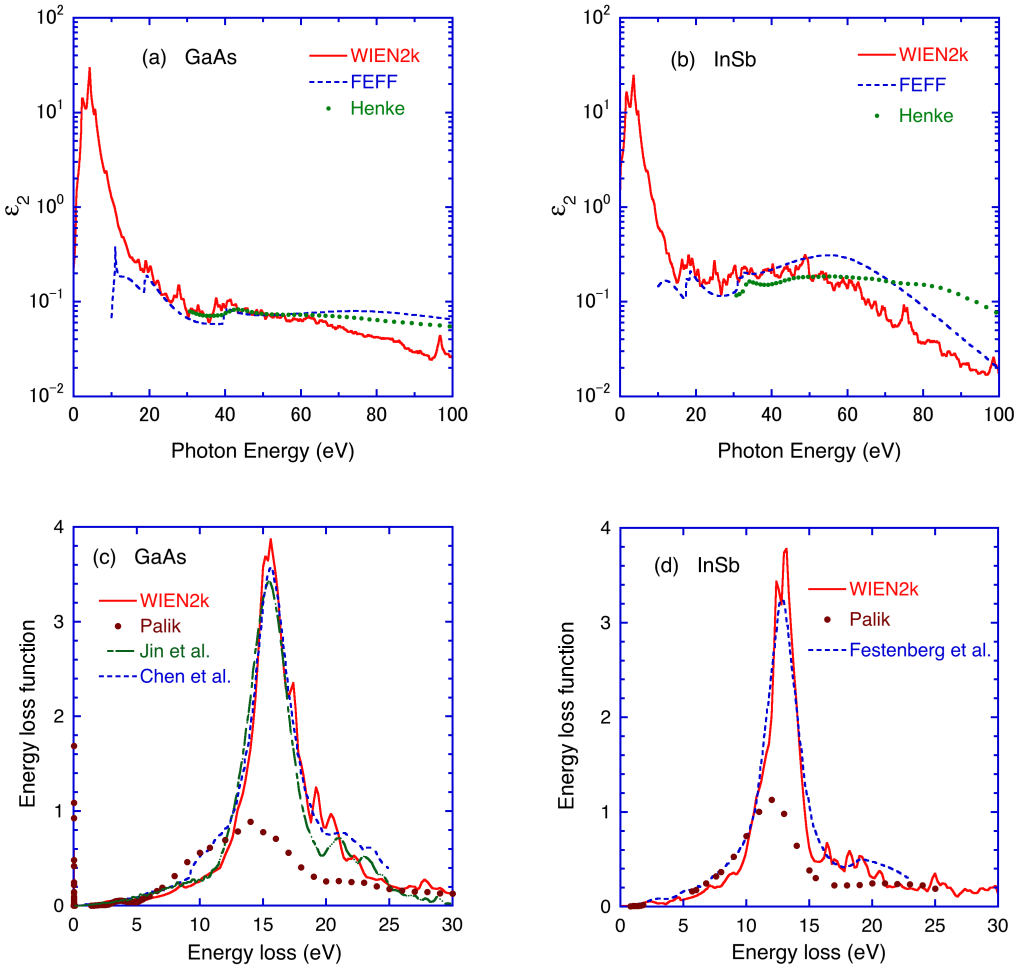

Figure 1. Plots of the imaginary part of the complex dielectric function, ε_2, as a function of photon energy and of the energy-loss functions (ELFs) as a function of energy loss for GaAs and InSb. (a) ε_2 for GaAs. The solid and dotted lines show calculated ε_2 values from the WIEN2k and FEFF codes, respectively. The solid circles indicate experimental data from Henke *et al.*[60]. (b) ε_2 for InSb. See caption to (a). (c) ELFs for GaAs. The solid line shows the optical ELF calculated from the WIEN2k code. The dot-dashed line is the ELF for GaAs measured by Jin *et al.*[63] and the dotted line is the ELF determined by Chen *et al.*[62]. The solid circles show the ELF from the optical data tabulated by Palik.[45] (d) ELFs for InSb. The solid line is the optical ELF from the WIEN2k code. The short-dashed line is the ELF measured by Festenberg *et al.*[61] The solid circles show the ELF from the optical data tabulated by Palik.[45]

Author Manuscript:
Published in final edited form as: *Surf. Interface Anal*. Volume 51, Issue 4, Pages 427-457, April 2019
https://doi.org/10.1002/sia.6598

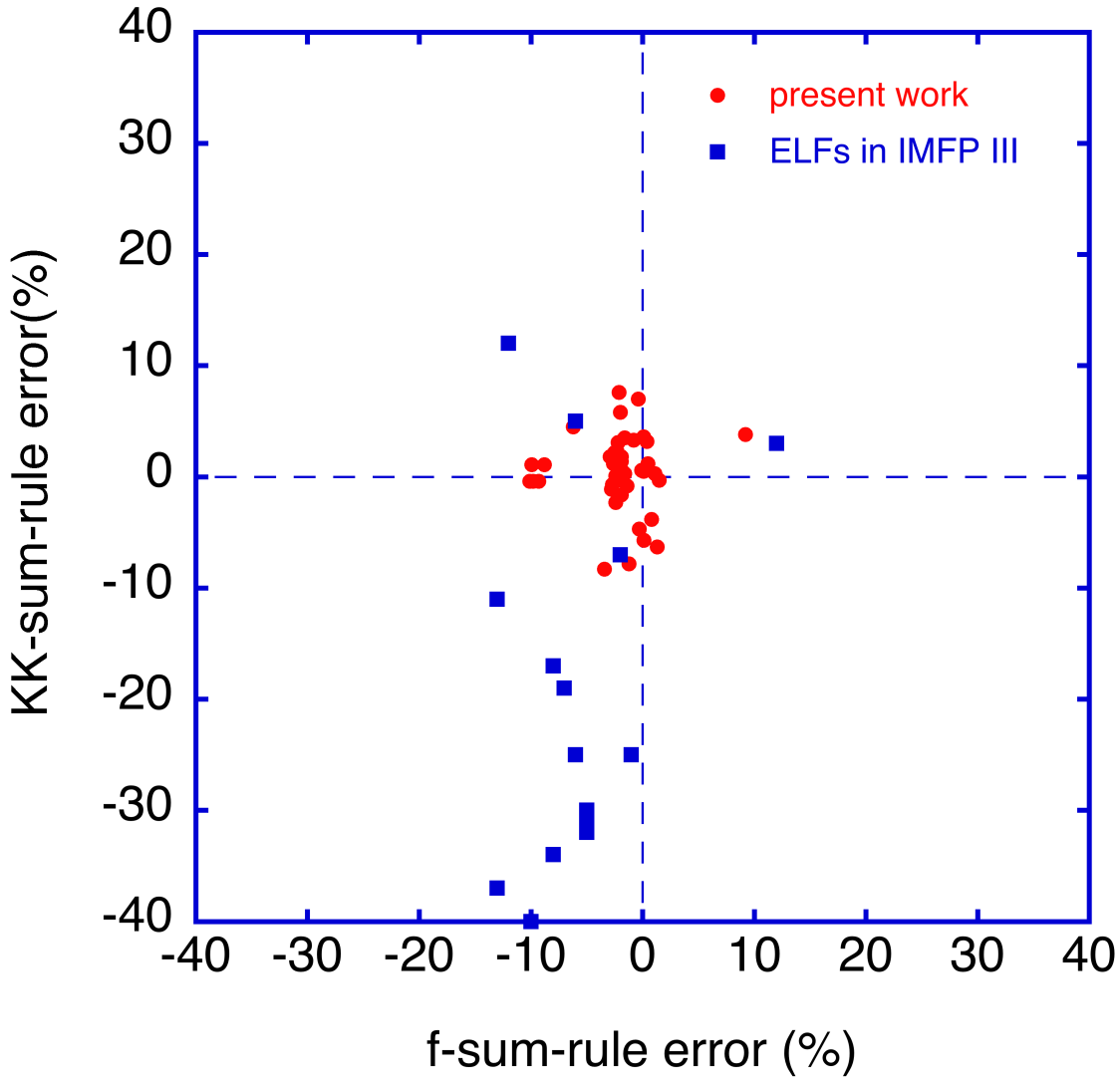

Figure 2. Plots of KK-sum rule errors *versus* f-sum rule errors for our group of 42 inorganic compounds (solid circles) and for the 15 compounds in our previous work (solid squares) [5].

Author Manuscript:
Published in final edited form as: *Surf. Interface Anal.* Volume 51, Issue 4, Pages 427-457, April 2019
https://doi.org/10.1002/sia.6598

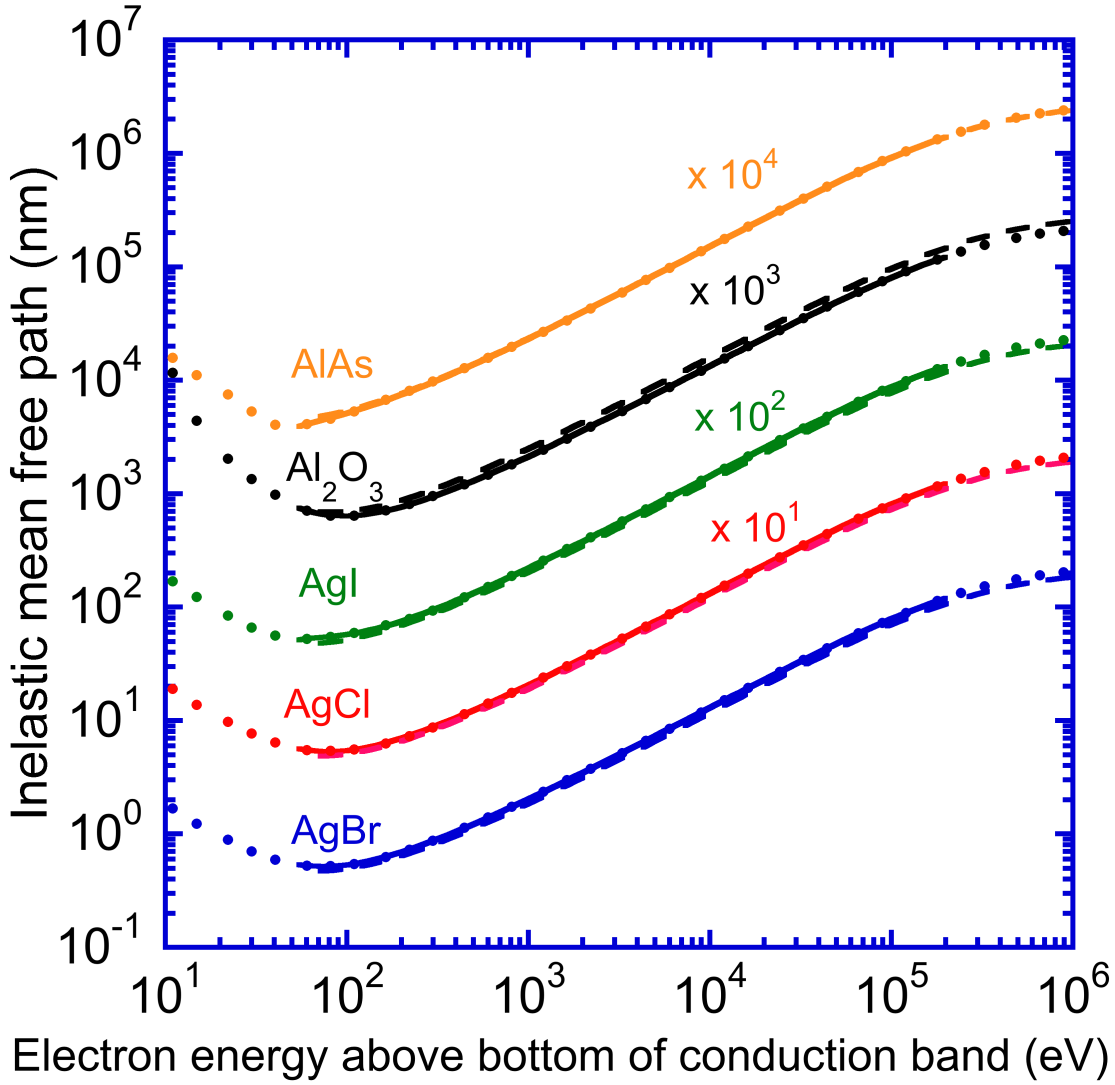

Figure 3. Plots of our calculated inelastic mean free paths as a function of electron kinetic energy for AgBr, AgCl, AgI, Al_2O_3, and AlAs. The solid circles show calculated IMFPs from the relativistic full Penn algorithm (Table 5). The solid lines show fits to these IMFPs with the relativistic modified Bethe equation [Eqns (12) and (13)] and the derived parameters are listed in Table 6. The long-dashed lines indicate IMFPs calculated from the relativistic TPP-2M equation [Eqns (12), (13) and (15)].

Author Manuscript:
Published in final edited form as: *Surf. Interface Anal*. Volume 51, Issue 4, Pages 427-457, April 2019
https://doi.org/10.1002/sia.6598

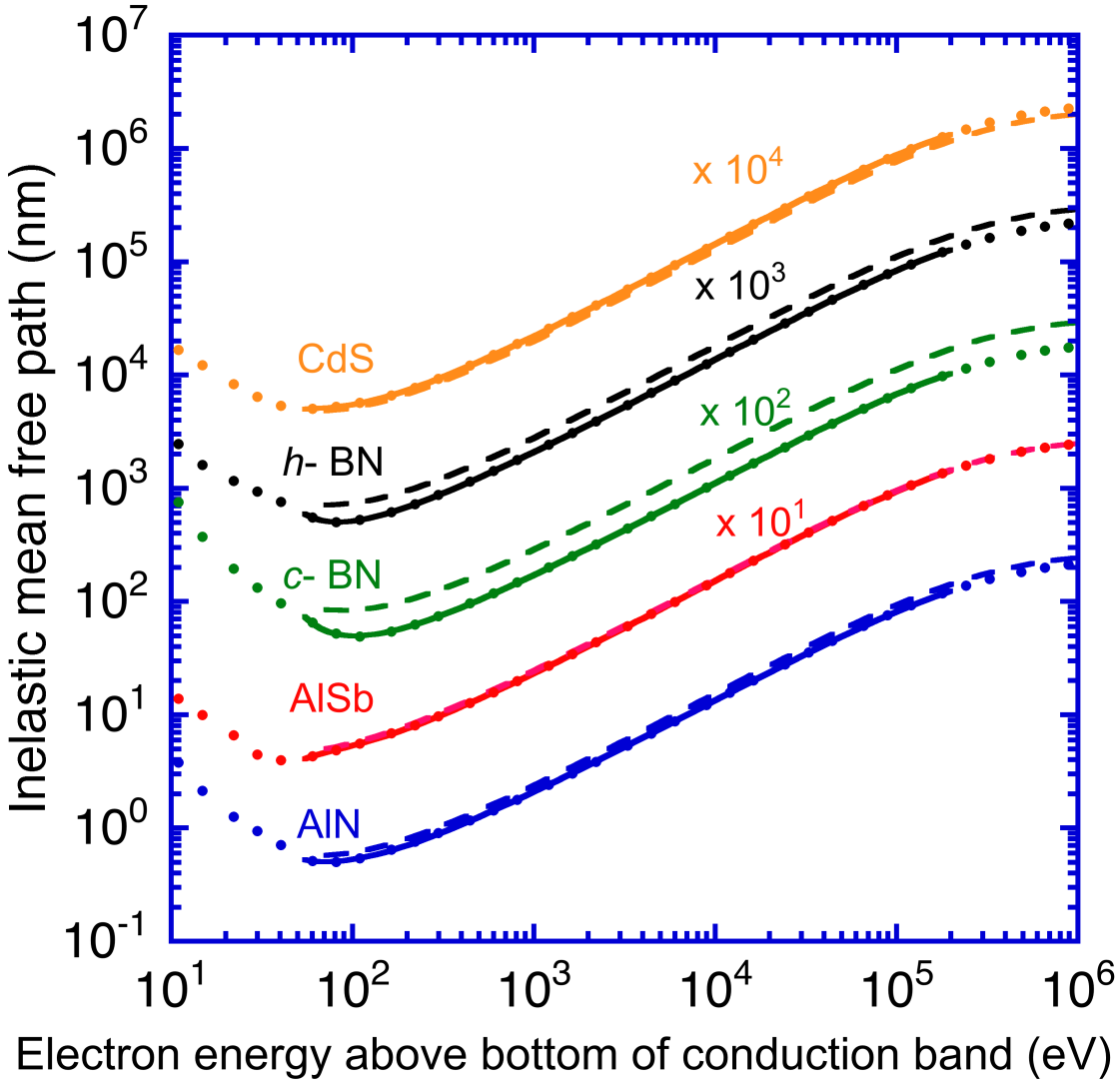

Figure 4. Plots of calculated electron inelastic mean free paths as a function of electron kinetic energy for AlN, AlSb, *c*-BN, *h*-BN, and CdS. See caption to Fig. 3.

Author Manuscript:
Published in final edited form as: *Surf. Interface Anal*. Volume 51, Issue 4, Pages 427-457, April 2019
https://doi.org/10.1002/sia.6598

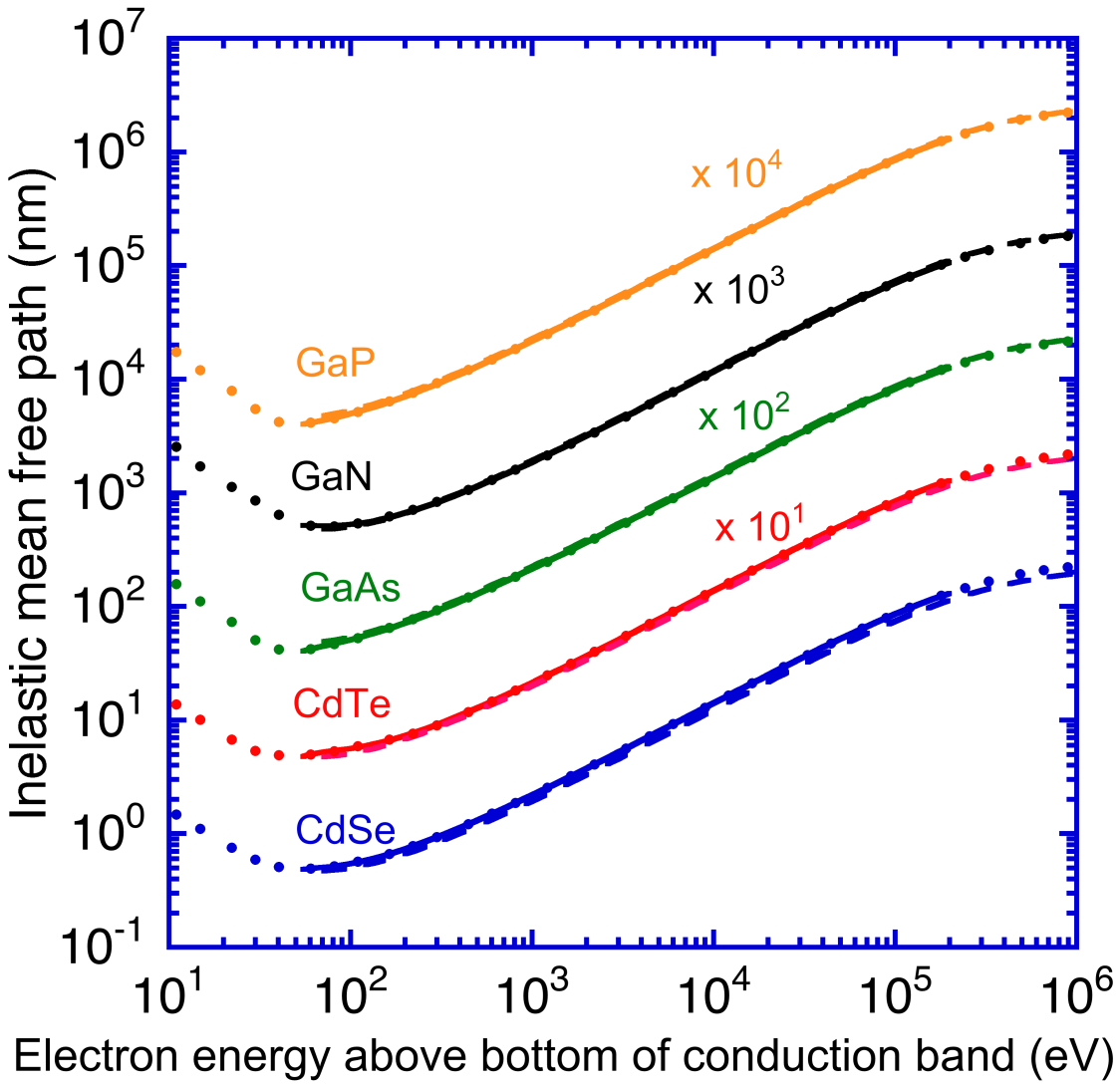

Figure 5. Plots of calculated electron inelastic mean free paths as a function of electron kinetic energy for CdSe, CdTe, GaAs, GaN, and GaP. See caption to Fig. 3.

Author Manuscript:
Published in final edited form as: *Surf. Interface Anal*. Volume 51, Issue 4, Pages 427-457, April 2019
https://doi.org/10.1002/sia.6598

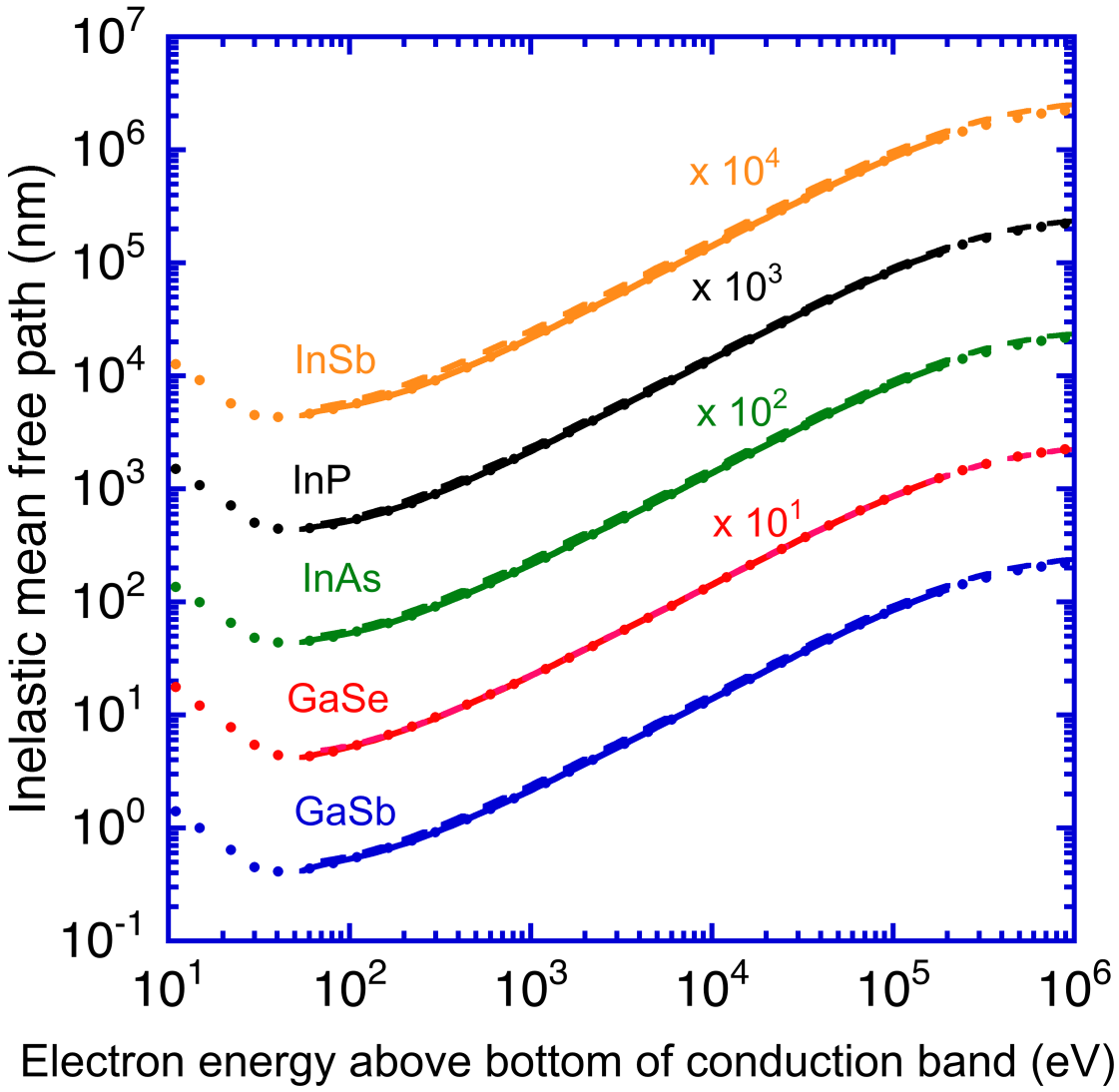

Figure 6. Plots of calculated electron inelastic mean free paths as a function of electron kinetic energy for GaSb, GaSe, InAs, InP, and InSb. See caption to Fig. 3.

Author Manuscript:
Published in final edited form as: *Surf. Interface Anal*. Volume 51, Issue 4, Pages 427-457, April 2019
https://doi.org/10.1002/sia.6598

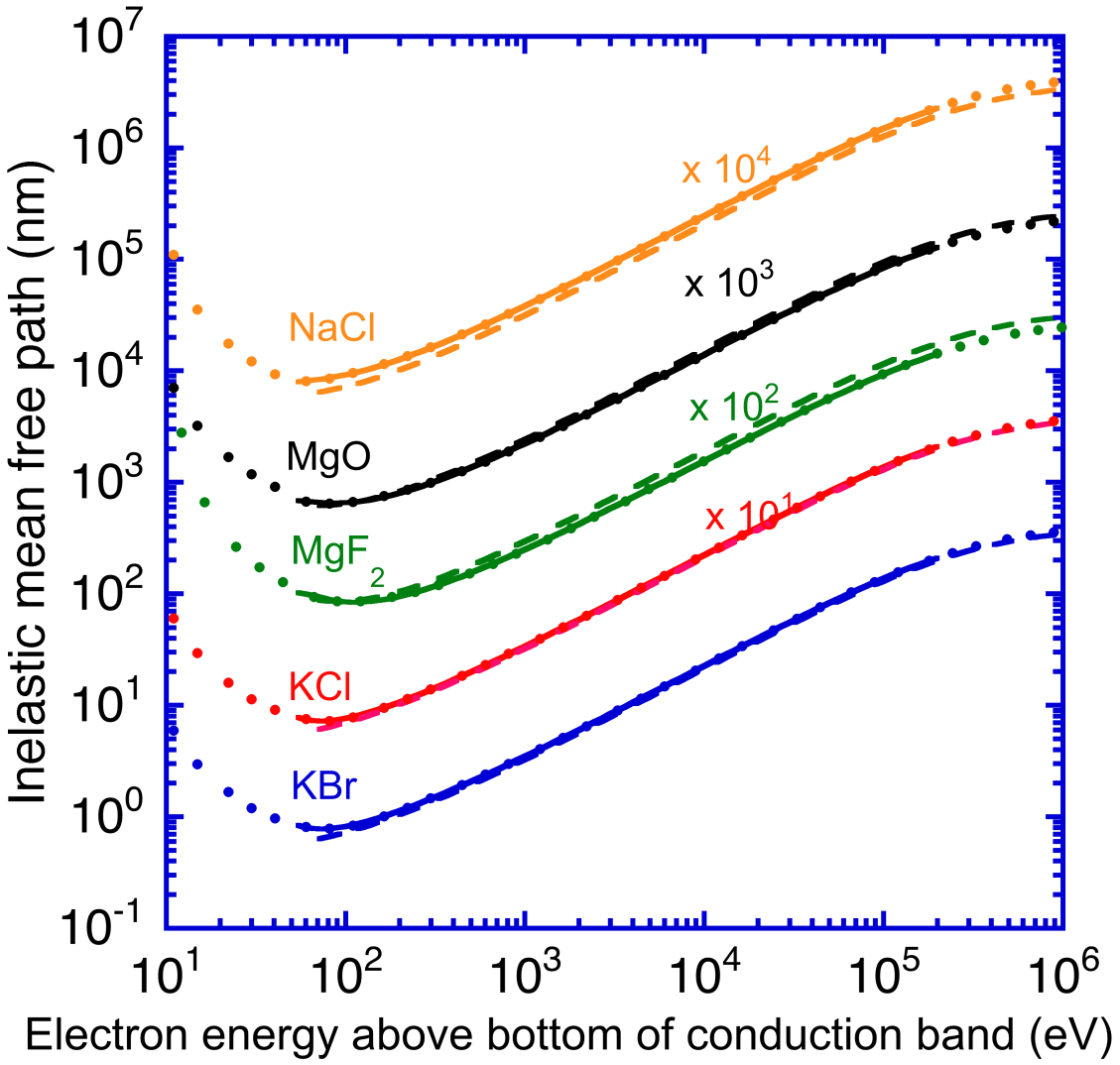

Figure 7. Plots of calculated electron inelastic mean free paths as a function of electron kinetic energy for KBr, KCl, MgF_2, MgO, and NaCl. See caption to Fig. 3.

Author Manuscript:
Published in final edited form as: *Surf. Interface Anal.* Volume 51, Issue 4, Pages 427-457, April 2019
https://doi.org/10.1002/sia.6598

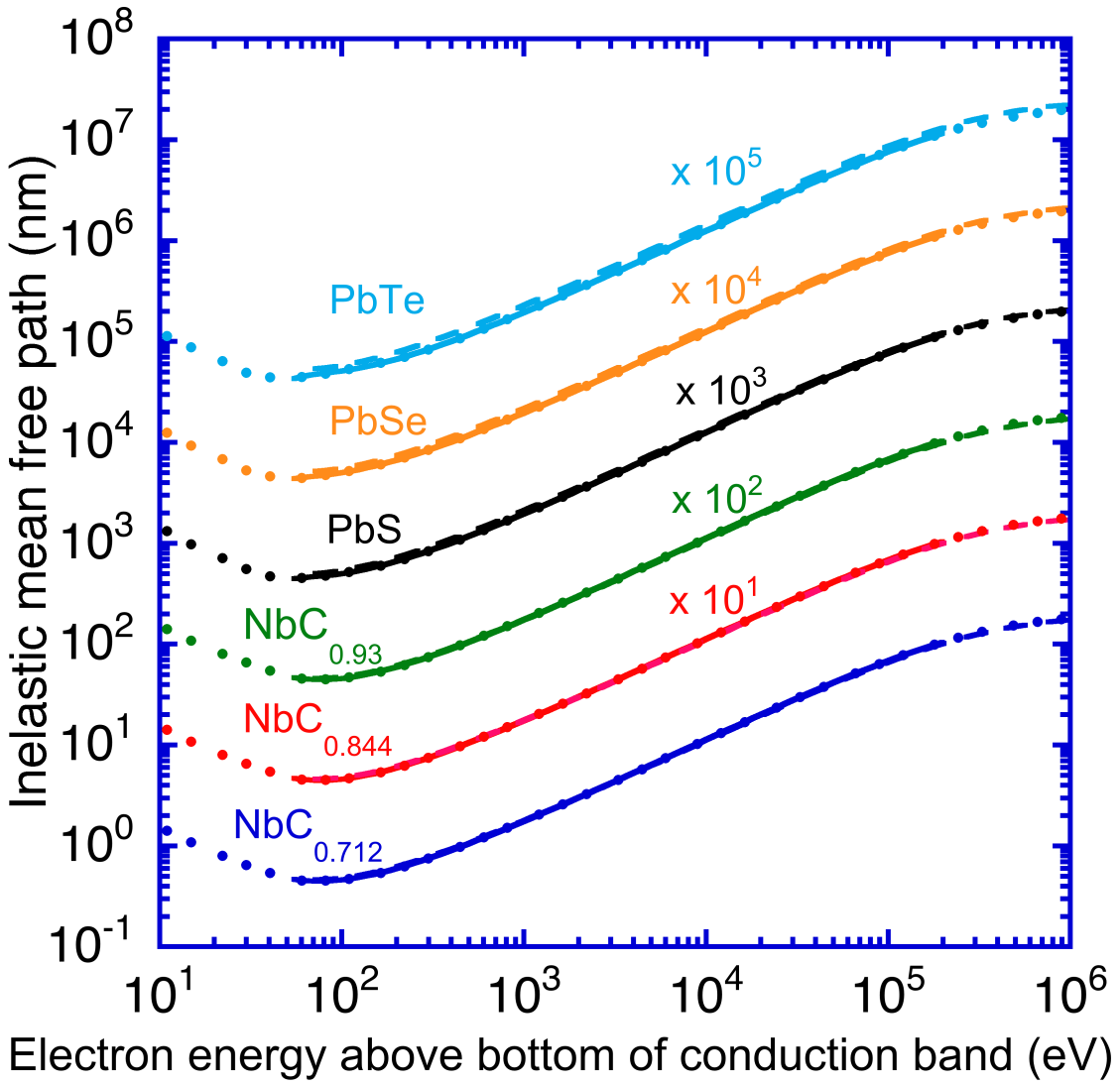

Figure 8. Plots of calculated electron inelastic mean free paths as a function of electron kinetic energy for $NbC_{0.712}$, $NbC_{0.844}$, $NbC_{0.93}$, PbS, PbSe, and PbTe. See caption to Fig. 3.

Author Manuscript:
Published in final edited form as: *Surf. Interface Anal*. Volume 51, Issue 4, Pages 427-457, April 2019
https://doi.org/10.1002/sia.6598

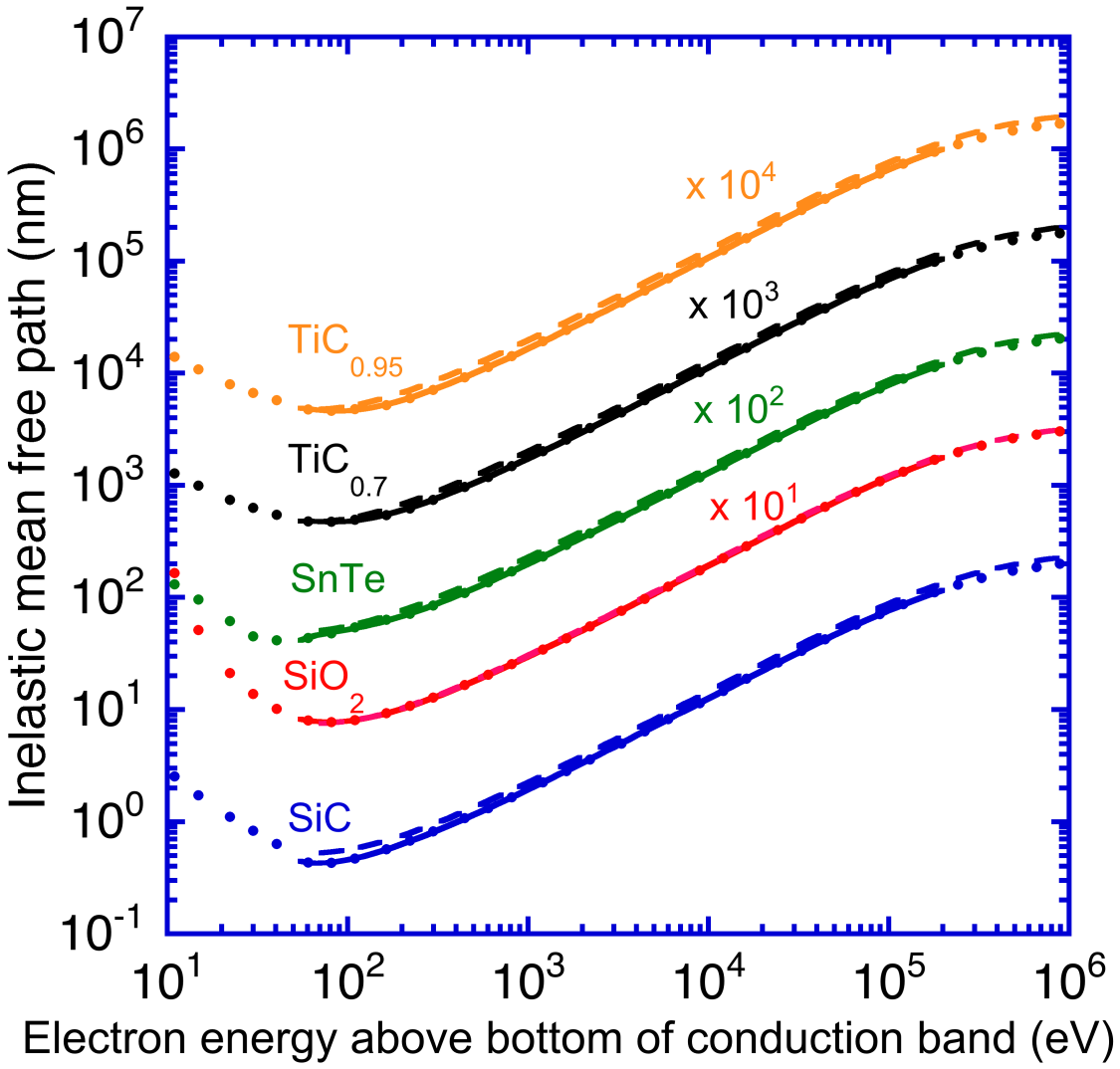

Figure 9. Plots of calculated electron inelastic mean free paths as a function of electron kinetic energy for SiC, SiO_2, SnTe, $TiC_{0.7}$, and$TiC_{0.95}$. See caption to Fig. 3.

Author Manuscript:
Published in final edited form as: *Surf. Interface Anal*. Volume 51, Issue 4, Pages 427-457, April 2019
https://doi.org/10.1002/sia.6598

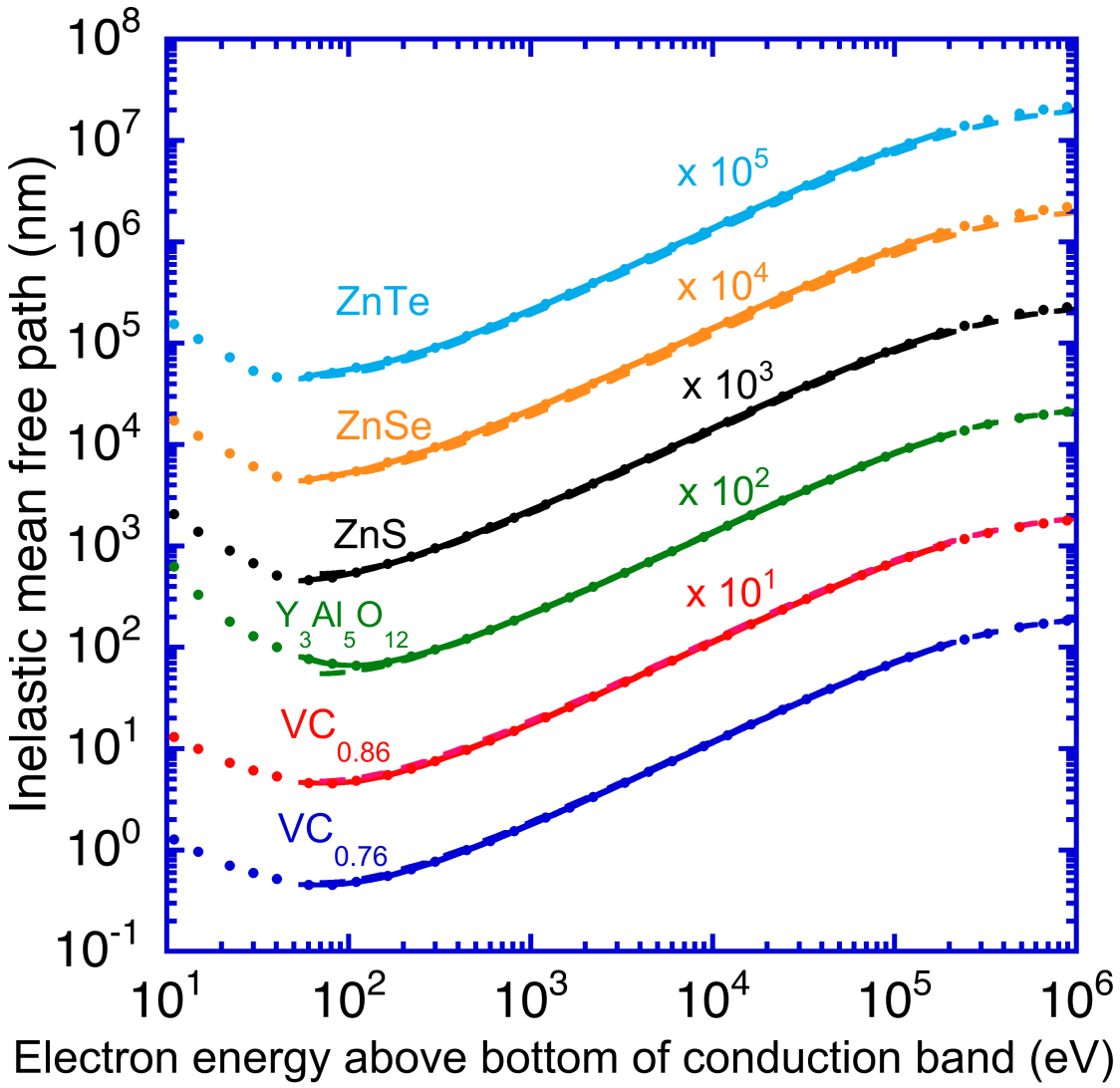

Figure 10. Plots of calculated electron inelastic mean free paths as a function of electron kinetic energy for $VC_{0.76}$, $VC_{0.86}$, $Y_3Al_5O_{12}$; YAG, ZnS, ZnSe, and ZnTe. See caption to Fig. 3.

Author Manuscript:
Published in final edited form as: *Surf. Interface Anal.* Volume 51, Issue 4, Pages 427-457, April 2019
https://doi.org/10.1002/sia.6598

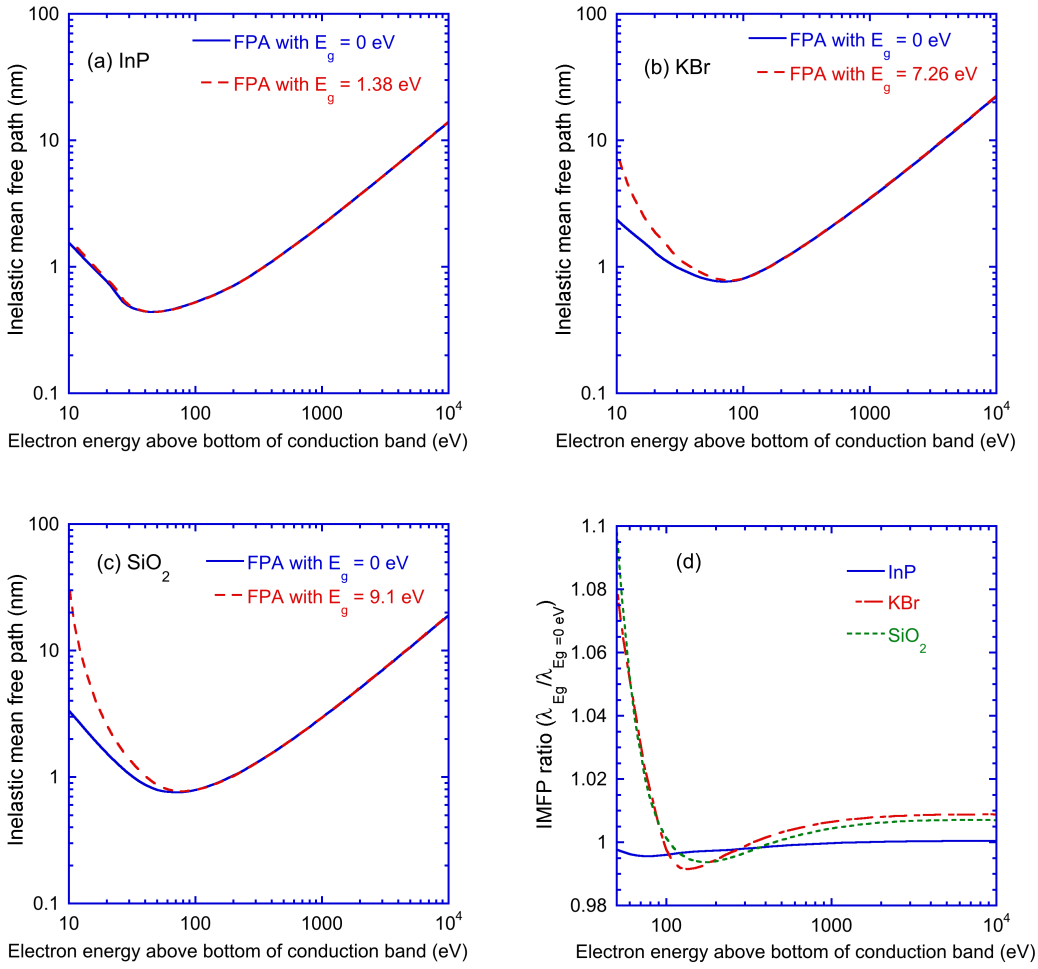

Figures 11. Plots of calculated electron inelastic mean free paths from the FPA-Boutboul approach (dashed lines) and from the FPA with E_g assumed to be zero (solid lines) for (a) InP, (b) KBr, and (c) SiO_2 as a function of electron kinetic energy between 10 eV and 10 keV.

(d) Ratios of IMFPs calculated from the FPA-Boutboul method to those from the FPA with E_g assumed to be zero for InP, KBr, and SiO_2 as a function of electron energy between 50 eV and 10 keV.

Author Manuscript:
Published in final edited form as: *Surf. Interface Anal*. Volume 51, Issue 4, Pages 427-457, April 2019
https://doi.org/10.1002/sia.6598

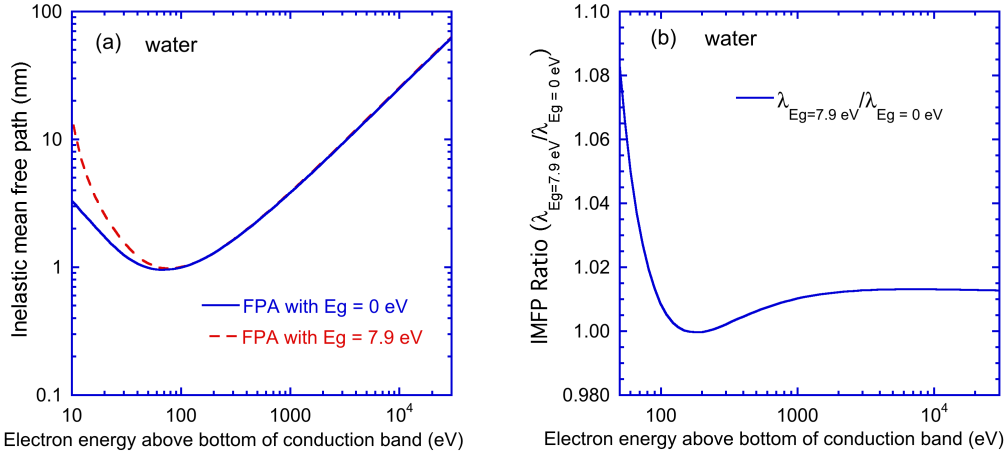

Figure 12. (a) Plots of calculated electron inelastic mean free paths for water from the FPA-Boutboul approach with E_g = 7.9 eV (dashed line) and from the FPA with E_g assumed to be zero (solid line) as a function of electron kinetic energy between 10 eV and 30 keV.
(b) Ratios of IMFPs calculated for water from the FPA-Boutboul method to those from the FPA with E_g assumed to be zero as a function of electron energy between 50 eV and 30 keV.

Author Manuscript:
Published in final edited form as: *Surf. Interface Anal*. Volume 51, Issue 4, Pages 427-457, April 2019
https://doi.org/10.1002/sia.6598

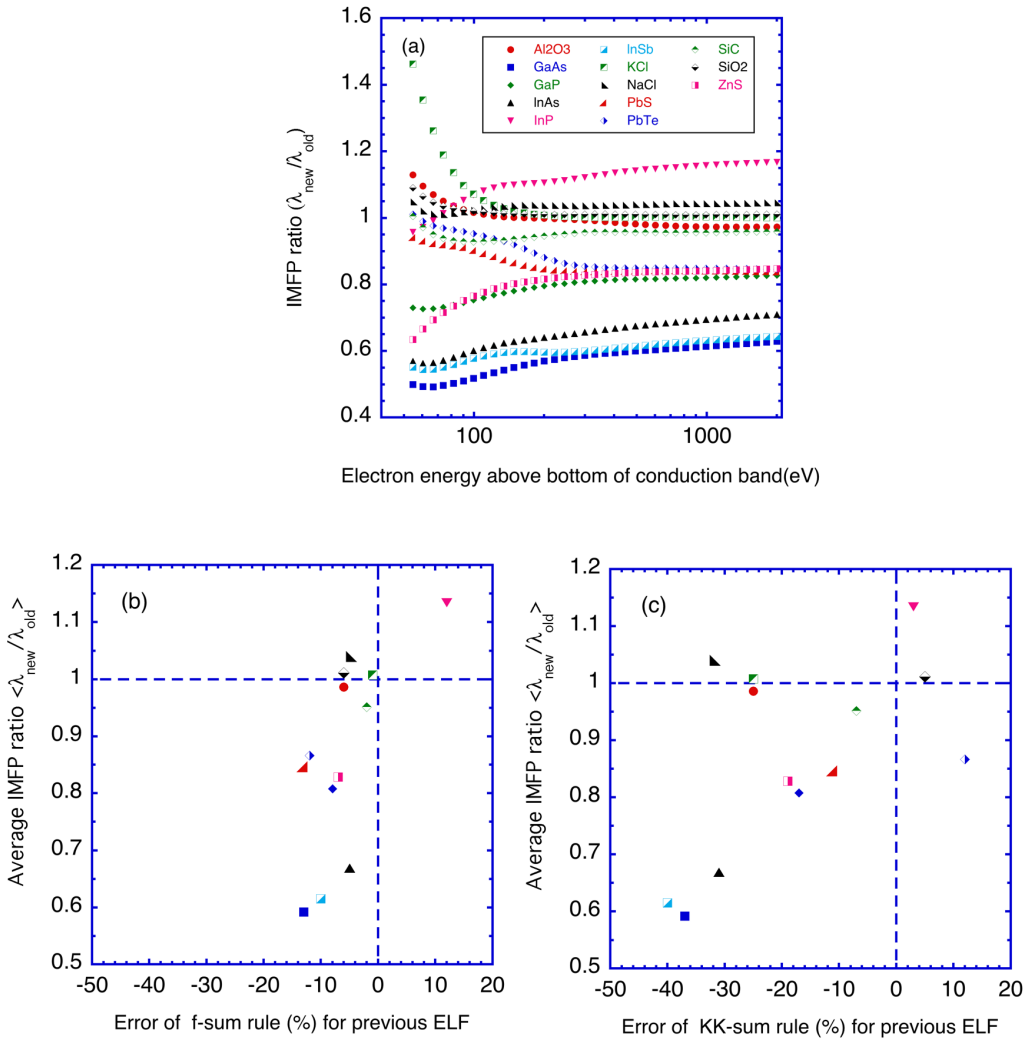

Figure 13. (a) Plots of ratios of IMFPs for 13 inorganic compounds with the newer ELFs to the corresponding previous IMFPs [5]. (b) Averages of the IMFP ratios, $<\lambda_{new}/\lambda_{old}>$, for each compound as a function of the f-sum rule errors for the previous ELFs. (c) Averages of the IMFP ratios, $<\lambda_{new}/\lambda_{old}>$, for each compound as a function of the KK-sum rule errors for the previous ELFs.

Author Manuscript:
Published in final edited form as: *Surf. Interface Anal*. Volume 51, Issue 4, Pages 427-457, April 2019
https://doi.org/10.1002/sia.6598

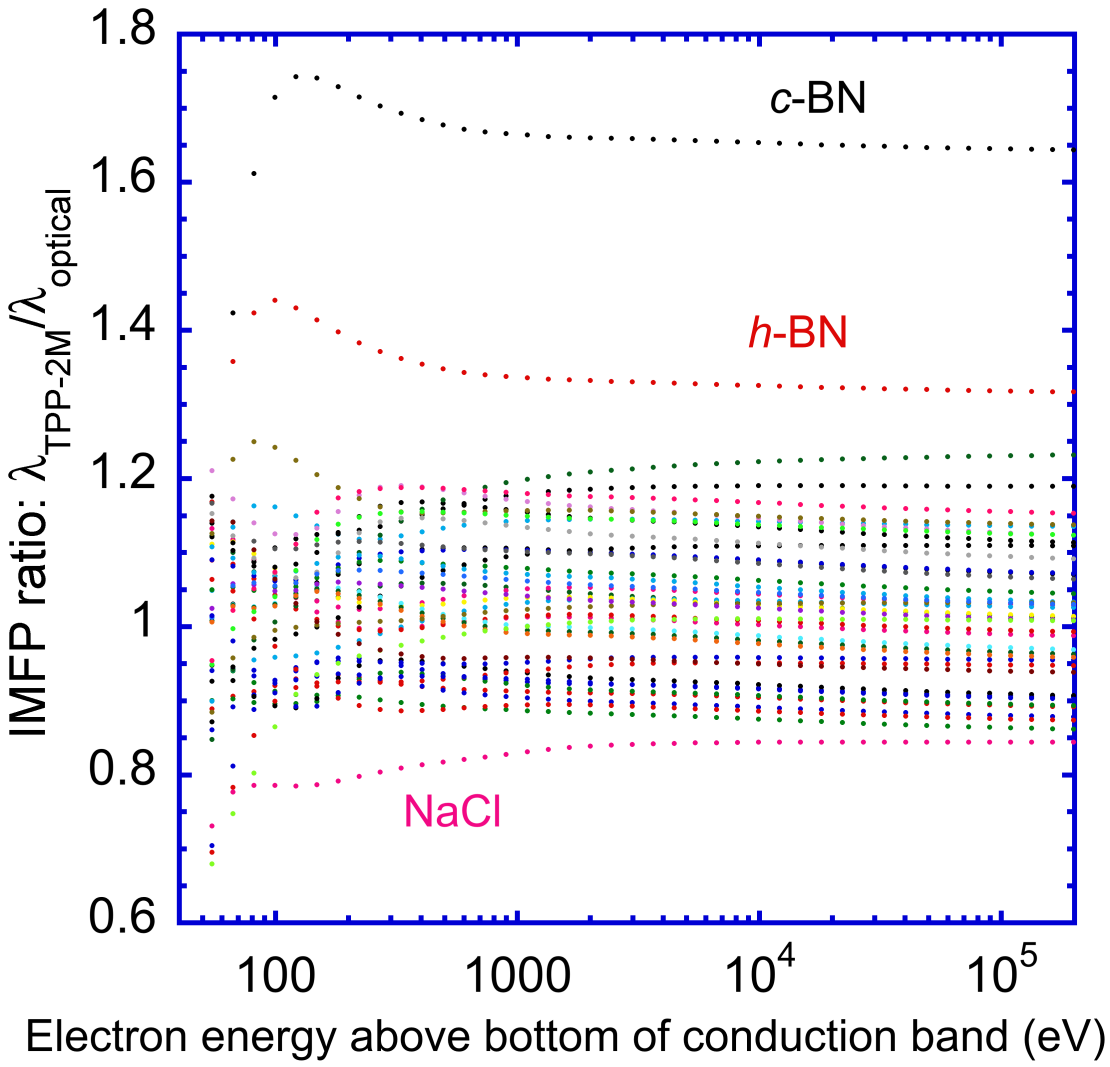

Figure 14. Ratio of IMFPs calculated from the relativistic TPP-2M equation [Eqns (12), (13), and (15)] to IMFPs calculated from optical data as a function of electron energy for our 42 inorganic compounds.

Author Manuscript:
Published in final edited form as: *Surf. Interface Anal.* Volume 51, Issue 4, Pages 427-457, April 2019
https://doi.org/10.1002/sia.6598

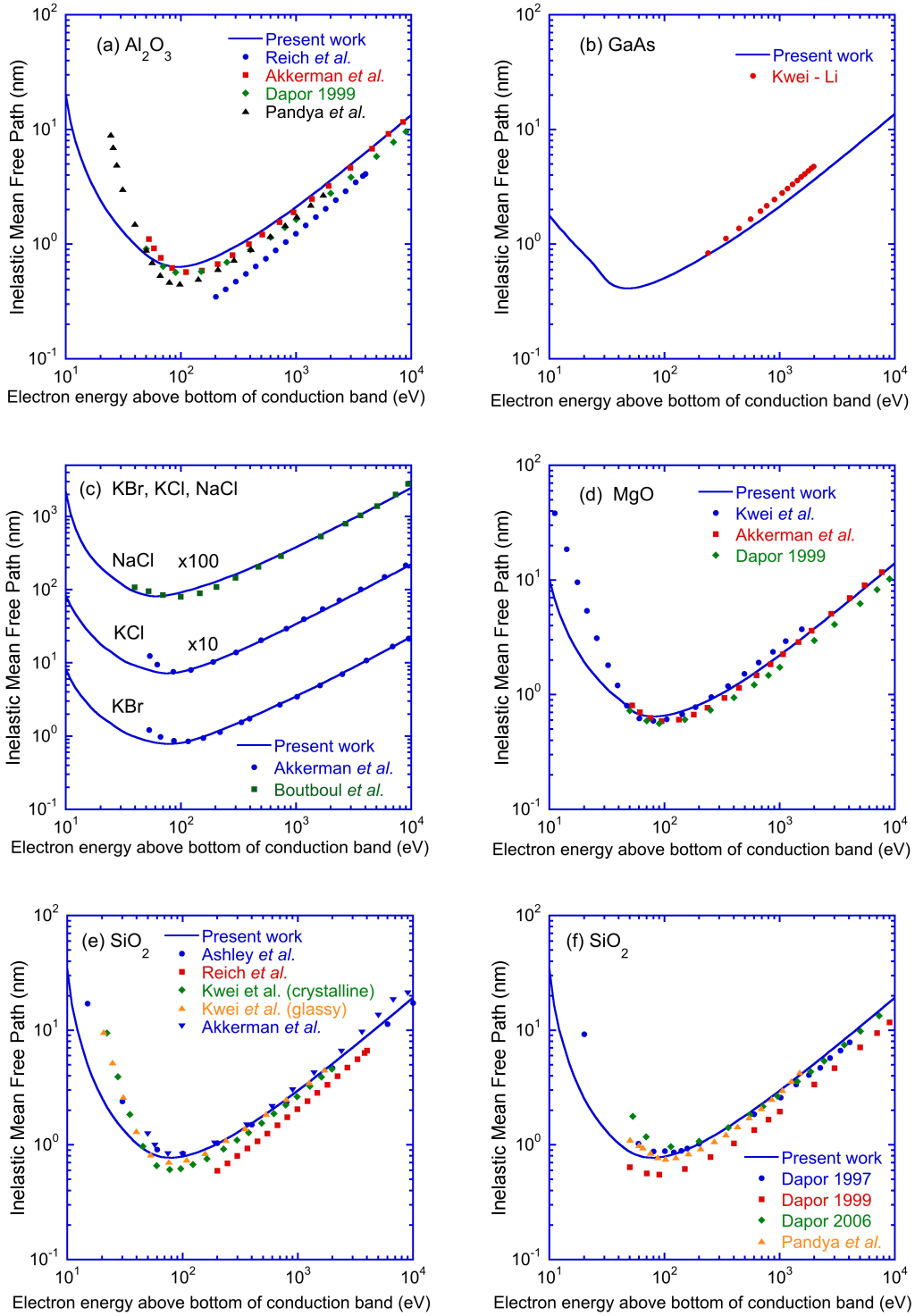

Figure 15. Comparison of our calculated IMFPs with IMFPs from other calculations for

Author Manuscript:
Published in final edited form as: *Surf. Interface Anal*. Volume 51, Issue 4, Pages 427-457, April 2019
https://doi.org/10.1002/sia.6598

(a) Al_2O_3, (b) GaAs, (c) KBr, KCl, and NaCl, (d) MgO, (e) SiO_2, and (f) SiO_2 for energies between 10 eV and 10 keV. The solid lines show our IMFPs that were calculated from optical ELFs with the FPA. The symbols indicate IMFPs calculated by Reich *et al.*[14] (for Al_2O_3 and SiO_2), Akkerman *et al.*[15] (for Al_2O_3, KBr, KCl, MgO, and SiO_2), Pandya *et al.*[16] (for Al_2O_3 and SiO_2), Kwei and Li [17] (for GaAs), Boutboul *et al.*[19] (for NaCl), Kwei *et al.*[18] (for MgO, glassy SiO_2 and crystalline SiO_2), Ashley and Anderson [20] (for SiO_2), Dapor and Miotello[21] (for Al_2O_3, MgO, and SiO_2), Dapor and Miotello[22] (for SiO_2), and Dapor[23](for SiO_2).

Author Manuscript:
Published in final edited form as: *Surf. Interface Anal*. Volume 51, Issue 4, Pages 427-457, April 2019
https://doi.org/10.1002/sia.6598

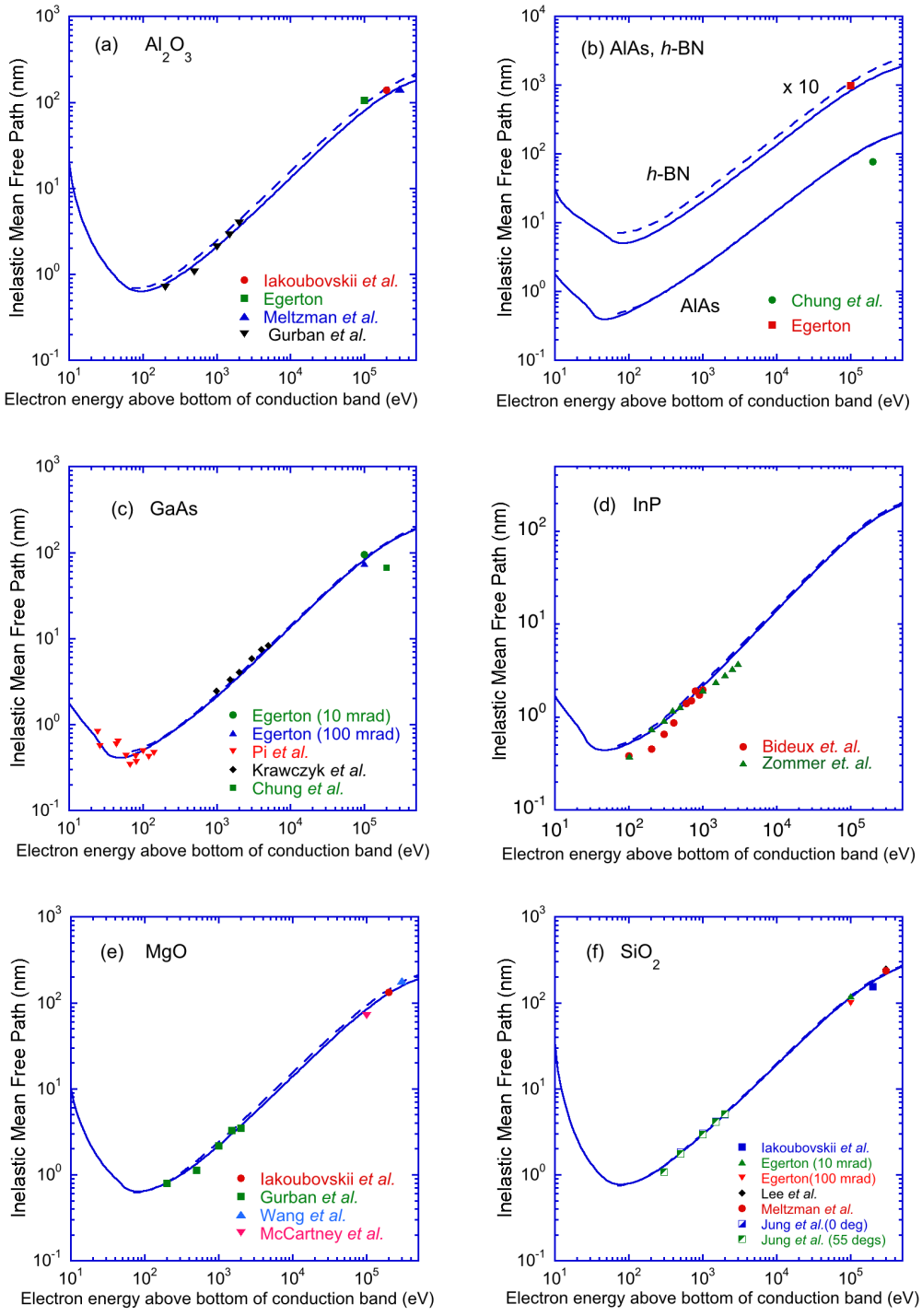

Figure 16. Comparison of our calculated IMFPs for (a) Al_2O_3, (b) AlAs and *h*-BN, (c) GaAs, (d) InP, (e) MgO, and (f) SiO_2 for energies between 10 eV and 500 keV. The solid lines show our IMFPs that were calculated from the FPA. The long-

Author Manuscript:
Published in final edited form as: *Surf. Interface Anal*. Volume 51, Issue 4, Pages 427-457, April 2019
https://doi.org/10.1002/sia.6598

dashed lines indicate IMFPs calculated with the relativistic TPP-2M equation [Eqns (12), (13) and (15)]. The symbols indicate IMFPs measured by Iakoubovskii *et al.*[24] (for Al_2O_3, MgO, and SiO_2), Egerton[25, 26] (for Al_2O_3, *h*-BN, GaAs, and SiO_2), Meltzman *et al.* [27] (for Al_2O_3 and SiO_2), Gurban *et al.*[28] (for Al_2O_3 and MgO), Chung *et al.*[31] (for AlAs and GaAs), Pi *et al.*[29] (for GaAs), Krawczyk *et al.*[30] (for GaAs), Bideux *et al.*[35] (for InP), Zommer *et al.*[36] (for InP), Wang *et al.*[32] (for MgO), McCartney *et al.*[33] (for MgO), Lee *et al*.[34] (for SiO_2), and Jung *et al.* [37] (for SiO_2).

Author Manuscript:
Published in final edited form as: *Surf. Interface Anal*. Volume 51, Issue 4, Pages 427-457, April 2019
https://doi.org/10.1002/sia.6598

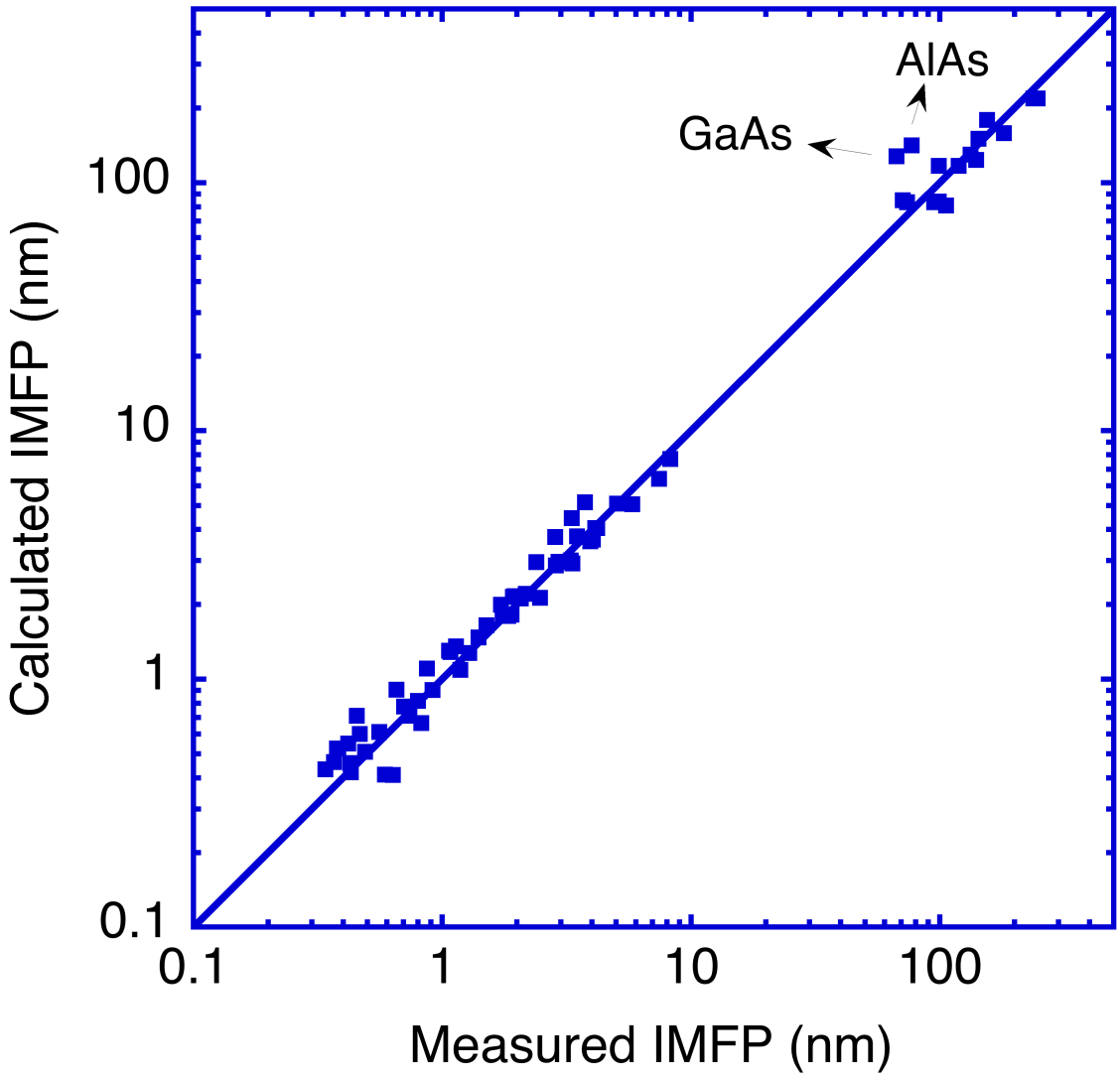

Figure 17. Plots of our calculated IMFPs as a function of measured IMFPs for Al_2O_3, AlAs, *h*-BN, GaAs, InP, MgO, and SiO_2 shown in Fig. 16 for energies between 24 eV and 300 keV. The solid line indicates perfect correlation between the calculated and measured IMFPs.

Author Manuscript:
Published in final edited form as: *Surf. Interface Anal*. Volume 51, Issue 4, Pages 427-457, April 2019
https://doi.org/10.1002/sia.6598

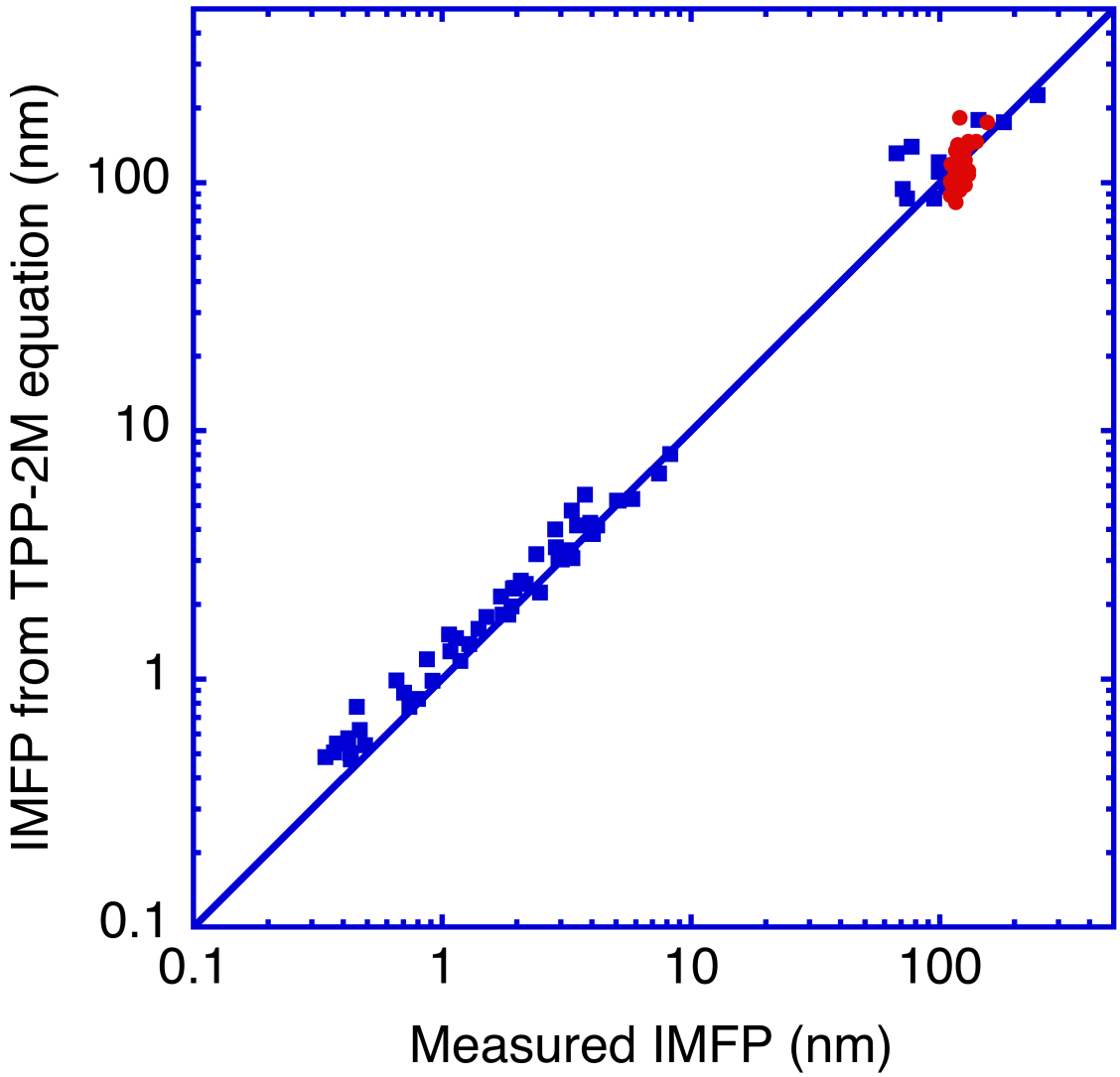

Figure 18. Plots of IMFPs calculated from the relativistic TPP-2M equation [Eqns (12), (13) and (15)] as a function of measured IMFPs for the seven compounds (solid squares) shown in Fig. 16 and for the 37 oxides (solid circles) measured by Iakoubovskii *et al.*[24] (B_2O_3, CaO, Sc_2O_3, TiO, V_2O_5, CrO_3, Fe_2O_3, CoO, NiO, ZnO, GeO_2, SeO_2, SrO, Y_2O_3, ZrO_2, MoO_3, PdO, Ag_2O, SnO_2, TeO_2, BaO, La_2O_3, Ce_2O_3, Pr_2O_3, Nd_2O_3, Sm_2O_3, Eu_2O_3, Gd_2O_3, Tb_2O_3, Dy_2O_3, Ho_2O_3, Er_2O_3, Yb_2O_3, WO_3, HgO, PbO, Bi_2O_3) for energies between 50 eV and 300 keV. The solid line indicates perfect correlation between the calculated and measured IMFPs.

Author Manuscript:
Published in final edited form as: *Surf. Interface Anal*. Volume 51, Issue 4, Pages 427-457, April 2019
https://doi.org/10.1002/sia.6598

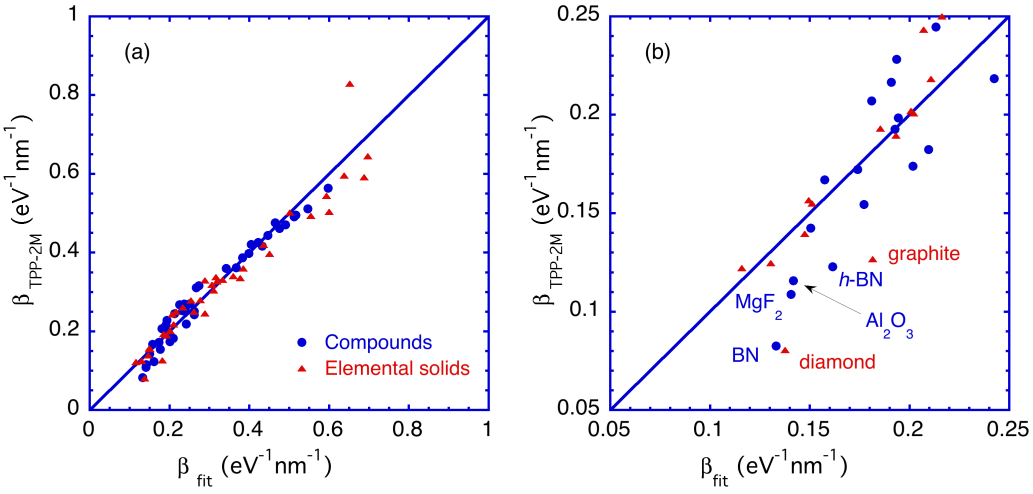

Figure 19. Values of β for TPP-2M calculated from Eqn (15a), $\beta_{\text{TPP-2M}}$, as a function of β values obtained by the fit to the IMFPs, β_{fit}, with Eqns (12) and (13) (Table 5). The solid line indicates perfect correlation between the calculated and fitted β values. The solid circles and squares show our results for compounds (present work) and elemental solids[8], respectively.

Author Manuscript:
Published in final edited form as: *Surf. Interface Anal.* Volume 51, Issue 4, Pages 427-457, April 2019
https://doi.org/10.1002/sia.6598

References

[1] C. J. Powell, A. Jablonski, *Nucl. Instrum. Meth. Phys. Res.* A. **2005**, 601, 54.
[2] C. J. Powell, A. Jablonski, *J. Electron Spectrosc. Relat. Phenom.* **2010**, 178-179, 331.
[3] S. Tanuma, C. J. Powell, D. R. Penn, *Surf. Interface Anal.*, **1988**, 11, 577.
[4] S. Tanuma, C. J. Powell, D. R. Penn, *Surf. Interface Anal.*, **1991**, 17, 911.
[5] S. Tanuma, C. J. Powell, D. R. Penn, *Surf. Interface Anal.*, **1991**, 17, 927.
[6] S. Tanuma, C. J. Powell, D. R. Penn, *Surf. Interface Anal.*, **1994**, 21, 165.
[7] S. Tanuma, C. J. Powell, D. R. Penn, *Surf. Interface Anal.,* **2011**, 43, 689.
[8] H. Shinotsuka, S. Tanuma, C. J. Powell, D. R. Penn, *Surf. Interface Anal.* **2015**, 47, 871; *ibid*, *Surf. Interface Anal.,* **2015**, 47, 1132.
[9] D. R. Penn, *Phys. Rev. B* **1987**, 35, 482.
[10] H. Bethe, *Ann. Phys.* **1930**, 5, 325.
[11] http://www.wien2k.at/; P. Blaha, K. Schwarz, G. K. H. Madsen, D. Kvasnicka, J. Luitz, WIEN2k, An Augmented Plane Wave + Local Orbitals Program for Calculating Crystal Properties (Karlheinz Schwarz, Tech. Universität Wien, Austria), 2001. ISBN 3-9501031-1-2.
[12] http://feffproject.org/; A. L. Ankudinov, C. Bouldin, J. J. Rehr, J. Sims, H. Hung, *Phys. Rev. B* 65, 104107 (2002).
[13] W. S. M. Werner, K. Glantschnig, C. Ambrosch-Draxl, J. Phys. Chem. Ref. Data **2009**, *38*, 1013.
[14] T. Reich, V. G. Yarzhemski, V. I. Nefedov, *J. Electron Spectrosc. Relat. Phenom.* **1988**, 46, 255.
[15] A. Akkerman, T. Boutboul, A. Breskin, R. Chechik, A. Gibrekhterman, Y. Lifshitz, *Phys. Stat. Sol. B* **1996**, 198, 769.
[16] S. H. Pandya, B. G. Vaishnav, and K. N. Joshipura, *Chinese Physics B* **2012**, 21, 093402.
[17] C. M. Kwei and Y. C. Li, *Appl. Surf. Science* **2004**, 238, 151.
[18] C. M. Kwei, Y. F. Chen, C. J. Tung, and J. P. Wang, *Surf. Science* **1993**, 293, 202.
[19] T. Boutboul, A. Akkerman, A. Breskin, and R. Chechik, *J. Appl. Phys.* **1996**, 79, 6714.
[20] J. C. Ashley, V. E. Anderson, *J. Electron Spectrosc. Relat. Phenom.* **1981,** 24, 127.
[21] M. Dapor and A. Miotello, *European Physical Journal Applied Physics* **1999**, 5, 143.
[22] M. Dapor and A. Miotello, *Phys. Rev. B* **1997**, 56, 2234.
[23] M. Dapor, *J. Electron Spectrosc. Relat. Phenom.* **2006**, 151, 182.
[24] K. Iakoubovskii, K. Mitsuishi, Y. Nakayama, K. Furuya, *Phys. Rev. B* **2008**, 77, 104102.

Author Manuscript:
Published in final edited form as: *Surf. Interface Anal.* Volume 51, Issue 4, Pages 427-457, April 2019
https://doi.org/10.1002/sia.6598

[25] R.F. Egerton, A data base for energy-loss cross sections and mean free paths. In *50th Ann. Proc. Electron Microsc. Soc. Am.*, San Francisco Press, San Francisco, CA, pp. 1264 - 1265.

[26] R. F. Egerton, *Electron Energy-Loss Spectroscopy in the Electron Microscope*, third edition, Springer, New York, **2011**.

[27] H. Meltzman, Y. Kauffmann, P. Thangadurai, M. Drozdov, M. Baram, D. Brandon, W. D. Kaplan, *Journal of Microscopy* **2009**, 236, 165.

[28] S. Gurban, G. Gergely, J. Toth, D. Varga, A. Jablonski, M. Menyhard, *Surf. Interface Anal.* **2006**, 38, 624.

[29] T.-W. Pi, B.-R. Chen, M.-L. Huang, T.-H. Chiang, G. K. Wertheim, M. Hong, J. Kwo. *J. Phys. Soc. Jpn.* **2012**, 81, 064603.

[30] M. Krawczyk, A. Jablonski, S. Tougaard, J. Toth, D. Varga, G. Gergely, *Surface Science* **1988**, 402–404, 491.

[31] S. Chung, D. J. Smith, M. R. McCartney, *Microscopy and Microanalysis* **2007**, 13, 329.

[32] Z. L Wang, A. J. Shapiro, *Ultramicroscopy* **1995**, 60, 115.

[33] M. R. McCartney, M. Gajdardziska-Josifovska, *Ultramicroscopy* **1994**, 53, 283.

[34] C.W. Lee, Y. Ikematsu, D. Shindo, *J. Electron Microsc.* **2002**, 51, 143.

[35] L. Bideux, C. Robert, S. Merle, B. Gruzza, E. Goumet, E. Gil-Lafon, *Surf. Interface Anal.* **1998**, 26, 903.

[36] L. Zommer, B. Lesiak, A. Jablonski, G. Gergely, M. Menyhard, A. Sulyok, S. Gurban, *J. Electron Spectrosc. Relat. Phenom.* **1998**, 87, 177.

[37] R. Jung, J.C. Lee, G.T. Orosz, A. Sulyok, G. Zsolt, M. Menyhard, *Surf. Sci.*, **2003**, 543, 153.

[38] J. M. Fernandez-Varea, F. Salvat, M. Dingfelder, D. Liljequist, *Nucl. Instrum. Meth. Phys. Res.* B **2005**; 229, 187.

[39] J. M. Fernandez-Varea, D. Liljequist, S. Csillag, R. Raty, F. Salvat, *Nucl. Instrum. Methods Phys. Res. B* **1996**, 108, 35.

[40] U. Fano, *Ann. Rev. Nucl. Sci.***, 1963**, 13, 1.

[41] J. Lindhard, *K. Dan. Vidensk. Selsk. Mat.-Fys. Medd.* **1954** , 28(8), 1.

[42] W. H. Strehlow, E. L. Cook, *J. Phys. Chem. Ref. Data*, **1973**, 2, 163.

[43] I. Vurgaftman, J.R. Meyer, L. R. Ram-Mohan, *J. Appl. Phys.* **2001**, 89, 5815.

[44] S. Adachi, *Optical Constants of Crystalline and Amorphous Semiconductors. Numerical Data and Graphical Information*, Kluwer, Boston ,**1999**.

[45] E. D. Palik, *Handbook of Optical Constants of Solids*, Academic Press, New York, **1985**.

[46] E. D. Palik, *Handbook of Optical Constants of Solids II*, Academic Press, New York, **1991**.

[47] E. D. Palik, *Handbook of Optical Constants of Solids III*, Academic Press, New York, **1998**.

[48] M. J. Weber (Ed.), *Handbook of Optical Materials*, CRC Press, New York, **2003**.

[49] S. Nagakura, H. Inokuchi, H. Ezawa, S. Iwamura, F. Sato, R. Kubo, *Rikagaku*

Author Manuscript:
Published in final edited form as: *Surf. Interface Anal*. Volume 51, Issue 4, Pages 427-457, April 2019
https://doi.org/10.1002/sia.6598

Jiten, in Japanese, Iwanami Syoten, Tokyo , **2006**.
[50] S. Thomas and P. M. A. Sherwood, J. Chem. Soc. Faraday Trans. **1993**, 89, 263.
[51] B. R. Strohmeier, Surface Science Spectra **1995**, 3, 135.
[52] R. T. Poole, J. G. Jenkin, J. Liesegang, and R. C. G. Leckey, Phys. Rev. B **1975**, 11, 5179.
[53] R. T. Poole, J. Szajman, R. C. G. Leckey, J. G. Jenkin, and J. Liesegang, Phys. Rev. B **1975**, 12, 5872.
[54] R. P. Vasquez, Surface Science Spectra **1993**, 2, 13.
[55] K. Hirose, H. Nohira, K. Azuma, and T. Hattori, Prog. Surf. Science **2007**, 82, 3.
[56] Yong-Nian Xu and W. Y. Ching, Phys. Rev. B. **1999**, 59, 10530.
[57] AtomWork database, http://crystdb.nims.go.jp/index_en.html.
[58] J. P. Perdew, K. Burke, M. Ernzerhof, *Phys. Rev. Lett.* **1996**, 77, 3865.
[59] G.D. Mahan, *Many-Particle Physics*, 3rd ed., Kluwer Academic/Plenum Publishers, New York, 2000. ISBN: 0-306-46338-5.
[60] B. L. Henke, J. C. Davis, E. M. Gullikson, R. C. C. Perera, Lawrence Berkeley Laboratory Report 26259, 1988; B. L. Henke, E. M. Gullikson, J. C. Davis, *At. Data Nucl. Data Tables* **1993**, 54, 181.; http://ftp.esrf.eu/pub/scisoft/xop2.3/DabaxFiles/.
[61] C. V. Festenberg, *Z. Physik* , **1969**, 227, 453.
[62] Y. F. Chen, C. M. Kwei, C. J. Tung, *Phys. Rev. B*, **1993**, 48, 4373.
[63] H. Jin, H. Shinotsuka, H. Yoshikawa, H. Iwai, M. Arai, S. Tanuma, S. Tougaard, *Surf. Interface Anal.* **2013**, 45, 985.
[64] H. R. Philipp, H. Ehrenreich, *Phys. Rev.*, **1963**, *129*, 1550.
[65] S. Tanuma, C. J. Powell, and D. R. Penn, *J. Electron Spectrosc. Relat. Phenom.* **1990**, 52, 285.
[66] S. Tanuma, C. J. Powell, D. R. Penn, *Surf. Interface Anal.* **1993**, 20, 77.
[67] S. Tanuma, C. J. Powell, D. R. Penn, *Surf. Interface Anal*. **2005**, 37, 1.
[68] H. Bethe, *Ann. Phys.* **1930**, 5, 325.
[69] H. Shinotsuka, S. Tanuma, C. J. Powell, D. R. Penn, *Surf. Interface Anal*. **2017**, 49, 238.
[70] M. Gryzinski, *Phys. Rev. A,* **1965**, *138*, 336.
[71] J. C. Ashley, *J. Electron Spectrosc. Rel. Phenom*. **1990**, *50*, 323.
[72] U. Buechner, *J. Phys. C* ,**1975**, *8*, 2781.
[73] H. A. Bethe, J. Ashkin in *Experimental Nuclear Physics*, Vol. 1, edited by E. Segre, Wiley, New York, **1953**, pp. 166-357.
[74] J. C. Ashley, *J. Electron Spectrosc. Rel. Phenom*. **1988**, *46*, 199.
[75] B. L. Henke, P. Lee, T. J. Tanaka, R. L. Shimabukuro, B. K. Fujikawa, *At. Data Nucl. Data Tables* **1982**, *27*, 1.
[76] K. N. Joshipura, S. Gangopadhyay, C. G. Limbachiya, M. Vinodkumar, J. Phys.: Conf., **2007,** *Ser. 80*, 012008.
[77] F. Salvat, J. Parellada, *J. Phys. D: Appl. Phys*.**1984**, *17*, 1545.

Author Manuscript:
Published in final edited form as: *Surf. Interface Anal*. Volume 51, Issue 4, Pages 427-457, April 2019
https://doi.org/10.1002/sia.6598

[78] J. D. Bourke, C. T. Chantler, J. Electron Spectrosc. Relat. Phenom., **2014**, *196*, 142.
[79] C. J. Powell,, A. Jablonski. *J. Phys. Chem. Ref. Data* **1999**, *28*, 19.
[80] S. Tanuma, T. Shiratori, T. Kimura, K. Goto, S. Ichimura, C. J. Powell, *Surf. Interface Anal.* **2005**, 37, 833.
[81] G. K. Wertheim, D. M. Riffe, N. V. Smith, P. H. Citrin, *Phys. Rev. B*, **1992**, *46*, 1955.
[82] M. Inokuti, *Rev. Mod. Phys*. **1971**, *43*, 297.
[83] X. Llovet, C. J. Powell, F. Salvat, A. Jablonski, *J. Phys. Chem. Ref. Data* **2014**, 43, 013102.
[84] C. J. Powell, X. Llovet, F. Salvat, *J. Appl. Phys*. **2016**, *119*, 184904.
[85] D. E. Cullen, J. H. Hubbell, L. Kissel, *EPDL97, The Evaluated Data Library, 1997 Version,* UCRL-50400, Vol. 6, Rev. 5 (Sep 19, 1997); http://ftp.esrf.eu/pub/scisoft/xop2.3/DabaxFiles/.
[86] T. Koide, T. Shidara, H. Fukutani, A. Fujimori, T. Miyahara, H. Kato, S. Otani, Y. Ishizawa, *Phys. Rev*. B, **1990**, *42*, 4979; T. Koide, Private communication.
[87] T. Koide, T. Shidara, H. Fukutani, A. Fujimori, S. Otani, Y. Ishizawa, *Jpn. J. Appl. Phys*., **1993**, *32*, 1130.